

DATE: 7 MAY 1971

~~71-24938~~
N71-24974
Report S-989

**REFRACTORY COMPOSITE MATERIALS
for
SPACECRAFT THRUST CHAMBERS**

**FINAL REPORT
for
THE PERIOD
23 JULY 1968 to 22 FEBRUARY 1970**

**CONTRACT: NAS7-555 MOD-3 & 4
Subcontract 700149 (Raytheon)**

PROJECT 5033

**CASE FILE
COPY**

DATE: 7 MAY 1971

REPORT S-989

REFRACTORY COMPOSITE MATERIALS
for
SPACECRAFT THRUST CHAMBERS

Final Report
for
The Period
of
23 JULY 1968 to 22 FEBRUARY 1970

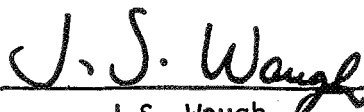
CONTRACT: NAS7-555 MOD-3 & 4
SUBCONTRACT 700149 (RAYTHEON)

PROJECT 5033

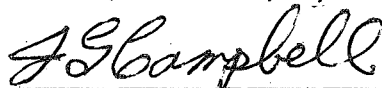
Prepared By:



C.D. Coulbert
Marquardt Program Manager



J.S. Waugh
Raytheon Company



J.G. Campbell
The Marquardt Company

Approved By:



T. Linton
Manager, Rocket Programs

FOREWORD

This report covers Phase III and Phase IV work performed by The Marquardt Company under Prime Contract NAS7-555, Modifications 3 and 4, and by the Research Division of the Raytheon Company under Marquardt Subcontract 700149, during the period 23 July 1968 to 22 February 1970. This program was a continuation of work reported in Marquardt Report 6142 on Phase I and Phase II investigations of pyrolytic refractory composites.

The work was sponsored by NASA-OART, Washington, D.C. The NASA Technical Manager was Mr. William Tyler (JPL).

The Program Manager, Mr. C. D. Coulbert (Marquardt), was responsible for the overall program direction and supervision. Dr. J. S. Waugh (Raytheon) was responsible for the technical supervision of the Raytheon subcontract. Mr. J. G. Campbell (Marquardt) was responsible for all the theoretical thermal, stress, thermodynamic and chemical analyses.

Mr. M. S. Wilson (Marquardt) performed heat transfer and thermodynamic analyses and oxidation testing. Mr. M. L. Haas (Marquardt) performed stress analysis and established analysis methods for multilamina composites.

TABLE of CONTENTS

<u>SECTION</u>	<u>TITLE</u>	<u>PAGE</u>
I	SUMMARY	1
II	INTRODUCTION	2
III	PYROREFRACTORY ALLOY FABRICATION UNDER RAYTHEON SUBCONTRACT	5
	A. Multilamina Thrust Chambers	5
	B. Pyrocarbide/Carbon Felt Composites	9
	C. Monolithic Deposits	11
IV	MATERIALS CHARACTERIZATION	12
	A. Pyrolytic Graphite/Carbitex Composites	12
	B. Thornel Reinforced Pyrolytic Graphite	14
	C. Vitreous Carbon	18
	D. Oxidation Tests	19
	E. Copper Impregnated POCO Graphite	20
V	THRUST CHAMBER DESIGN and FABRICATION	21
	A. Thrust Chamber Designs	22
	B. Thrust Chamber Fabrication and Evaluation	23
	C. Metal-Carbon Bonding	26
VI	TEST FIRING WITH FLOX/METHANE	30
	A. Test Period I	31
	B. Test Period II	32
	C. Test Period III	34
VII	STRESS ANALYSIS	36
	A. Stress Analysis Program	37
VIII	THERMAL and THERMOCHEMICAL ANALYSIS	37
	A. Heat Transfer Analysis	38
	B. Thermochemical Analysis	40
	C. Thrust Chamber Concepts	44
IX	CONCLUSIONS	48
X	REFERENCES	49
	DISTRIBUTION	151

LIST of ILLUSTRATIONS

<u>FIGURE</u>	<u>TITLE</u>	<u>PAGE</u>
1	Free Standing Pyrolytic Chamber History	81
2	Layouts of Structural Thrust Chambers for Pyrobond Fabrication Studies	82
3	Raytheon Multilamina Chambers	83
4	Chamber MRS-50	84
5	Schematic Diagram of Filament Orientation in a Carbitex Thrust Chamber	85
6	Dimensions of Pyrolytic Graphite/Carbitex Composite Test Cones	86
7	Pyrolytic Graphite/Carbitex Test Cones	87
8	Fixture for Pressurization of Test Cones	88
9	Variation of Circumferential Modulus of Elasticity of Carbitex with Wrap Angle	89
10	Variation of Axial Modulus of Elasticity of Carbitex with Wrap Angle	90
11	Variation of Axial Strength of Carbitex Cones with Wrap Angle	91
12	Dimensions of PG/Thornel Test Sample Spool	92
13	PG/Thornel Test Sample Spools	93
14	PG/Thornel NOL Ring Specimens for Tensile Tests	94
15	Results of Tensile Tests of PG/Thornel NOL Ring Specimens	95
16	Microstructure of PG/Thornel Ring Specimen 1C	96
17	Microstructure of PG/Thornel Ring Specimen 2C	97
18	Microstructure of PG/Thornel Ring Specimen 3C	98
19	Microstructure of PG/Thornel Ring Specimen 4C	99
20	Photomicrographs of Representative Sections of PG Infiltrated Thornel, Spools Nos. 1 and 2	100
21	Photomicrographs of Representative Sections of PG Infiltrated Thornel, Spools Nos. 3 and 4	101
22	PG/Thornel/PG Chamber	102
23	PG Infiltrated Thornel-50 Carbon Yarn	103
24	PG/Thornel/PG Tensile Test Apparatus	104
25	PG/Thornel/PG Tensile Test Rings after Failure	105

List of Illustrations - (Continued)

<u>Figure</u>	<u>Title</u>	<u>Page</u>
26	Carbon Materials Erosion Rate - Oxyacetylene Flame in Air	106
27	Loss of Copper from AXF-5QC	107
28	Copper Impregnated Graphite After Cyclic Heating	108
29	Composite Chamber, FLOX/LPG	109
30	POCO Graphite Heat Sink Thrust Chambers	110
31	Uncooled Copper Adapter Section for Testing Coated Tantalum-Tungsten Chambers	111
32	Copper Impregnated POCO Chamber Segment	112
33	100 Pound Thrust Carbitex 713 Chambers	113
34	PG/Carbitex Thrust Chamber with RPG Nozzle Extension	114
35	X-Ray Photograph of PG/Carbitex Thrust Chamber with RPG Nozzle Extension	115
36	100 Pound Thrust FLOX/LPG Engine Assembly	116
37	PG/Carbitex 100 Pound Thrust Sea Level Chamber with Coating on the Inside Only	117
38	PG Liners Used for PG/Thornel Composite Altitude Thrust Chambers	118
39	Thornel Wound Sea Level Chamber before PG Infiltration	119
40	Thornel Wound Altitude Chamber before PG Infiltration	120
41	Filament Winding Setup for PG/Thornel Thrust Chamber	121
42	Electrodeposited Nickel on RPG/PG Cylinders before Machining	122
43	Electrodeposited Nickel on RPG/PG Cylinder after Machining	123
44	Test Specimen Used for Thermal Cycling Test of Bond of Electrodeposited Nickel on RPG	124
45	Setup for Thermal Cycling Test of Electrodeposited Nickel on RPG	125
46	Typical Cycles of Thermal Cycling Test of Electrodeposited Nickel on RPG	126
47	Photomicrographs of Plasma Sprayed Nickel - RPG Interface	127
48	Final Configuration of the 100 Pound Thrust FLOX/Methane Injector, S/N 002	128
49	Final Configuration, S/N 002 Injector	129
50	100 Pound Thrust FLOX/Methane Engine	130
51	Erosion Pattern of PG Chamber S/N 006 after Test Run 45	131

List of Illustrations - (Continued)

<u>Figure</u>	<u>Title</u>	<u>Page</u>
52	Carbon Deposition in Sea Level PG Streak Chamber after 20 Seconds Firing	132
53	Water Flow Test of a Modified Injector Showing Film Spreading in a Lucite Chamber, $\Delta P = 80$ PSI	133
54	Spray Pattern from Cold Flow Tests of the 100 Pound Thrust FLOX/Methane Injector with 18 Fuel Film Holes	134
55	Layout of 100 Pound Thrust PG/Carbitex Altitude Chamber with Nozzle Extension	135
56	PG/Carbitex Chamber with RPG Nozzle Extension after 322 Seconds Firing	136
57	HfC Coated Tantalum-Tungsten Chamber	137
58	Predicted Transient Temperature Distribution in a ZrC Composite Fired with FLOX/Methane	138
59	Inner Surface Stresses in a ZrC Composite Chamber Fired with FLOX/Methane	139
60	Outer Surface Stresses in a ZrC Composite Chamber Fired with FLOX/Methane	140
61	1K Chamber Geometry for Thermal Analysis	141
62	Combustion Temperature of OF_2/B_2H_6	142
63	Chamber Heating Rate	143
64	Sensible Heat Capacity - Vs - Supply Temperature	144
65	B_2H_6 Cooling Capacity	145
66	Enthalpy of Gaseous Diborane	146
67	Equilibrium Chamber Wall Temperature	147
68	Combustion Products of OF_2/B_2H_6	148
69	Heat Transfer Mechanisms in an Endothermically Cooled Pyrolytic Graphite Nozzle	149
70	Composite Materials Chamber	150

LIST OF TABLES

<u>TABLE</u>	<u>TITLE</u>	<u>PAGE</u>
I	Explanatory Notes for Figure 1	51
II	Thrust Chamber Process Data	53
III	Thrust Chamber Physical Property Data	54
IV	Thickness Profile	55
V	Process Data for Felt Impregnation	59
VI	Average Physical Properties	59
VII	Local Density of Run No. MQF-5	59
VIII	Flexure Strength	60
IX	Process Data - Monolithic Deposits	60
X	Results of NOL Ring Tensile Tests of PG/Thornel - 50	61
XI	Summary of the Test Period II Injector Evaluation Firings	62
XII	Summary of Erosion of Three Free Standing PG Chambers and One POCO Graphite Chamber	64
XIII	Test Period II - Summary of Ambient Thrust Chamber Firing Tests in Magic Mountain Cell M-2	65
XIV	Summary of Average Thrust Chamber Throat Erosion Data, Test Period II, December 1968 to February 1969	70
XV	Extended Range Film Temperature Data, Phase II Tests	71
XVI	Test Period III - 100 Pound Thrust FLOX/Methane Engine Test Data	72
XVII	Summary of Stresses in ZrC/PG Composite Thrust Chambers	74
XVIII	Throat Heating Rates - $\text{OF}_2/\text{B}_2\text{H}_6$	75
XIX	Combustion Products of $\text{OF}_2/\text{B}_2\text{H}_6$	76
XX	Graphite Equilibrium with $\text{OF}_2/\text{B}_2\text{H}_6$	77
XXI	B_4C Equilibrium with $\text{OF}_2/\text{B}_2\text{H}_6$	78
XXII	Boron Nitride Equilibrium with $\text{OF}_2/\text{B}_2\text{H}_6$	79
XXIII	Tungsten Equilibrium with $\text{OF}_2/\text{B}_2\text{H}_6$	80

(This Page Intentionally Left Blank)

REFRACTORY COMPOSITE MATERIALS FOR SPACECRAFT THRUST CHAMBERS

SECTION I SUMMARY

Pyrolytic refractory materials using vapor deposition techniques and combined in composites with new carbon fiber materials have demonstrated a unique potential for high temperature structural service in a severe rocket thrust chamber environment. A family of these pyrolytically bonded (Pyrobond) materials has been formulated which combines the erosion resistance of a pyrolytic refractory thrust chamber inner wall with the high strength and fabrication flexibility of a carbon fiber composite structure.

These material systems were evaluated theoretically and experimentally in structural and hot firing tests with FLOX/methane propellants. A total of nine different 100-lb thrust refractory composite chambers, plus a hafnium carbide coated tantalum-10 tungsten chamber, seven POCO heavy wall graphite chambers, and six free standing pyrolytic graphite chambers were test fired with FLOX/methane propellants at 100 psia. A total of 2800 seconds of hot firing was accumulated during three test periods. Combustion efficiencies between 89 and 98 percent were attained as a function of chamber L^* values between 10 inches and 18 inches. During these tests, both chamber erosion and carbon deposition were evaluated locally in the chamber from the injector to the nozzle throat as a function of fuel film flow, wall material, O/F, L^* , and duty cycle.

Two of the most promising structural materials evaluated were the PG/Carb-I-tex and PG/Thornel composites. The PG/Carb-I-tex system has been incorporated into thrust chamber designs ranging from 25 to 3000 pounds thrust for evaluation in at least four fluorinated propellant combinations. Test specimens of the PG/Thornel composites have demonstrated tensile strengths in the 50,000 to 100,000 psi range for different filament orientations.

New strength and modulus data were obtained on Carbitex filament wound components and are presented as a function of fabrication parameters. Axial strength of Carbitex is from 400 to 2000 psi, depending on wrap angle.

In studies of forming metal-to-carbon joints with carbon fiber composites, both plasma spraying and electrodeposition of nickel appear to be promising techniques for attachment of carbon composites to metal injector components.

Thermochemical and heat transfer studies were made to define the severity and composition of the thrust chamber environment in a 1000-lb thrust $\text{OF}_2/\text{B}_2\text{H}_6$ rocket engine. Heat transfer analyses were made of heating rates with $\text{OF}_2/\text{B}_2\text{H}_6$ and compared with the results of other investigators. The chemical composition of the combustion gases

were used in a thermodynamic equilibrium analysis using various chamber wall materials including graphite, boron carbide, boron nitride and tungsten to evaluate chemical compatibility as a function of temperature.

On the basis of these thermochemical studies, it was concluded that tungsten is the least reactive material with the combustion products of $\text{OF}_2/\text{B}_2\text{H}_6$. The feasibility of using graphite was found to be dependent on rates of reaction which must be determined by engine test firings, since heterogeneous reaction rates cannot be predicted theoretically. It was also concluded that boron nitride might have less chemical reaction with the combustion products of $\text{OF}_2/\text{B}_2\text{H}_6$ than graphite up to a temperature of 4,000°R.

Deposition of an anisotropic form of pyrolytic boron nitride coating on a Carb-I-tex structural wall was not as successful as PG and pyrocarbide coatings due to the larger thermal expansion differences for the boron nitride. However, an isotropic form of pyrolytic boron nitride was successfully deposited on a graphite tube. This form of boron nitride may be of value as a chamber liner for $\text{OF}_2/\text{B}_2\text{H}_6$.

SECTION II INTRODUCTION

This technical report covers work accomplished under Contract NAS7-555, Phases III and IV, on the development and evaluation of pyrolytic refractory thrust chamber materials during the nineteen-month period from August 1958 through February 1970. This program is a continuation of the investigation of improved pyrolytic thrust chamber materials conducted under NASA Contracts NAS7-54, NAS7-262 and NAS7-373 (References 1 through 4). Marquardt Report 6142 (Reference 5) covers the work on Contract NAS7-555 from March 1967 through July 1968 and presents the background and initial developments on the materials work presented in this report.

A. Objective

The basic objective of this continuing program has been to provide the necessary technology to design, fabricate and test spacecraft liquid rocket thrust chambers using advanced state-of-the-art pyrolytic refractory materials and composites. The scope of work undertaken in achieving this goal has included:

1. New Materials Research - To develop new material concepts to achieve strength at high temperature, chemical compatibility and fabrication flexibility.
2. Material Characterization - To evaluate experimentally, material properties and structural capabilities which are critical to the practical application of these materials in severe rocket thrust chamber environments.

3. Application Studies - To demonstrate by the design, analysis, fabrication and testing of complete thrust chamber assemblies, the feasibility of the material systems which appear the most promising and define problem areas, structural limitations and criteria for improved material and fabrication concepts.

B. Related Programs

In earlier work on pyrolytic refractories, thrust chambers were fabricated and tested with N_2O_4 /hydrazine blend earth storable propellant combinations. During this current program, all test firings were conducted with FLOX/ CH_4 propellants. However, analytical and design studies included application to both FLOX/ CH_4 and OF_2/B_2H_6 propellant systems. During concurrent contracted programs at Marquardt (References 6, 7 and 8), pyrolytic refractory composite thrust chambers were designed and fabricated for testing with the following propellant combinations at the indicated thrust levels:

Air Force RPL	3000-lb	$CLF_3/BA1014$ (hydrazine blend)
NASA-LeRC	100-lb	FLOX/methane
NASA-JPL	200-lb	OF_2/B_2H_6
Air Force RPL	25-lb	CLF_5 /Hydrazine blend

The material system used in each of the above thrust chamber designs was PG/Carb-I-tex, which consists of a pyrolytic graphite chamber inner wall deposited on a structural shell of Carb-I-tex 713, a filament wound graphite yarn composite manufactured by the Carborundum Co. The initial development work on this material system at Marquardt under Phase I and Phase II of Contract NAS7-555 was reported in Reference 5.

The PG/Carb-I-tex system was one of several new thrust chamber fabrication concepts investigated during Phase I and Phase II of this program. Others which were conceived and included in the evaluation program were:

1. Multiple lamina pyrolytic carbide alloys including ternary and radially graded compositions.
2. High modulus carbon yarn wound over a free standing pyrolytic graphite thrust chamber and pyrolytically infiltrated and bonded.
3. Pyrolytic graphite infiltrated carbon felt combined with free standing pyrolytic graphite and filament wound reinforcing.
4. The use of vitreous carbon, stacked pyrocarbide washers, high density graphite impregnated with copper, and pyrolytic boron nitride materials in composite structures.

The technology for these newer materials had advanced sufficiently by the summer of 1968 that thrust chamber components could be fabricated and test fired with high-energy fluorinated propellants. A concurrent coordinated program to continue the development and test firing evaluation of the PG/Carb-I-tex system for a 100-lb thrust FLOX/LPG reaction control engine was supported by a contract with NASA-LeRC (NAS3-11215) (Reference 6).

A historical outline of the development of pyrolytic refractory thrust chambers at Marquardt, including PG, PG alloys, and composites is presented in Figure 1, which outlines the development of free standing thrust chambers of pyrolytic refractory materials and composites. Concurrent work under these same contracts included material development and property measurement as well as work on flat plate stock and washer-type nozzle designs. Explanatory notes for Figure 1 are given in Table I.

Details of the 100-lb FLOX/LPG injector design and its test firing evaluation are presented in Reference 6, which covers the NASA-LeRC-supported engine program. Over 900 seconds of firing on FLOX/methane, with one injector, were achieved with no plugging or overheating during operation at C^* efficiencies between 89 to 98 percent of theoretical for chamber L^* values of 10 inches and 18 inches, respectively. During these tests with FLOX/methane, both chamber erosion and carbon deposition were evident and varied locally in the chamber from the injector to the nozzle throat as a function of fuel film flow, wall material, O/F, L^* , and duty cycle.

It was concluded that the injector design approach was successful and that with additional effort, the design could be optimized to provide high performance and minimum erosion and carbon deposition.

Thrust chambers of nine different material systems, including pyrolytic refractories, fiber composites, vitreous carbon, and refractory metals were designed and fabricated for structural evaluation and test firing with FLOX/methane propellants.

Fabrication studies, property measurement, and design analyses were continued to explore and evaluate newer material concepts for specific application to the OF_2/B_2H_6 propellant combination.

The Raytheon Company, participating as a major subcontractor, under a continuing subcontract, fabricated multilamina pyrocarbide alloy thrust chambers and investigated fabrication techniques for producing pyrocarbide/carbon fiber composites and pyro-nitride/carbon fiber composites.

SECTION III

PYROREFRACTORY ALLOY FABRICATION UNDER RAYTHEON SUBCONTRACT

A. Multilamina Thrust Chambers

1. Previous Chamber Experience

Seven 100-lb thrust, thick (≈ 0.25 -in.) walled, laminated chambers with graded ZrC-PG composition were fabricated and proof tested during Phase II of this program (reported in Reference 5). The highest internal pressure withstood by this group of chambers was 650 psi. Four of the chambers failed during internal pressure testing due to tensile cracking in the inner lamina. Inasmuch as achieving the potential strength of the thick walled chamber at low initial temperatures during rocket ignition depends upon uniform transfer of the pressure loads to the outer shells, the inner lamina must be tight or even in compression if possible. Apparently this was not the case, so several alternative fabrication variations were evaluated during Phase III and Phase IV of the contract which are documented in this report.

Three interacting anisotropic physical phenomena occur in the material which vary in degree with chemical composition, temperature, and duration of elevated temperature. These are the anisotropic thermal expansion, compressive creep, and crystal lattice transformation (or growth). Initial simplified analysis indicated that it would be desirable to grade the chemical composition of the laminae from a higher ZrC content on the outside to pure PG on the inside, so that the laminae would tend to tighten during cool down to room temperature from the 1850°C (3400°F) deposition temperature.

In order to assess the effect of growth and creep on a composite cylinder, a ZrC-PG graded composition multilamina cylinder made of five laminae was annealed for two hours at 2500°C . The laminae appeared to be loosened at cool down.

The nominal wall thickness of these multiple lamina chambers was 0.25-inch. This thickness had been selected primarily to evaluate the quality of material which could be achieved in the multiple step deposition process, and fabricate a chamber capable of withstanding ignition overpressures above 3000 psi. Subsequent analytical stress studies (presented later in this report) indicated excessive external transient thermal stresses would be experienced for a 0.25-inch wall thickness during firing. Reducing the maximum wall thickness to 0.125-inch reduced the maximum thermal stresses in a 2-inch diameter cylinder by a factor of three, while maintaining a potential burst strength above 2000 psi if tight laminae could be achieved.

2. New Chamber Design

Raytheon undertook the fabrication of additional 100-lb thrust chambers to improve the maximum burst pressure attainable and provide pyrocarbide alloy thrust chambers for evaluation of erosion in FLOX/LPG test firings. The typical thrust chamber configurations are shown in Figure 2. The design parameters to be covered included:

- a) Wall thickness of 0.125 (ZrC-PG) with three laminae and 0.050 (HFC-PG) for single wall.
- b) Alloy composition - ZrC-PG (25, 12 and 0 wt % Zr) with constant radial composition.
- c) Post run anneal or heat treatment.
- d) Use of male and female mandrels for deposition.
- e) Exit expansion cones of 1.5:1 and 12:1.

3. Results of Chamber Deposition Runs

Four of the chambers fabricated by Raytheon and delivered to Marquardt are shown in Figure 3. Eighteen furnace deposition runs were made to fabricate thrust chambers for structural and test firing evaluation. The furnace process conditions, physical data and dimensional data are presented in Tables II, III and IV. Descriptions of the furnace runs and the chambers obtained from each run are given in the following paragraphs. The thrust chamber numbering sequence for the Phase III and Phase IV furnace deposition runs was MRS-50 through MRS-67.

Chamber MRS-50 (Figure 4) was deposited in a similar fashion to the earlier sea level chambers with the exception that the composition of ZrC-PG was held constant during the run rather than being graded to pure PG on the inner lamina. The purpose of this change was to try to bind the inner laminae tightly to the outer layers so that the entire shell would be load bearing, but this was not accomplished. MRS-51 was a pure PG deposition designed for the same purpose as MRS-50, to obtain a tightly bound multi-lamina chamber. An exit plug was used in this run to divert the gases after passing from the throat to improve the deposit in the expansion cone. Unfortunately, the plug caused turbulence in the gas stream and nodules on the inner lamina that ran the full length of the chamber. Both chambers were shipped to Marquardt.

The ZrC composition of MRS-50 was uniform at both ends, but the thickness profiles for both chambers showed thinning toward the exit cone. The deposition conditions were changed for the following runs in order to: 1) improve the structure of the deposit in the exit cone area and 2) decrease the thickness gradient throughout the length of the chamber.

While waiting for additional graphite female mandrels to be fabricated, two male mandrel deposits were made to evaluate the feasibility of making the altitude chambers by the external deposition technique. MRS-52 was a PG deposit and MRS-53 a ZrC-PG deposit. The mandrels were machined from single pieces of CS grade graphite into a shape that approximated a finished thrust chamber. The pyrolytic deposit was removed from the mandrel for examination by slicing it along the axis, yielding two halves of a chamber. The thicknesses for both MRS-52 and MRS-53 are listed in Table IV. MRS-53 was a repeat of -52, except that the deposit was ZrC-PG. In both runs, the deposit was smooth and fairly uniform in thickness. Upon removal from the mandrel, the deposit closed on itself indicating that the outside was in compression.

Chamber MRS-54 was the first deposit using the newly received female mandrels. A plug was used in the expansion cone to improve the deposit thickness in that region. The running conditions were identical (Table II) to those used for previously deposited (MRS-50, -53) chambers. The chamber exit plugged after 2-1/2 hours because the deposit completely filled the region where the throat and the plug tip met. Undoubtedly, the plug was too close to the throat; therefore, for MRS-55, the plug tip was raised above the throat. This deposit ran for the full term, but after removal of the mandrel and plug, it was apparent that again the plug constricted the gas flow and the inside of the chamber was coated with a rough deposit. The profile was also poor (Table IV).

For Run MRS-56, changes were needed to improve the profile and improve the deposit in the expansion cone region. The plug was raised again, the pressure was lowered to 7.5 mm Hg from 10.0 mm Hg, and the temperature was lowered to 1825°C from 1850°C. This procedure resulted in a sound chamber which was very smooth over the inside surface. The wall thickness profile was thinner than desired, varying from 0.118-inch at the injector end to 0.040-inch at the exit.

Chambers MRS-57 through -62 were deposited in the same way, that is, a diffuser plug was positioned in the expansion cone area. The pressure was lowered for this series to 6.0 mm Hg from 7.5 mm Hg for MRS-56. This change eliminated the choking that occurred in the throat area in previous chambers. Chambers MRS-57 and -58 were identical depositions except for time adjustments to obtain a more desirable thickness.

Chambers MRS-59 and -60 were 0.050-inch thick single wall chambers and were identical depositions except for run time adjustments. Both of these chambers were HfC-PG depositions to achieve 25 percent Hf. Mandrel removal was a problem because of the thinner chamber wall thicknesses, and both chambers cracked during removal. A redesign of the mandrel allowing for easier removal was undertaken. MRS-61 and -62 were ZrC composition graded, that is, the chlorine flow was varied from 0.15 lpm to 0.05 lpm. The 0.15 lpm flow was maintained during the first laminate, a flow of 0.10 lpm Cl_2 was maintained during the middle laminate, and 0.05 lpm Cl_2 was maintained during the final laminate. The depositions were ideal, being free of nodules and other deleterious

effects, but both of the chambers cracked while the mandrels were being removed. The graded structure apparently either changed: 1) the growth at temperature or 2) the average expansion coefficient, so that when the mandrels were removed, cracking occurred in the expansion cone area. A redesign of the mandrel may help to correct this problem for graded structures. MRS-62, however, had sufficient sound material remaining after mandrel removal to be used as a sea level chamber. MRS-56, -57 and -58 were altitude chambers with 12:1 expansion cones (Figure 3).

The metal content in these chambers was considerably lower than that reported for MRS-50, even though the only significant process change was a reduction of pressure from 10 mm Hg to 6 mm Hg. A reduction of this magnitude was totally unexpected. Apparently the relative rates of decomposition of the methane and metal tetrachloride changed with pressure, resulting in reduced metal content in the deposition. The precise explanation for this result is not clear.

MRS-63 was deposited under conditions similar to those used in deposition of the previous chambers, but with a slightly higher chlorine flow to yield a higher zirconium content chamber. The deposition was successful, but the chamber cracked during mandrel removal because of isolated sticking between the deposit and the mandrel. This is an unusual, but not unprecedented occurrence, and no particular reason has been singled out as the cause of this problem.

MRS-64 was a repeat of run MRS-58. During the last portion of the run (the final third), the gas inlet tube plugged due to a malfunction in the retort system used to generate the $ZrCl_4$. The chamber deposition was thin and the inside layer, which was only about 10 mils thick, buckled and rendered the chamber useless. MRS-65 was deposited using identical conditions as those for MRS-64 and a sound chamber was obtained. After deposition and before cool down, the chamber was subjected to a one-hour anneal at the deposition temperature while still on the mandrel. The reason for this operation was to promote "growth" and thereby tighten the three laminae against each other. Visual observation of the chamber indicates that this did not happen. The growth-anisotropic stress relationship is sufficiently complex to make predictions of this kind rather difficult.

Chamber MRS-66 was deposited as a 0.050 wall thickness HfC-PG altitude chamber. The deposition was good and the chamber was sound but cracked during mandrel removal. Further mandrel modification to provide a weaker mandrel would solve this problem, but available time was too short to try another mandrel design.

MRS-67 was deposited utilizing identical operating conditions (Table II) as for MRS-58. A one-inch section was cut from the bottom of the chamber (excess material), and this section was heat treated after removing the mandrel at the deposition temperature (1825°C) in argon in order to tighten the laminae. Previous heat treating experiments have been: 1) conducted at temperatures far above the deposition temperature and significant

graphitization occurred, or 2) at the deposition temperature with the sample restricted within the mandrel, resulting in growth stresses sufficiently high to buckle the inner lamina. The present experiment was designed to allow the inner lamina to grow, unrestricted by the mandrel, and thereby tighten against the outer laminae. After the heating cycle, the laminae were found to have loosened.

During the final thrust chamber fabrication study in which 18 chamber deposition runs were completed, there were seven thrust chambers shipped to Marquardt (MRS-50, 51, 56, 57, 58, 62 and 65). Chamber MRS-58 was received in time to be test fired with FLOX/methane during the January 1969 test period reported in Section VI.

4. Current State-of-the-Art

Based on the results of these chamber deposition studies, it was concluded that:

- a) Multilamina thrust chambers of controlled geometry and thickness can be fabricated reproducibly and with good internal surface finish.
- b) Production controls and fabrication techniques need to be improved by further development and design studies.
- c) Tightening of the laminae of thick pyrorefractory cylinders was not achieved by any of the techniques tried and thus the burst pressure potential of this material system was not realized.

B. Pyrocarbide/Carbon Felt Composites

Composites made of carbon felts infiltrated with pyrolytic graphite have demonstrated ultimate flexure strengths of 10,000 psi using rayon precursor and 19,000 psi using a wool precursor, with compressive strengths as high as 65,000 psi (Reference 9). Tensile strengths for the pyrocarbide materials (ZrC-PG and HfC-PG) measured for earlier Raytheon materials (Reference 4) exceeded 40,000 psi and flexure strengths above 100,000 psi were measured. Since these values were more than double the values measured for pure PG, it seemed reasonable to expect an appreciable increase in carbon fiber composite strength if the felts could be similarly infiltrated with the pyrocarbides. Additional potential advantages over PG/Carbon felt and pure ZrC-PG materials would be fabrication flexibility, hardness, and oxidation resistance.

Initial exploratory furnace deposition runs were conducted by Raytheon as reported in the Phase I and Phase II report (Reference 5). These initial runs were attempts to obtain uniform impregnation of the felt without sealing off the surface. The feasibility of the material system was demonstrated, but the flow and process conditions required to achieve a uniform high density composite needed further investigation.

Ten furnace deposition runs were made during the Phase IV program to further define the impregnation process parameters for the uniform densification of 3/4-inch thick carbonized rayon felt with the ZrC-PG alloy.

The furnace setup for run MQF-1 was a square box design, inside dimensions of approximately 1-1/2 x 1-1/2 x 10 in. Two of the sides of the box were made of 3/4-inch thick carbonized rayon felt. The incoming gases were made to pass through a preheat chamber so that by the time the gases were in the felt chamber, they were hot enough to crack and react with the substrate. Deposition conditions (Table V) similar to those used to successfully deposit pyrolytic carbon in felt structures, were used as starting points. The run plugged after 15 hours in the preheat chamber, indicating that the enhancement of gas phase reaction in the pyrocarbide system, even at such a low temperature as 1200°C, is greater than was anticipated.

The setup for run MQF-2 was of similar design as MQF-1, except that the preheat chamber was eliminated, the temperature lowered to 1100°C, and the chlorine flow was reduced to 0.05 lpm. All these changes were designed to reduce the rate of cracking of the gases so that the carbide would be deposited in the interior of the felt. After 35 hours of deposition the run plugged and examination of the box after cool down indicated a surface coating of sooty material on the felt approximately 10 mils thick. This rate of deposition was about 50 times greater than that observed for the pyrocarbon system deposited under similar conditions.

For run MQF-3, the box dimensions were the same. The pressure was reduced to 10 mm Hg, the rationale being that the lower pressure would reduce gas phase reaction by reducing the number of gas molecules available for collision prior to contact with the fiber surfaces. The run duration was 40 hours. The material was found to be sooty and not usable.

Larger boxes than those for the first three runs were made for the furnace setup for the next three runs. The sides were 3 x 10 x 3/4-inch, but in all other respects the setup was the same.

Deposition MQF-4 was run for 20 hours, MQF-5 for 40 hours and MQF-6 for 28 hours, although it was scheduled to be run for 60 hours. The increased deposition temperature (1500°C) increased the efficiency of the process over those runs using the lower temperatures, whereas the reduced pressure of MQF-6 improved, at least from visual appearances, the homogeneity of the deposits throughout the thickness of the felt. MQF-6 did not run full term. The gas inlet tube plugged for indeterminate reasons.

The average bulk and toluene densities of material from runs MQF-4, -5, -6, -7, and -10 are presented in Table VI. The variation in densities is due both to degree of buildup and to metal composition of the deposit.

The local density data from MQF-5 given in Table VII show some interesting information. The density gradient at the top is greater than the gradient at the bottom because: 1) the gas is coldest at the top and is the most rich, and 2) the bottom exhaust arrangement allows the gas to deposit on the outside as well as the inside walls. The increase of the toluene density from bottom to top shows that the carbide phase is preferentially deposited, a fact observed many times before in this program (during cylinder and chamber depositions).

The carbide infiltration runs (MQF-7 through -10) were deposited utilizing the methods described before as the $\Delta T - \Delta P$ techniques. The sample consisted of a felt pad formed into a closed shape such that the gases were required to pass through the fiber network. In addition, a temperature gradient was imposed across the thickness of the felt, similar to the method developed by the Sandia Corp. (Reference 10). The gases enter the network of fibers, decompose and deposit carbide-pyrolytic carbon onto the hot side of the felt. As material builds up on the surface of the fibers the temperature gradient moves in toward the cold side of the felt and deposits additional material. This process is self limiting in that once the hot side of the felt becomes filled with material, no additional gas flow is permitted and surface coating of the inside surface occurs. However, this technique is relatively rapid and the heavily coated side of the felt can be trimmed from the remainder and used for the measurements intended.

MQF-8 and -9 were not successful runs in that both terminated early due to malfunctions of equipment.

MQF-4, -5 and -6, deposited by a different technique, were made by simply passing gases over the felt with no pressure or temperature differential imposed with only surface diffusion operating to densify the felt. Their compositions were considerably lower than the later runs mainly because of lower chlorine to methane ratios.

Table VIII presents flexural strength data measured on the felt infiltration runs. A comparison of the room temperature flexure data between MQF-6 and MQF-10 shows the effect of carbide content on flexural strength (~4000 psi for 3% Zr vs. 5700 psi for 27% Zr), and the increased test temperature shows the increase in strength observed in other carbon systems (i. e., PG). All of the flexure tests were conducted with the load parallel to the ab plane. Since the rayon precursor is not isotropic, loading in the direction perpendicular to the ab plane would probably yield lower values of flexure strength.

C. Monolithic Deposits

Monolithic deposits (MQP-106, -107 and BN-794) were made on the inside of Carbitex mandrels, the purpose of the runs being to determine the compatibility of the deposited material with the substrate. Process conditions are given in Table IX.

MQP-106 was a standard ZrC-PG run, MQP-107 an anisotropic pyrolytic boron nitride run, and BN-794 an isotropic pyrolytic boron nitride run made under proprietary conditions. The ZrC-PG deposit appeared to adhere well to the mandrel, whereas neither of the boron nitride materials were compatible with the carbitex. Raytheon has successfully deposited isotropic BN on the inside of a commercial graphite tube.

SECTION IV MATERIALS CHARACTERIZATION

A. Pyrolytic Graphite/Carbitex Composites

In order to design composite thrust chambers of PG/Carb-I-tex and to calculate the axial and circumferential stress distributions, it was necessary that values of axial and circumferential elastic moduli for Carb-I-tex be known. In pressure tests of Carb-I-tex 713 chambers, the mode of failure was a gross axial tensile failure of the wall. The approach to improving the axial strength was to decrease the wrap angle (Figure 5) of the filament winding.

In order to obtain data on strength and elastic properties applicable to chamber design as a function of wrap angle, twelve Carb-I-tex 713 cones were purchased from Carborundum Co. The design of the cones is shown in Figure 6. Six of the cones were filament wound with a 60° wrap angle and six with a 75° wrap angle. The cones are shown in Figure 7, with strain gages installed.

The following properties of Carb-I-tex 713 in the filament wound axisymmetric form were determined using both the 60° and 75° cones as structural test specimens:

1. Modulus of elasticity in the circumferential direction.
2. Modulus of elasticity in the axial direction.
3. Ultimate tensile strength in the axial direction.

The cones were held at the large end and internally pressurized, with the small end sealed (Figure 8). This setup created maximum stresses in the large end of the cone. At an internal pressure of 600 psig, the axial stress 0.6-inch from the large end was 1880 psi, perhaps exceeding the axial strength. The circumferential stress was only 5500 psi, well below the expected hoop strength of the Carb-I-tex. Therefore, it was expected that the axial strength determined in this cone under biaxial pressure loading would be more representative of the loading in a thrust chamber than that obtained from loading of a flat test specimen.

The wrap angle of the cones actually varied with diameter because of the type of filament winding machine used. The wrap angle varies as follows:

$$\frac{\text{Diameter}}{\tan \alpha} = \text{Constant}$$

where

α = Wrap angle as defined in Figure 5.

It was possible to break the cones more than once at successively smaller diameters, thus obtaining more data on the variation of axial strength with wrap angle.

Six of the twelve Carb-I-tex cones obtained were used in the uncoated condition to measure axial and circumferential properties. The remaining six cones were coated with PG for the measurement of composite properties.

The Carb-I-tex cones and tubes were fitted with strain gages and pressurized to obtain modulus and strength data as a function of the wrap angle. Figure 9 shows circumferential modulus values from cone data and from tube No. 1. The circumferential modulus varies from 2×10^6 to 5×10^6 psi. The axial modulus (Figure 10) follows the opposite trend and is considerably lower than the circumferential modulus, ranging from 0.9×10^6 to $.2 \times 10^6$ psi. One data point was obtained by compressing tube No. 2 (from Phase II, Ref. 5) axially on a Baldwin loading machine.

Figure 11 shows axial tensile strength as a function of wrap angle as obtained from cones pressure stressed to destruction. Most cones were tested to failure twice, once near the large end and then near the small end by remounting the remainder of the cone. All cones failed axially with the exceptions of Cone No. 1-60, which had a hole blown in the side and Cone No. 2-60, which could not be broken because of excessive leakage. Some cones with high leakage rates were broken when a very thin plastic liner was used inside as a seal. The axial strength was much lower than the circumferential strength. Several 60° cones showed circumferential stresses as high as 9600 psi when failing axially. The circumferential strength of 75° cones would be expected to be higher.

The surfaces of the Carb-I-tex cones were not as good quality as those of previous Carb-I-tex tubes (2-inch diameter) and 100-pound thrust chambers (Reference 5). Numerous rough areas with graphite filament breakage existed on both the ID and OD. Polishing techniques were used to alleviate this condition. Part of the problem seems to be small voids in the Carb-I-tex. A smooth Carb-I-tex surface is desired to produce a good quality PG coating with minimum size and number of nodules. Other observations made during inspection of the cones were as follows:

1. The 75° wrap angle cones were smoother inside and outside than the 60° cones.
2. The delaminations in the Carb-I-tex wall were common at the small end of the 60° cones.
3. None of the cones were completely smooth or free from small rough areas.

Six of the Carb-I-tex cones were coated with PG according to the following schedule:

<u>Cone Wrap Angle (Minimum) (degrees)</u>	<u>Inside PG Coating (in.)</u>	<u>Outside PG Coating (in.)</u>
60	0.025	None
75	0.025	None
60	0.050	None
75	0.050	None
60	0.025	0.025
75	0.025	0.025

The resulting tubes had good quality, well bonded coatings both inside and outside. Surface flaws in the Carb-I-tex are still apparent in the PG surface after coating. The cones are still available for further testing of the effect of these flaws on pressure failure modes.

B. Thornel Reinforced Pyrolytic Carbon

1. Description of Test Specimens

Testing was completed on the Thornel-50 wound, pyrolytic carbon infiltrated, NOL-type composite ring specimens which were prepared and partially tested during the course of the Phase II program (Reference 5). The specimens were prepared by winding the Thornel yarn around four foam carbon, spool shaped mandrels - each divided into four sections as shown in Figure 12. Two ring specimens were obtained from each section. The spools, after winding and pyrolytic carbon infiltration, are shown in Figure 13, and examples of test rings are shown in Figure 14.

Spool No. 1 was filament wound without additives or special treatments to the filaments before PG infiltration. Chopped carbon fibers were added to Spool No. 2 during the winding process to form a network of fibers to fill the space between the graphite yarn bundles. The objective of this addition was to improve the shear strength of the composite. The same objective was pursued in preparing Spool No. 3 by causing frayed fibers of the Thornel yarn itself to bridge the space between adjacent yarn or yarn layers. To accomplish this, the yarn was lightly abraded with a sharp tool during winding. Spool No. 4 was wound with the addition of carbon black and furfural binder to fill the potential pores and also for the purpose of improving the composite shear strength. The subsequent PG infiltration process provided inter-filament bonding within the yarn for effective load transfer.

2. Discussion of Test Results

The results of the tensile test of the rings using the NOL Split-D technique are shown in Table X and plotted in Figure 15 as a function of specimen thickness. Because of the effect of bending moment on the test section, the thinnest ring would be expected to produce the highest apparent tensile strength, provided the materials are uniform and without major defects. Without a prior knowledge of the magnitude of this bending moment, its actual effect cannot be accurately assessed. The effect depends not only on the magnitude of the maximum strain which the composite undergoes, but also on other factors such as its modulus and the mismatch between the diameter of the Split-D fixture and the inner diameter of the specimen.

If the cross section of the test region of the specimen contains major pores or other defects, a defect of a given size would have the largest influence on the thinnest specimen. In the macrographs and micrographs of these specimens, it was noted that many lacked uniformity and denseness in packing. Figures 16 through 19 show the Section C from each spool as examples of the cross sectional microstructure. The influence of porosity and other defects on the mechanical properties can be seen in the degree of data scatter for the thin specimens (Section A) in Figure 15.

The 10X photomacrographs show the full cross section of the specimen. The 50X photomicrographs show an enlarged section of the specimen under polarized light conditions to bring out the highly anisotropic pyrolytic graphite (white areas). Much of the thick pyrolytic graphite on the outer surface was machined off during the preparation of these specimens. The presence of the chopped fiber or the frayed fiber effect in the windings of Spools Nos. 2 and 3, respectively, are not readily evident in the photomicrograph (Figures 17 and 18), except for a few individual PG-coated fibers in the void area. However, the carbon black with furfural binder added during the winding of Spool No. 4 is clearly seen as the smoother gray areas (Figure 19). In Section D of each spool, the

Thornel filaments were wound over pyrolyzed felt. Although the felt layer was designed to be 0.20-inch thick with a Thornel wrapping of 0.050-inch, it was noted in the 10X micrographs (not shown) that some variation in these values was obtained in the actual windings. On the average, there was approximately 0.10-inch of felt, with approximately 0.10-inch of Thornel. Since the underlying felt/PG material contributes little to the total strength, the actual PG/Thornel strength is much larger than the indicated strength.

The 750X photomicrographs (Figures 20 and 21) of representative sections of each spool show the details of pyrolytic coating over each fiber within the yarn, and in some cases, regions of more massive depositions around the yarns. The pyrolytic graphite deposition around each filament in Spool No. 1 (Figure 20A) was uniform (approximately 0.05×10^{-3} -in.) with no preferentially high deposition rate over the outer fiber of the yarn. In Spools Nos. 2 and 3 (Figures 20B and 21A, respectively), however, the coating rates were higher. Each fiber was coated with approximately 0.10×10^{-3} to 0.20×10^{-3} in. of PG, whereas heavy coatings occurred around the periphery of yarn bundle adjacent to the voids (which constitute the primary passageway for infiltrants). The absence of the corresponding heavy coating in the large voids of Spool No. 1 is not adequately explained. It would appear that the chopped fibers introduced in Spool No. 2 and the frayed yarns in Spool No. 3 served to open up the primary passageways to allow free flow of infiltrants to permit the heavier deposits. In Spool No. 4 (Figure 21B), however, the PG coating of the fiber was less than in the others, indicating the effect of the carbon black and furfural binder in closing up the primary passages. Although not readily evident in the polarized light photomicrograph, the stray outer strands of the yarn are tightly embedded in the pyrolyzed, furfural-bonded carbon black. Because of the blocked primary passages, the coating rates of the inner fibers are reduced, and longer time would be required to infiltrate for adequate inter-filament bonding.

On the basis of very limited data, the following observations are noted:

1. The addition of the chopped carbon fibers into the Thornel windings was effective in increasing the strength of PG impregnated Thornel reinforced composite, probably by partially filling the void between yarn with PG-bonded chopped fibers, thereby increasing the overall interlaminar shear strength.
2. The abrasion of filament while winding the spool did not improve the properties despite good PG infiltration; rather, the properties degraded, probably from the direct damage incurred by the filament during the knife edge abrasion. The admonition to handle the filaments with care should be well heeded.

3. The beneficial effect of the furfural and carbon black additions was not clearly evident. These additions can be expected to provide improved shear strength of the composite by bridging the space between yarns. On the other hand, the presence of the filler material can prevent the thorough penetration by the infiltrant, or decrease its rate. The inter-filament bonding within the yarn would require a longer processing time.
4. Improved winding techniques under conditions of constant tension should provide better filament packing. Judicious choice of impregnants and impregnation techniques can lead to improvements in high strength, high modulus graphite, filament wound structures.

As noted in the microstructure of Spool No. 4 specimens with the carbon black/furfural impregnant, some of the outer filaments of the graphite yarn were completely encased in the pyrolyzed impregnant. If means were devised to impregnate thoroughly into the inner regions of the yarn, it may result in a produce superior to the PG infiltrated structure. Currently, all resin materials undergo considerable shrinkage ($\approx 20\%$ or more) requiring re-impregnation to obtain reasonably low porosities. The use of PBI (polybenzimidazole) resin with high char yield is an attempt to accomplish this purpose. The shrinkage of PBI during carbonization is claimed to be approximately 10%. Preliminary studies conducted by the Narmco Research and Development Division of the Whittaker Corporation showed carbonized PBI resin impregnated, thornel re-inforced, uniaxial composite laminates to be stronger than corresponding PG infiltrated materials. Additional work is required to substantiate these early observations.

Better testing techniques which do not impose bending moments are available in measuring the circumferential tensile strength of ring specimens. A common technique involves the hydraulic pressurization of an axially restrained internal bladder. A method using an axial compression of a solid rubber cylinder to provide radial expansion inside the ring specimen has recently been described (Reference 11).

3. Filament Wound Thrust Chamber Tensile Tests

Three composite thrust chambers utilizing PG infiltrated high modulus carbon fiber were fabricated for structural and test firing evaluation.

The PG/Thornel/PG chambers (Figure 22) consists of free standing PG chambers with .050 walls which were filament wound with Thornel-50 to a 0.125 wrap thickness at an 80° lead angle. The chambers were then infiltrated with PG during a 96-hour furnace run. The free standing PG liners had been previously pressure checked

to 200 psig before filament winding. During the trimming and finishing of one of the composite chambers, the PG liner cracked and would not hold pressure. Therefore, the PG liner was removed leaving a shell of the Thorne1-50/PG composite. The structure of the Thorne1 50/PG composite is shown in Figure 23. The cylindrical chamber section of this part was cut into three NOL tensile rings. A set of "D" blocks (Figure 24) was made and the three NOL rings were pulled at room temperature. The tensile strength results are tabulated below for the broken specimens shown in Figure 25.

NOL Ring Test Results

Sample	I.D. In.	Wall Thickness		Height In.	Area In. ²	Failure Load Lb.	Aver. Stress psi
		Max. In.	Min. In.				
1	1.53	.100	.092	.758	.145	8400	57,700
2	1.53	.109	.102	.761	.161	7420	46,200
3	1.53	.096	.093	.760	.144	7720	53,800

The above level of available strength in the chamber wall would provide a chamber pressure capability of over 7,000 psi if the cold start pressure stresses could be transferred to the composite before an inner liner failure. As the PG chamber liner heats due to combustion heating, the inner liner does transfer the load and, in fact, the PG liner goes into compression.

The carbon composite material consisting of high strength carbon filaments and PG bonding appears to have excellent potential for high strength at high temperature. However, there are several fabrication parameters subject to variation for tailoring the material to a specific application. The carbon yarn Young's modulus may be varied from 1 to 100×10^6 psi with a corresponding increase in tensile strength. A number of other different types of high modulus carbon fibers are also being developed. At the present time, some of these PG/fiber material concepts are being developed for other applications by Super Temp Co.

C. Vitreous Carbon

Compared to the better known forms of carbon, vitreous carbon possesses properties which are desirable for structural applications. It is isomorphous, relatively strong and stiff, has good thermal shock resistance, and its glassy structure is stable (does not graphitize) to over 3000°C. It is also very hard and it should exhibit good erosion resistance.

However, it also has a serious weakness in its sensitivity to mechanical shock, and a crack once started propagates easily and rapidly. It is therefore important to protect a vitreous carbon structure from impact-type loads and from high stress concentrations. Vitreous carbon as produced by Beckwith Carbon was investigated for application as thrust chamber liners.

Initial investigations involved the use of available cylindrical crucible shapes for the combustion chamber section and washer-type inserts for the throat section. A principal, nonrecurring expense for such items is the fabrication of a metal transfer mold. Once this item is amortized, the cost of vitreous carbon liners would be significantly less than the cost of pyrolytic graphite liners.

In preparation for the use of vitreous carbon parts in a thrust chamber, preliminary machining tests were conducted at Marquardt. The hardness and brittleness of vitreous carbon precludes the use of carbide cutting tools as used in lathe operations. Diamond tools were effective in cutoff, core drilling, or grinding operations. Procedures generally used for ceramic materials are useful on vitreous carbon. Vitreous carbon is sufficiently conductive that EDM (electrical discharge machining) processes are very effective, although time consuming. Brass and carbon electrodes were used; both suffered erosion, but the metal electrode resulted in a better finish. Because this technique is very slow, it should be used for intricate shape cuts where the more rapid, diamond cutoff, drilling, or grinding operations are not practical. Ultrasonic machining techniques should also prove to be well suited to vitreous carbon materials.

The brittle fracture characteristic of vitreous carbon by which a crack in the material propagates readily through the whole piece could possibly be overcome by introducing fibrous carbon reinforcements. This possibility was explored in cooperation with Beckwith Carbon Corporation. However, due to several furnace run malfunctions, the results were inconclusive. Two approaches were being evaluated. The first was to pyrolyze a phenolic/carbon fiber composite through the same furnace cycle used in vitrifying a normal phenolic molded component. Due to the 20 percent shrinkage in the phenolic during processing, it would be expected that voids would develop in the composite, while the normal vitreous carbon is impervious and free of all porosity. An alternate approach would be to formulate a resin/rayon composite in which the pyrolyzation shrinkages would be matched for each material. The furnace runs on the phenolic carbon fiber samples developed operating problems before satisfactory material was obtained and this limited effort was terminated.

D. Oxidation Tests

An oxyacetylene torch test was performed to determine the relative oxidation resistance of a number of advanced carbon materials. Samples of each material were supported on alumina blocks and exposed to the oxyacetylene flame. Throughout the heating time, the maximum surface temperature was monitored with an optical

pyrometer. The exposure time was set for each material to give significant erosion without burnthrough. Some samples were limited to 2-1/2-minute runs, and others were run 8 minutes. When more than one sample of each material was available, test runs were made at different surface temperatures by adjusting the torch-to-sample distance.

The materials evaluated included:

1. Pyrolytic graphite (as a reference)
2. POCO graphite (AXF-5Q)
3. Copper impregnated POCO (AXF-5QC)
4. Vitreous carbon (Beckwith)
5. Fluidized bed pyrolytic carbon (isotropic)
6. PG/Thornel composite

Figure 26 shows erosion rate as a function of surface temperature for the materials tested. The small sample of graphite coated with isotropic pyrolytic carbon burned through during the test so that an exact erosion rate could not be determined. It can be stated, however, that the erosion resistance of this material was not greater than anisotropic PG.

Of the materials tested, POCO graphite (AXF-5Q) showed the least erosion resistance. Copper impregnated POCO (AXF-5QC) gave nearly identical results. Both materials eroded about six times faster than PG. The erosion rate of PG impregnated Thornel was about twice that of PG. Vitreous carbon eroded at a rate about three times that of PG. The vitreous carbon sample cracked in two after 30 seconds of heating, but the test was continued with one piece without additional cracking.

The oxidation rates of vitreous carbon in oxygen, argon, and CO₂ gas mixtures at temperatures up to 3000°K have been compared to the rates for pyrolytic and molded graphite in Reference 12. The oxidation rates of vitreous carbon and PG were similar and they are somewhat lower than those for molded graphite. At a surface temperature of 3000°K (4900°F), vitreous carbon had an oxidation rate in carbon dioxide less than one-half that of PG.

E. Copper Impregnated POCO Graphite

Copper impregnated POCO-AXF-5Q graphite is being evaluated as a potential chamber lining material. The potential advantages of the material include:

1. Strength equal to or better than POCO-AXF-5Q graphite
2. Double the thermal conductivity at temperatures to 3500°F
3. Capable of structural operation to the temperature limits of graphite

4. Reduced brittleness and increased resistance to thermal stress failure
5. Improved heat sink and conduction cooling capability
6. Potential for combining with a PG/fiber composite for operation at high temperature.

Two other characteristics which have been evaluated in tests were oxidation resistance in an oxidizing flame and effect on carbon deposition in a FLOX/LPG test chamber. In both tests the performance of the copper impregnated graphite was essentially the same as the pure graphite.

Another characteristic evaluated was the mechanism of copper loss during high temperature heating. In one series of tests, samples of Cu/POCO were heated in a vacuum furnace to nominal temperatures of 2300^o, 3000^o and 3400^oF for times of 10 and 20 minutes. The results are shown in Figure 27. In a second series of tests, a sample of Cu/POCO was heated to 3300^oF four times. During the first heat up cycle, molten copper exuded from the sample surface and the total weight loss was 31.3 percent. During subsequent heating cycles the weight loss was 3.0 percent per cycle. After each cycle a part of the sample was cut off and the loss of copper examined visually (Figure 28). After each cycle the copper boundary within the sample was well defined indicating that the loss of copper is from an internal effective copper surface. After the first heating cycle the molten copper is exuded from the pores of the graphite by the difference in thermal expansion. On subsequent cycles, no molten copper is seen on the surface and the copper is apparently lost by evaporation.

A similar heating test was conducted with Cu/POCO sample in which a 1/2-inch diameter tantalum tube was inserted. After heating to 3000^oF three times, it was found that the interface gap between the tube and graphite remained filled with copper while the copper loss boundary was again seen at the outside of the sample (Figure 28).

SECTION V THRUST CHAMBER DESIGN and FABRICATION

The results of preliminary design studies and fabrication experiments demonstrated the feasibility of fabricating complete lightweight, all carbon, composite thrust chambers with the potential of very high burst pressures and high operating temperatures. At the same time, a number of design variables remained uncertain for the various composite structures. These unknowns included:

1. The values of thermal conductivity, thermal expansion, elastic modulus and creep rates of the PG/carbon fiber composites as a function of process parameters and operating temperatures.

2. The residual stresses and nature of the bonds in the various composite structures.
3. The optimum choice of thickness, carbon fiber modulus, wrap orientation, etc. to achieve the maximum rocket chamber strength at ignition heat up and steady state conditions.

These design unknowns are all amenable to experimental and analytical determination in time, but it was decided that a screening program to evaluate fabricability, structural soundness and erosion resistance of the chamber liners in a single environment would be worthwhile at the present time.

A. Thrust Chamber Designs

The chamber design concepts described below were incorporated into chamber designs for fabrication, pressure testing and test firing with FLOX/methane propellants. Along with the advanced composite designs, additional materials and chambers also described below were fabricated to broaden the base of comparison and provide additional data on the operating characteristics of the 100-lb thrust FLOX/methane injectors used.

1. Multilamina Pyrocarbide Chambers

These chambers have been described in Section III-A.

2. Free Standing Thin Wall HFC-PG Chambers

Chamber fabrication described in Section III-A.

3. Free Standing Pyrolytic Graphite

Chambers with 0.050 walls were used both as streak test chambers to evaluate injector performance in short runs and as the liner for the PG/Thornel/PG chambers below.

4. PG/Thornel/PG Chambers

A high quality PG free standing liner filament wound with high modulus carbon yarn to a thickness 0.125 or 0.25 and then infiltrated with pyrolytic graphite to bond the carbon fibers and PG liner into a high strength composite, pressure tight thrust chamber.

5. PG/Thornel/Resin Chambers

Same as above, except the Thornel wrapped chambers were PG/resin impregnated and pyrolyzed in multiple steps to achieve a pyrolyzed resin/Thornel composite over the PG liner.

6. Carb-I-tex 713 Chambers

With and without PG coatings.

7. Vitreous Carbon Chamber Liner (Figure 29, bottom)

8. Pyrocarbide Alloy (ZrC-PG) Stacked Washer Nozzle Insert (Figure 29, top)

9. High Density Isotropic Graphite (POCO) (Figure 30)

Used for long run evaluation of injector streaking and deposition plus graphite erosion characteristics.

10. Refractory Metal Chambers (Figure 31)

Ta-10W chambers coated by ITTRI (Reference 13) with the carburized Hf-10Ta-4, 5C-0.4S: slurry coating.

11. High Density POCO Graphite Impregnated with Copper (Figure 32)

Cylindrical section inserted between injector and POCO graphite chamber.

All of the above design concepts were carried through the design stage and to various stages of fabrication, structural evaluation and test firing as described in the following sections.

B. Thrust Chamber Fabrication and Evaluation

1. PG/Carb-I-tex Chambers

a) Three 100-lb thrust size Carb-I-tex 713 chambers (Figure 33) were received from the Carborundum Co. for coating with PG. These chambers were to have 0.25-inch Carb-I-tex walls, but the thicknesses of the delivered shells varied from 0.19 to 0.25-inch. Because the shells were thin, the outside surfaces were not machined smooth except at the attach end. The inside surfaces had been machined using a standard tool bit which left several rough places where fibers had been torn loose.

The three Carb-I-tex chambers were proof pressure tested with nitrogen to 200 psig without failure. However, the chambers leaked gas through the walls, indicating a degree of porosity.

Previous experience showed that the quality of the PG coating depended directly on the surface finish of the PG mandrel substrate. All surface blemishes and machining marks are picked up and propagated through the PG coating, often resulting in large nodules. These, in turn, might become points of initiation of failure.

One Carb-I-tex chamber was sent with its existing finish to Super Temp Co. to have a 12:1 nozzle extension added. The 12:1 nozzle exit cone was fabricated of RPG and attached to the Carb-I-tex by a threaded joint. The Carb-I-tex chamber and nozzle were then coated inside and outside with a 0.040-inch layer of PG. The chamber as received from Super Temp is shown in Figure 34. An X-ray photograph of the chamber (Figure 35), as well as visual examination, revealed that the outer layer of PG separated from both the RPG and the Carb-I-tex. An axial crack occurred in the outside PG on the exit cone. In finish machining the chamber, most of the loose PG on the exit cone was removed. The finished chamber is shown in Figure 36 attached to the injector and bipropellant valve.

The remaining two Carb-I-tex chambers were used for surface finishing studies. The surface finishes on the Carb-I-tex chambers and test cones were not as good as on the previously received tubes. There were numerous rough spots which appeared to be voids in the material. In some cases, loose fiber ends were exposed.

A number of methods of grinding and polishing was attempted to eliminate the rough spots. A very sharp tool bit at 300 rpm was tried, but the finish was not improved. Hand finishing with fine (600 grit) emery paper gave a reasonably good finish in some cases, but rough areas were uncovered on other samples by the sanding. As with other finishing techniques, it was found advantageous to sand in the same direction in which the Carb-I-tex was wrapped to prevent the edge of the paper from picking up fiber ends.

The inside surfaces of the Carb-I-tex cones were finished by lapping using an anodized aluminum tapered plug. A good finish was obtained on 75° cones, but the 60° cones still had rough areas. A reasonably good PG coating was obtained on the cones without large nodules, but rough areas still existed, especially on the 60° cones.

Grinding wheels were tried in an attempt to get a good finish on the Carb-I-tex tubes. A 1-1/2-inch Cratex rubber wheel turning at 5000 rpm was tried with fair results, but other rough areas were uncovered. A 60 grit Al_2O_3 wheel was tried and also a 46 grit open wheel. Neither gave good results.

The best surface finish was obtained using diamond tools. A single diamond cutting tool gave a reasonably good finish, but best results were obtained with a small diamond grinding wheel (about 0.5-inch in diameter) mounted on a balance quill. A surface free from serious rough areas was obtained. The insides of two Carb-I-tex 100-lb thrust chambers were finished in this way using a template to guide the wheel. A surface grinding speed of 40 ft. per second was used. Equally good results were obtained with two tubes ground with the same wheel at 6 ft. per second.

One of the Carb-I-tex 100-lb thrust chambers was finished for firing without a PG coating and the other chamber was coated with a 0.04-inch layer of PG on the inside only (Figure 37).

2. PG/Thornel Composite Chambers

Two pyrobond thrust chamber fabrication concepts were evaluated using a free standing PG chamber over-wrapped with Thornel and bonded. These chambers consist of thin (0.050-inch wall), pyrolytic graphite liners wrapped with multilayer helical windings of high modulus graphite yarns with matrices of either infiltrated pyrolytic carbon or impregnated and pyrolyzed PBI resin. The high modulus reinforcements used for these chambers were Thornel-50 (Union Carbide). The impregnant resin was PBI (Polybenzimidazole).

The PG liners for the altitude thrust chambers are shown in Figure 38. The Thornel-wound sea level and altitude chamber structures are shown in Figures 39 and 40, respectively, before PG infiltration. Two-piece graphite inserts which extended beyond the liner ends were placed into the PG liners in order to provide a cylindrical end section to prevent slippage during winding of the yarn down the conical section of the chamber liner. These extensions were machined off after the completion of the infiltration and impregnation and pyrolyzation process. A steel bolt through the axis served to hold the graphite mandrel in place and to provide a chucking medium for the lathe. The filament winding setup at Narmco-Whittaker is shown in Figure 41 showing the chamber in the lathe and the Thornel feed bobbin with the lathe in the background. On removing the bolts before PG infiltration at Super Temp, one of the filament-wound chambers, the altitude chamber, broke in the chamber region. The broken sections were placed in the infiltration furnace along with the two sea level chambers for production of material test samples.

Although it was intended to leave the stainless steel bolts in the three filament-wound chambers for PBI impregnation during the impregnation-pyrolyzation treatments at Narmco, the bolts were removed after the experience at Super Temp. No difficulties were encountered in the removal of the bolts from these chambers and the impregnation-pyrolyzation cycles were completed without difficulty.

3. Vitreous Carbon Thrust Chambers

Three vitreous carbon crucibles (1.5-in. dia. x 6.0-in. length x 0.09-in. wall) were purchased for use as thrust chamber liners to be encased in a POCO graphite, heavy walled chamber. Prior to use, one of the crucibles was machined by grinding to obtain a true outer surface that was round and uniformly tapered. The closed end of the crucible was removed by grinding. During grinding of the outer crucible surface, cracks developed in the wall at the ground surface. Since the material is isotropic and the heating and cooling cycles were very gradual, the existence of residual stresses would not be expected. One possibility was the stresses due to mounting during machining. Also considered was the heating effect of the grinding operation. This heat should have been small due to the light cuts taken and the ease of carbon removal.

The characteristic glass-like propagation of the wall crack during machining demonstrates the need to overcome this property limitation by the use of some re-inforcement technique.

The two remaining crucibles on hand were also broken during attempts to fill the crucibles with a potting material to facilitate mounting the part while grinding. A low temperature metal alloy was used to fill the crucible in one case and a plastic was used in the other. The reason for these failures was not clear. However, this experience with cracking of the vitreous carbon while grinding, mounting, heating and potting point out the brittleness of vitreous carbon above normal commercial graphite and the pyrolytic graphites.

4. Stacked Pyrocarbide Washer Nozzle

A chamber of graphite, steel and reinforced plastic was designed (Figure 29) to hold exit nozzle inserts for test firing evaluation. Two sets of ZrC-PG washers were fabricated with a 0.868 throat diameter by Raytheon during Phase II. One nozzle set was test fired with N_2O_4 /MMH (Reference 5). The second set was available for evaluation with FLOX/Methane. Fabrication of the chamber was postponed because it could not have been completed in time for the January 1969 time period. Therefore, a set of exit nozzle insert washers is available for test evaluation.

C. Metal-Carbon Bonding

All current carbon composite and PG thrust chamber attachment designs employ a clamping action to seal the carbon to the metal interface. Work done by Solar (Contract NAS 7-100) demonstrated that PG could be brazed to Ta-10W alloys. However, the mechanical integrity of such a joint was poor under thermal cycling conditions due to

thermal expansion stresses. However, in a thrust chamber design using a carbon fiber composite with a PG inner wall, the possible techniques of bonding metal to the carbon fiber composite were re-examined. Three techniques have been studied in exploratory experiments, namely, brazing, electroforming and plasma spraying. The objective of these initial studies was to form a metal-to-carbon joint for operation and thermal cycling at temperatures below 2000°F such as those allowable at an injector/chamber interface.

1. Brazing

A study at Marquardt was conducted to determine the practicality of brazing PG/Carbon felt (RPG) to itself and to 321 stainless steel and also of brazing Carb-I-tex to itself and to stainless steel. An attempt was made to braze the following materials using small samples:

<u>Materials</u>	<u>Braze Alloy</u>
RPG-RPG	Coast 53
RPG-RPG	Palniro 7
RPG-Cres 321	Coast 53
PRG-Cres 321	Palniro 7
Carbitex-Cres 321	Coast 53
Carbitex-Cres 321	Palniro 7

The composition of Coast 53 braze alloy is 83.5Ni-6.5Cr-3B-4.5Si-2.5Fe. The composition of Palniro 7 is 70Au-22Ni-8Pa. The braze material was applied as a paste using Nicrobraz cement as the binder. Brazing was done in a vacuum at 1975°F.

In no case was a good braze achieved. On the RPG-RPG samples, neither alloy would wet the material; the braze material did not flow to the interface. The results for the RPG-Cres 321 samples were the same except that the steel was uniformly wetted. There was no bond to the RPG.

Likewise, no success was achieved in brazing Carbitex to Cres 321. The Carbitex and the steel were wetted by both alloys (more uniformly by Coast 53), but the joints failed in cooling. A thin layer of Carbitex was found adhering to the steel sample. This failure is due to the difference in thermal expansion between the two materials. The coefficient of thermal expansion of Carbitex is $1.2 \times 10^{-6} \text{ } ^\circ\text{F}^{-1}$, that of Cres, $9.3 \times 10^{-6} \text{ } ^\circ\text{F}^{-1}$. This problem is less severe for RPG which had a coefficient of thermal expansion of $4.5 \times 10^{-6} \text{ } ^\circ\text{F}^{-1}$.

Future work may include investigation of brazing metal infiltrated or metal coated RPG. It is hoped that infiltration of an appropriate material will cause the RPG to be wetted by the braze alloy and enable a good bond to be made. Several techniques of metal infiltration of RPG have been discussed with Super Temp and could be evaluated in the future.

2. Electroformed Nickel

Two short cylindrical specimens of RPG/PG composite were used as a substrate for electrodeposition of a thick layer of pure nickel. The appearance of the nickel deposit prior to machining is shown in Figure 42. After machining, a 50X photomicrograph of the nickel RPG interface (Figure 43) shows the penetration of the nickel into the RPG.

a. Thermal Cycling Test

To evaluate the structural integrity of the joint, a thermal cycling test was run to define the nature of the metal bond failure. The geometry of the test specimen is shown in Figure 44 and the experimental heating setup is shown in Figure 45.

Two thermocouples located as shown in Figure 44 were used to monitor the temperatures. Both thermocouples were imbedded in the RPG, the inner one being near the PG interface and the outer one near the nickel interface.

In order to simulate thrust chamber performance, the specimen was heated from the inside diameter portion by inductively heating the ends of a cylindrical graphite susceptor which passed through the ring specimen. The heating was conducted under a moderate vacuum of about 5×10^{-2} torr (50 micron Hg).

In an initial coil configuration, the split coil was placed too close to the specimen, causing direct susceptance by the specimen. The specimen heated more rapidly on the outside and caused heating beyond the temperature intended for the Ni-RPG interface, especially at the position opposite the side with the thermocouple.

The setup was modified by using a longer susceptor and placing the two coil sections farther apart. Figure 45 was taken during the high temperature phase of the heating cycle.

With this test configuration, thermal cycling tests were programmed for 5 cycles, each to nominal temperatures of 1000° , 1500° and 2000°F as monitored by the inner thermocouple. The low temperature portion of each cycle was determined by practical time considerations of thermal decay of the system. The actual typical cycles are shown in

Figure 46. The upper temperature for the last series of cycling tests (intended to be 2000°F) was not achieved, due to the indirect heating method for the heater-specimen geometry used, in which the thermal losses by radiation were excessive. At the peak of these cycles, the susceptor temperature within the induction coils was ~2320°F and the temperature in the region of the specimen was ~2025°F, as determined by optical pyrometry.

b. Discussion of Results

The temperature experienced by the nickel-RPG bond interface was very closely that indicated by the outer thermocouples. From the typical temperature cycles (Figure 46), it is noted that the bond interface reached temperatures of approximately 800°, 1200° and 1400°F during the three cycling series.

Under the conditions noted, that of three series of thermal cycling tests to the temperatures shown in Figure 46, the following observations are noted:

- (1) The inner PG ring remained intact.
- (2) Although most of the interface between the nickel and RPG remained apparently well bonded, a hair line crack developed in the RPG near the nickel interface.
- (3) The nickel surface appeared to have small blisters, probably due to the vaporization of occluded electrolyte material. This blistering effect began during the second cycling series. A slight distortion of the nickel band was also observable without the use of measuring devices.
- (4) Considerable outgassing occurred during the initial phase of the test leaving white deposits on the glass bell jar wall. It is suspected that most of the gaseous evolution took place in the RPG, possibly that of the electrolyte entrapped during the electro-forming process.

The physical bond between electroformed nickel and RPG is sufficiently stable to permit nickel to be used as an intermediate bonding medium for graphite structures under moderate steady or cyclic temperature conditions for a limited but undefined period of time. The most severe conditions encountered by the Ni-RPG interface during the final cyclic series was five 25 minute cycles between 700° and 1400°F with a hold

period of approximately 6 minutes at the maximum temperature in each cycle. Further testing is required to define the various time-temperature cycle conditions under which this system is stable. Electroforming conditions should be selected to minimize occlusion of electrolytes in the nickel, or entrapment in the graphitic structure. Preliminary thermal treatments which eliminate such entrapped electrolyte slowly may be beneficial to the stability of nickel-graphite structures.

c. Plasma Sprayed Nickel

Two short cylindrical specimens of RPG were supplied to the Wall Colmonoy Corporation of Santa Fe Springs, California, to have a layer of nickel deposited on the RPG by plasma spraying. After deposition of approximately a 0.010-inch layer of nickel, a tensile failure occurred in the outer layer of RPG and the band of nickel and a layer of RPG opened up due to the buildup of tensile residual stress in the nickel layer. The layer of nickel was still well bonded to the RPG and the nickel also exhibited fair ductility in bending the nickel layer over a 1/4-inch diameter rod. The nickel apparently wetted the carbon fibers without causing local failures. The interface is shown in Figure 47.

This type of joint may work much better on a material such as Carb-I-tex. The nickel layer would serve as an intermediate layer to which other metal parts could be joined by brazing or welding.

SECTION VI TEST FIRING WITH FLOX/METHANE

Test firings with FLOX/methane during the Phase III and Phase IV programs were conducted during three periods in Marquardt's Magic Mountain Cell M-2. These three test periods were:

- I. August 2 - September 9, 1968 - 47 runs
- II. December 28, 1968 - February 11, 1969 - 30 runs
- III. July 9 - July 25, 1969 - 27 runs

These test periods were cooperative test programs in support of two NASA programs (NAS3-11215 and NAS7-555) in order to achieve reduced hardware and test costs.

The main test objective of the NAS3-11215 testing was the demonstration of the maximum firing durability of the PG/Carb-I-tex thrust chamber with a 12:1 exit nozzle. The main objectives of the NAS7-555 testing were the determination of the structural and erosion resistance capabilities of a variety of advanced materials and fabrication concepts with the development of chamber design criteria and guides to improved materials and fabrication techniques.

A. Test Period I

During the test period I, the primary objective was the evaluation of the FLOX/methane 100-lb thrust injector designed under Contract NAS3-11215. Two injectors of the same design were fabricated, one under NAS3-11215 and one under NAS7-555.

The injector design utilized like doublet injection elements and fuel film boundary layer injection. The original injector was described in physical detail in Reference 6. The final configuration is shown in Figure 48 and the photograph of Figure 49. The injector and copper heat sink chamber are shown in Figure 50.

Evaluation tests of the injector were conducted at the Marquardt Magic Mountain Cell M-2 sea level test site utilizing both copper heat sink chambers for combustion performance evaluation and graphite chambers for thermal and erosion characteristics. A listing of all test firings and a summary of results are tabulated in Table XI.

These test results indicated that the prime injector requirements of efficiency and durability were satisfied since C* efficiency in excess of 95 percent was consistently demonstrated with smooth ignition and combustion. The requirement of film protection was not completely met, since excessive local erosion of the free standing PG chambers occurred at the plane of the injector face. Quantitative erosion data for three free standing PG chambers and one POCO graphite chamber are shown in Table XII. It is to be noted that the POCO chamber did not show evidence of upstream erosion or carbon deposition encountered by the free standing PG chambers, due to lower wall temperatures resulting from the much higher heat sink capacity of the POCO chamber. The PG chamber erosion pattern (Figure 51) and carbon deposition (Figure 52) were correlated with the regions which were covered by the fuel film jets. The erosion is also correlated with regions of relatively high oxidizer concentration as influenced by the injector spray fan pattern and combustion reactions. This possibility had been anticipated with provisions for modifying the injector to increase the boundary layer film protection at minimal compromise of C* performance.

The two existing injectors were modified prior to the next test period, which included long duration chamber tests at altitude conditions. The injector modification consisted of adding an additional ring of fuel film injection elements consisting of 12 equally spaced, 0.005 inch diameter jets impinging on the chamber wall in the plane of the injector face. The existing original set of 6 jets impinging at a plane approximately 3/4-inch from the injector face remained, since the film produced by them provided adequate protection to the downstream chamber and throat region. A plastic chamber section was used during cold flow injector tests to evaluate the film protection coverage and spreading pattern of the additional holes (Figure 53). The spray pattern during water flow tests of the modified injector is shown in Figure 54.

B. Test Period II

The objective of test period II was to evaluate the structural and erosion characteristics of widely diverse refractory materials and composites in a common FLOX/methane combination environment during long duration runs (60 - 1800 seconds). The fabrication of more than 30 thrust chambers was undertaken between test period I and II. A number of chambers experienced fabrication problems and were either completed too late for the January 1969 tests or were not available for testing due to structural problems as discussed in the previous section. Twelve thrust chambers were used during Period II with an additional ten thrust chambers fired during test period III in July 1969.

The test period II runs are summarized in Table XIII. Briefly, the test items and firing durations were as follows:

1. Heat sink copper - two chambers, No. 1, 8 runs, 45 seconds
No. 2, 3 runs, 141 seconds
2. Free standing PG - three chambers, 3 runs, 58 seconds
3. POCO graphite - one chamber - 5 runs, 5 runs, 194 seconds
4. Multilamina pyrocarbide (MRS 58) - one chamber - 1 run, 60 seconds
5. PG/Carb-I-tex (sea level) - one chamber - 1 run, 40 seconds
6. PG/Carb-I-tex (12:1 exit) - one chamber - 6 runs, 322 seconds.

Essentially, all of the 860 seconds of run time listed above was accumulated with one injector with no indication of injector plugging or overheating during operation.

Initial test firings during test period II with the injector modified by the additional fuel film jets showed wall erosion near the injector face. Accordingly, the final configuration also included the addition of a short deflection ring welded to the face of the injector just outside the circumference of the oxidizer doublets. This modification, shown in Figures 48 and 49, was very effective in reducing local erosion near the injector face. No overheating of the ring as shown was experienced.

The PG/Carb-I-tex chamber (SL-3) with an L^* of 18 inches, which was fired for 322 seconds, had been modified by attaching a 12:1 exit nozzle extension of a PG/carbon felt composite (RPG). The joint was formed by threading the exit nozzle and chamber. The inside and outside of the assembly were coated with a 0.040-inch layer of PG (Figure 55).

During the first 60 second firing run with the above chamber at altitude conditions using the no-flow ejector, the exit nozzle extension apparently failed early in the run. The mode of failure of the exit cone is not known since the parts of the cone were ejected sideways into the altitude bell rather than downstream. There was no sign of burning or erosion on the cone pieces. One possible explanation is that a lateral deflection of the chamber assembly against the diffuser inlet occurred during the start transient and cracked the exit cone.

After the first firing, the chamber was removed from the cell and examined. There was very little throat erosion. There was carbon deposit buildup within the chamber and throat. There was some minor local erosion at the injector end of the chamber. There did appear to be several hairline cracks in the PG inner wall. The appearance of the chamber was similar to that of the first PG/Carb-I-tex chamber (SL-1) (Figure 56) which had been fired for 40 seconds.

The first PG/Carb-I-tex chamber (Figure 56) (which also developed hairline cracks) was pressurized after the 40 second firing run. At 50 psi there was leakage through the wall at the throat. It should be noted that all the uncoated 100-lb Carb-I-tex chambers leaked gas at all pressures when they were pressurized to 100 psig prior to coating.

Test firing of PG/Carb-I-tex chamber SL-3 with FLOX/methane was continued for five more runs. The maximum firing durations were limited by the pressure drop increases across the FLOX line filter. It is postulated that this was due to solid crystals of HF, since after each run, when the filter was allowed to heat up, the blockage disappeared. It was the objective of this firing series to run until some definite failure occurred in the chamber. At the beginning of the sixth run, after successful runs of 60, 47, 60, 71 and 68 seconds, there was an apparent burn through. Examination of the chamber after the run showed failure due to gradual erosion through the PG coating on the wall ahead of the throat and then a more rapid burn through in the Carb-I-tex. The PG inner wall in the throat region showed nearly uniform circumferential erosion. At local areas, where a very thin coating of PG remained, the PG/Carb-I-tex bond remained intact. There was no tendency for the PG to separate from the inner wall of the Carb-I-tex. The hairline cracks did not initiate any local erosion or failure (Figure 56).

The estimated PG liner erosion rate over the total burn time was about 0.12 mil/second at the pressure, temperatures and mixture ratios involved.

Erosion rates for the free standing PG chambers, POCO graphite, and copper chambers are presented in Table XIV. Throat erosion rates in the multilamina (MRS-58) chamber which had an inner lamina of ZrC/PG alloy (12 wt. % Zr) were similar in appearance and magnitude (0.19 mil/sec) to PG materials. A local erosion streak in the combustion chamber also indicated that the erosion characteristics of the alloy were similar to PG.

Structurally the ZrC-PG alloy chamber was similar to a three laminae PG chamber fired with F_2 /BA1014 propellants during the Air Force PG chamber program (Reference 14). The maximum exterior wall temperature reached at the outside surface of the multi-lamina chamber was 3150°F as shown in Table XV. This table summarizes maximum wall temperatures measured using the calibrated extended-range photographic film technique. The estimated interior wall temperature based on heat transfer analyses was close to 5000°F .

C. Test Period III

The objective of test period III was to continue the test firing evaluation of advanced chamber material systems not available during the period II tests. Twenty-seven test firing runs were completed with ten chambers between 9 July 1969 and 25 July 1969. The test firing summary is shown in Table XVI. The ten chambers fired included:

1. POCO graphite (three)
2. PG/Thornel/Resin Composite (two)
3. PG/Thornel/PG Composite
4. PG/Carb-I-tex
5. Carb-I-tex (uncoated)
6. HfC coated tantalum-tungsten
7. Copper impregnated POCO graphite

From these test firings, data were obtained on erosion rates, carbon deposition and structural integrity of the different material and fabrication concepts. The results are discussed below:

1. POCO Graphite

Three POCO graphite chambers were test fired for durations up to 60 seconds. Despite relatively slow heating time because of the heat sink effect, the throat erosion was as much as 0.32 mils/sec (Run 15). The POCO oxidized on the outer surface during the longer runs, and it was noticed during post fire proof tests that the porosity was increased by the firings.

2. PG/Thornel/Resin Composite

Of the two PG/Thornel/Resin composite chambers tested, good erosion data was obtained on Run 9 of 82 seconds duration. The erosion rate (Table XVI) was 0.14 mils/sec, which is a typical value for pyrolytic graphite. The outer wrap was depleted by oxidation from the atmosphere during the test firings, with the residue having the appearance of loose Thornel. It was concluded that the Thornel/Resin reinforcement did not offer any advantages over free standing pyrolytic for the test conditions involved.

3. PG/Thornel/PG Composite

The PG/Thornel/PG chamber was trimmed and pressure checked to 200 psig. However, in mounting the chamber on the injector with the tapered seal attachment, the clamping load caused a crack in the PG liner at the attach flare. To allow the test firing to proceed, a sealing compound was used to fill the crack in the liner flare and the test firing was accomplished satisfactorily. During the 65 seconds of firing a small hole was eroded in the side of the chamber through both the PG liner and Thornel overwrap. No crack or further failure was initiated by the burn through.

4. PG/Carb-I-tex

Chamber SL-1, fired previously for 40 seconds during Test Period II, was fired for 40 and 105 seconds during Runs 11 and 12, respectively.

The chamber pressure varied erratically during Run 12 because of carbon buildup in the throat which periodically was ejected. The overall throat erosion rate was 0.15 mils/sec. Post test examination of the chamber revealed heavy carbon deposits about two inches downstream of the injector face, and thin carbon deposits in several portions of the throat. The rest of the combustion chamber and contraction region was free of carbon deposits. The PG had been smoothly eroded away in a 90° segment of the contraction region, but no evidence of leakage through the Carb-I-tex was found. There were about eight hairline cracks in the throat PG coating, which did not cause any further damage to the Carb-I-tex wrap.

5. Carb-I-tex (Uncoated)

An uncoated Carb-I-tex chamber was given four test firings. During the longest run of 61 seconds (Run 19), the throat erosion was 0.41 mils/sec. The chamber was in good condition after the tests except for the throat erosion.

6. HfC Coated Tungsten

A tantalum-10 tungsten chamber coated with hafnium carbide by ITRI was test fired for 10 seconds during Run 27 using the test installation shown in Figure 31. The chamber is shown in Figure 57. The coating was completely removed from the throat during the test firing.

7. Copper Impregnated POCO Graphite

The two-inch long cylindrical section of copper impregnated POCO graphite was clamped between the copper adapter and POCO chamber as shown in Figure 32. Looking at the inside of the chamber after Runs 22, 23 and 24, a total of 60 seconds of firing, the film cooling impingement patterns were clearly visible. The heating pattern was clearly visible by the boundary of copper melting and depletion and by the oxidized areas on the outside of the POCO and the copper impregnated (Cu/POCO) sections. Inside the chamber, carbon deposit streaks built up in line and downstream of the six inside fuel film jets. There was no difference noted between deposits on the Cu/POCO and POCO chamber sections. In regions of no deposit the outside wall temperatures were coolest in line with the six inside fuel film jets.

Based on this limited testing and previous heating tests with the Cu-POCO, it would be concluded that the chemical and structural performance of the Cu/POCO would be the same as straight POCO graphite with the possible advantage of higher thermal conductivity and heat capacity.

SECTION VII STRESS ANALYSIS

A stress analysis of a multilamina ZrC/PG thrust chamber was made to evaluate the possible advantages of this type of structure. The analysis was made for the conditions of a 100 lb thrust engine using FLOX/CH₄ at a chamber pressure of 100 psia, a mixture ratio of 4.0, a C* efficiency of 95%, and a combustion gas temperature of 6345° F.

The chamber wall consisted of six laminae of 0.040 inch thickness each, for a total wall thickness of 0.24 inch. Data for the thermal conductivity of ZrC in PG are very limited but are of the same order as pure PG. Therefore, the thermal conductivity was assumed to be identical to that of PG.

The specific heat was also assumed to be the same as for PG. Reference 4 data was used to obtain the density of ZrC/PG.

The transient temperatures in the combustion chamber wall (ID = 1.4 inches) for a 300 second firing are plotted in Figure 58. The outer chamber wall was assumed to be radiating to space with an emissivity of 0.8.

Several distributions of alloy composition were assumed. The first distribution studied consisted of 0% Zr content in the inner lamina, varying linearly to 30% Zr (by weight) in the outer lamina. The Zr content in each lamina was assumed constant, and increased between laminae by 6% increments.

A transient stress analysis was made of the cylindrical sections of the thrust chamber. The results are shown in Figures 59 and 60, which present the maximum stresses at about 300 seconds into a run at both surfaces.

The maximum stress on the inside surface (pure PG) is shown in Figure 59 to be about 11,000 psi in the axial direction. The maximum stress on the outside surface (30% ZrC) is shown in Figure 60 to be about 28,000 psi in the circumferential direction.

Alternate distributions of ZrC concentration (30% inside/0% outside; 30% constant; 0% inside/12% middle/0% outside; etc.) did not significantly reduce the stresses for the same basic chamber configuration. However, for the same ZrC distribution (0% inside, 30% outside), a large reduction in stresses is achieved by reducing the wall thickness to 0.12 or by increasing the chamber diameter to 2.8 inches. These comparisons are also shown in Table XVII.

A. Stress Analysis Program

The Marquardt non-homogenous, anisotropic stress analysis computer program was used to calculate stress profiles for the engine configuration being studied. This program calculates stresses and radial displacements in a cylindrical tube of constant wall thickness. The mathematical model assumes an axially symmetric temperature distribution and incorporates internal pressure and residual stresses. The program was originally written for studies on pyrolytic graphite, which is a transversely isotropic material. The program can handle end conditions of complete axial restraint, finite end loads, or free ends; and it also takes into account growth (permanent deformation), creep, and temperature dependent material properties, together with differing material compositions. This is done by dividing the cylinder into a specified number of concentric cylindrical shell elements and considering the material properties at the mid-point of each element. The material properties are assumed constant for each element, and a composite stress distribution is obtained by determining the unknowns in each element and matching corresponding quantities on the boundaries. The calculations involve the solution of a set of $(2N+1)$ linear equations, where N is the number of cylindrical shell elements.

Another feature of the program is the so-called post run analysis, which corresponds to a cooling down of the cylinder under no external loads. The resulting final stresses in this case are due to the anisotropic residual stresses and to any growth during the loaded case.

In addition to this basic program, a version of the program was modified to handle chambers with delaminations. This was done by requiring that a positive (or tensile) radial stress could not exist between two delaminations. If the original calculations predicted such a situation, the stresses were redistributed so that this situation did not exist.

SECTION VIII

THERMAL and THERMOCHEMICAL ANALYSES

Thermochemical and heat transfer studies were made to define the severity and composition of the thrust chamber environment in a 1000 lb. thrust $\text{OF}_2/\text{B}_2\text{H}_6$ rocket engine. Heat transfer analyses were made of heating rates with $\text{OF}_2/\text{B}_2\text{H}_6$ and compared with the results of other investigators. The chemical composition of the combustion gases were used in a thermodynamic equilibrium analysis to evaluate chemical compatibility of various chamber wall materials including graphite, boron carbide, boron nitride, and tungsten as a function of temperature.

A. Heat Transfer Analysis

Heat transfer analysis was done to predict the wall temperatures for several chamber design concepts. All analysis was done for a thrust chamber producing a space rated thrust of 1000 lbs. at a chamber pressure of 100 psia and a mixture ratio of 3.0, using a throat diameter of 2.6 inches.

The thrust chamber contours used in the materials selection are shown in Figure 61. Contraction ratios of 2.0 and 6.0 were used, with L^* values of 16 and 46, respectively. The portion of the chamber more than two inches downstream of the throat was not considered in calculating heat loads.

The combustion temperature of $\text{OF}_2/\text{B}_2\text{H}_6$ at 100 psia is shown in Figure 62 over a range of mixture ratios. At a mixture ratio of 3.0 and a C^* efficiency of 95 percent, the combustion temperature is about 6000° F, which was used in the calculations of chamber heat loads.

The convective heating of the thrust chamber wall was calculated from the Bartz equation modified by the reference enthalpy method. The heat transfer coefficient and heat flux at the throat for a wall temperature of 1000°F is compared in Table XVIII with experimental data from several sources. It can be seen that the throat heat flux from all sources is fairly uniform, approximately $5 \text{ BTU/in}^2 \text{ sec.}$, regardless of the contraction ratio or type of propellant stratification used.

The total heating rate to isothermal chambers at various wall temperatures is shown in Figure 63. The total heating rate is somewhat greater for the contraction ratio of 2.0 than for the contraction ratio of 6.0. Turbulent convective heating without any film cooling was assumed throughout the chamber. An attempt to induce laminar heating rates at the throat of a 1K chamber with a contraction ratio of 8:1 is reported in Reference 15. However, the throat heat flux, shown in Table XVIII was still about $5.4 \text{ BTU/in}^2 \text{ sec.}$

The cooling capacity by sensible heat absorption of various liquid propellants is shown in Figure 64. The amount of sensible heat which can be absorbed in the liquid phase depends on the supply temperature at which the propellant is provided. The maximum possible amount of cooling corresponds to supply just above the freezing point, with subsequent heating to the boiling point at the chamber pressure. Actual cooling systems would have to operate over a somewhat narrower temperature range to maintain liquid propellant throughout the system. The maximum possible sensible heat absorption of liquid B_2H_6 is 140 BTU/lb. , compared to 260 BTU/lb. for MMH.

The cooling capacity of diborane is indicated in Figure 65, which presents the potential heat absorption rate of fuel cooling as a function of the percent of the total fuel flow (0.68 lb/sec) which is used for cooling. If all of the diborane could be heated from the freezing point and vaporized, about 250 BTU/sec. could be absorbed. Additional heat could be absorbed by the vaporized diborane if the cooling system could transfer heat into the diborane gas. The enthalpy-temperature relationship for gaseous diborane (Figure 66) shows that gaseous diborane could absorb 740 BTU/lb. by being heated to 1000°F , which is approximately the limit temperature to avoid decomposition (Reference 15).

The temperature to which an isothermal 1K chamber (contraction ratio of 6:1) could theoretically be cooled by the diborane are shown in Figure 67. If all of the diborane were used for chamber cooling, and only the sensible heat capacity of the liquid were used, the isothermal wall temperature could not be reduced below 4400°F . This condition (the line labeled QSENS(LIQ) in Figure 67 defines the theoretical limit of regenerative cooling with a liquid.

If regenerative cooling could use the heat of vaporization of the diborane, the lower line in Figure 67 could theoretically be achieved. However, the isothermal wall temperature is still too high for conventional types of regeneratively cooled structures. In order to achieve wall temperatures below the lower curve, the cooling of gaseous diborane would have to be utilized, perhaps by gaseous film cooling or by gaseous regenerative cooling. Both of these methods would be difficult to implement.

The principal conclusion to be drawn from the heat transfer analysis is that the cooling capacity of the diborane for the 1K engine is very limited, even for the optimistic and idealized heat balances used in this analysis.

B. Thermochemical Analysis

Thermochemical calculations were performed to evaluate the suitability of a number of materials when exposed to the combustion products of $\text{OF}_2/\text{B}_2\text{H}_6$. Those materials evaluated were graphite, boron carbide, boron nitride and tungsten.

The analysis consisted of calculating the composition of mixtures of the combustion species in thermodynamic equilibrium with a large amount of the candidate wall material at temperatures from 1000°R to 7000°R .

The weight ratio of initial wall material to the combustion products was usually assumed to be 20:1. Any reduction in the initial amount of the wall material may indicate the potential for chemical reactions between the wall and the combustion species. However, it is impossible to estimate the rate of such reactions unless experimental data are available describing the kinetics of the reactions. Such kinetics data is not presently available for most of the combustion species and wall materials studied.

1. Chamber Environment

The principal gaseous combustion species of $\text{OF}_2/\text{B}_2\text{H}_6$ for a mixture ratio of 3.0 and a chamber pressure of 100 psia are plotted in Figure 68 for temperatures from 1000°R to 7000°R . The principal gaseous species above 3000°R are H_2 , BOF , H and HF . A more precise compilation of combustion products is given in Table XIX which is normalized to include solid species such as B_2O_3 . Therefore, the mole fraction of gaseous species at low temperatures is somewhat smaller in Table XIX than in Figure 68.

Below 3000°R , the principal gaseous species are H_2 and BF_3 . The combustion products of $\text{OF}_2/\text{B}_2\text{H}_6$ also produce solid B_2O_3 at low temperatures. Boric oxide (B_2O_3) is a glassy substance which melts at approximately 650°F , forming a viscous liquid with a boiling point of about 4000°F . This implies that B_2O_3 will deposit or condense on portions of the chamber wall which are below 4000°F .

Another factor to consider in evaluating the chamber environment is the possibility that the B_2H_6 will be used for film cooling of the chamber wall. In that case, the mixture ratio adjacent to the wall would be much lower than the overall value of 3.0 assumed in the analytical study. The use of B_2H_6 film cooling would result in decomposition of the B_2H_6 , creating a boundary zone with a large amount of H_2 and boron. The boron might deposit on the chamber wall. This effect was found in the experimental measurements in Reference 15, which reported that about 90% of the gaseous species adjacent to the wall of chamber film cooled with B_2H_6 was hydrogen. Wall deposits near the injector consisted of about 94% boron and 4% B_2O_3 . Near the throat, the effect of the decomposition of B_2H_6 film coolant had diminished so that only 31% of the solid wall deposits was boron, while 61% was B_2O_3 .

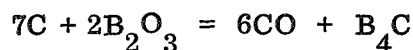
2. Graphite

a. Compatibility with Combustion Species

The equilibrium composition of a mixture of the combustion products of OF_2/B_2H_6 and a 20:1 weight addition of graphite is presented in Table XX. Reactions are indicated by the presence of carbon bearing reaction products. Therefore, it can be seen that reactions occur at all temperatures. Methane is the predominant product at temperatures below $4000^\circ R$, while carbon monoxide and acetylene become more prevalent above $4000^\circ R$.

b. Compatibility with B_2O_3 —

A calculation of the free energy change for the reaction



shows that the reaction will begin at about $3500^\circ R$.

c. Compatibility with Boron

Graphite is predicted on the basis of free energy change to react with boron at all temperatures. Again, as in the reactions with the combustion gases, the rate of the reaction cannot be predicted.

d. Compatibility with H_2 —

Graphite is predicted on the basis of thermodynamic equilibrium to react with hydrogen at all temperatures. There is some data on the reaction rates between hydrogen and graphite (Reference 16), which becomes appreciable at about $3000^\circ R$.

3. Boron Carbide

a. Compatibility with Combustion Species

The equilibrium composition of a mixture of the combustion products of $\text{OF}_2/\text{B}_2\text{H}_6$ and a 20:1 weight addition of boron carbide (B_4C) is given in Table XXI. The behavior of B_4C is similar to that of graphite, in that some amount of carbon bearing reaction products are predicted at all temperatures. Boron carbide would be inert to attack by boron wall deposits, but would react with B_2O_3 .

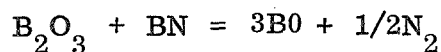
4. Boron Nitride

a. Compatibility with Combustion Species

The composition of equilibrium mixtures of boron nitride with $\text{OF}_2/\text{B}_2\text{H}_6$ is given in Table XXII. It is not possible to determine potential reaction by looking for the presence of boron bearing species, because there are many boron species present in the nominal combustion products. However, reactions or decomposition of BN may be indicated by the presence of nitrogen bearing species. Examination of the equilibrium compositions, listed in Table XXII, reveals some very small amounts of NH_3 and N_2 at 1000°R . The amount of these species is at a constant value at 2000°R and 3000°R , and the amount of solid BN is greater at these temperatures than at 1000°R . This behavior probably indicates insignificant reactions at these temperatures. The presence of small amounts of N_2 at 4000°R and 5000°R may indicate slight reactions, vaporization or dissociation.

b. Compatibility with B_2O_3

Boron nitride was predicted to react with B_2O_3 at 4300°F (4750°R) according to the equation:



c. Compatibility with Boron

Boron nitride would be inert to boron wall deposits.

d. Compatibility with Hydrogen

Boron nitride would react with hydrogen at temperatures above about 2800°F , but the rates are not known since heterogeneous reaction rates cannot be predicted theoretically.

5. Tungsten

a. Compatibility with Combustion Species

The compatibility of tungsten with the products of $\text{OF}_2/\text{B}_2\text{H}_6$ is very good, as shown by the equilibrium composition at 6500°R shown in Table XXIII. Only small amounts of WF or tungsten oxides are predicted, implying little reaction. Tungsten borides were not included in this calculation because of the lack of thermodynamic properties, which also precluded calculating the compatibility of tungsten with boron or B_2O_3 .

b. Compatibility with Hydrogen

Tungsten does not react with hydrogen at any temperature.

6. Summary

The results of the thermochemical analysis lead to the following conclusions:

a. Of the materials evaluated, tungsten is the least reactive with the combustion products of $\text{OF}_2/\text{B}_2\text{H}_6$. Tungsten has the disadvantages of high density (19.3 gm/cc) and marginal ductility, despite its high melting point (6120°F) and resistance to chemical erosion.

b. The feasibility of using graphite as the thrust chamber material for $\text{OF}_2/\text{B}_2\text{H}_6$ must be evaluated by engine test firings, since the rates of predicted reactions are unknown. Graphite has the advantage of low density (1.5 - 2.2 gm/cc) and a very high sublimation temperature (6600°F). Toughness or effective ductility of graphite is attainable with composite graphitic structures such as Carb-I-tex.

c. Boron nitride will probably have somewhat less reaction with the combustion products of $\text{OF}_2/\text{B}_2\text{H}_6$ than graphite up to a temperature of 4000°R .

d. Boron nitride may have advantageous properties for use in intermediate temperature regions, compatible with its sublimation temperature ($4500 - 5400^\circ\text{F}$) adjacent to the injector, due to its inertness in contact with boron and B_2O_3 wall deposits.

e. Boron carbide (B_4C) is probably similar to graphite in its chemical reactions with the combustion products of $\text{OF}_2/\text{B}_2\text{H}_6$, and is limited to lower temperatures because of its melting point of 4260°F . Brittle behavior of B_4C would also be of concern.

C. Thrust Chamber Concepts

Various types of thrust chamber construction and cooling were evaluated in order to devise thrust chamber concepts to meet the following requirements:

Propellants:	$\text{OF}_2/\text{B}_2\text{H}_6$
Thrust (space):	1000 lbs
Chamber pressure:	100 psia
Mixture ratio:	3.0
C* efficiency:	95 percent
Firing duration:	1000 seconds

1. Graphite - Film Cooled

The feasibility of using graphite thrust chambers must be evaluated by test firings, since the preceding section indicates possible chemical erosion, but does not answer the question of reaction rate. Reaction with the combustion gases could be excessive for wall temperatures as low as 3000°F . It is not possible to keep the wall temperature below 3000°F by film cooling with reasonable amounts of film cooling or propellant stratification. For example, the analysis of Reference 15 shows that 40 percent of the propellant would be required in stratified flow (mixture ratio = 1.0) along the wall of a 1K chamber to reduce the boundary layer temperature at the throat to 5000°R (4540°F). The performance loss expected for even larger amounts of boundary layer cooling required to obtain a 3000°F boundary layer temperature would be unacceptable.

2. Conduction Cooling

Conduction cooling is achieved by conducting heat from the throat through a high thermal conductivity chamber wall to a low wall temperature region near the injector. The low wall temperature is obtained by film cooling from the injector, ordinarily by a liquid fuel. The effectiveness of conduction cooling is limited by the tendency of the liquid fuel to boil off of the wall as the wall temperature exceeds the boiling point of the fuel. The cooling effectiveness of the gaseous film downstream of the liquid film is also low because of mixing with the combustion gas core.

3. Pyrolytic Graphite/Carb-I-tex Composite

A composite graphitic thrust chamber made by depositing pyrolytic graphite on Carb-I-tex has been tested at the 3K thrust level with ClF_5 /Hydrazine blend with excellent results (Reference 17). Chambers of this type will be tested with $\text{OF}_2/\text{B}_2\text{H}_6$ by JPL.

A pyrolytic graphite/Carb-I-tex chamber has characteristics of very light weight, an impervious wall which permits good sealing at the injector attachment, and the lowest chemical erosion rates of any type of graphite material. The thickness of pyrolytic graphite which can be produced in this configuration is limited to a thickness/radius ratio of approximately 0.10. The inside wall temperature at the throat will approximately equal the local boundary layer temperature within 60 seconds and therefore the erosion rates by the products of $\text{OF}_2/\text{B}_2\text{H}_6$ may be excessively high.

4. Edge Oriented Pyrolytic Graphite

A thrust chamber made of stacked washers of pyrolytic graphite would have the greatest durability and lowest erosion of any graphitic material.

The restart capability and low erosion of such a nozzle designed and fabricated by Marquardt was recently demonstrated by the AFRPL (Reference 18) during test firings with ClF_3 /Hydrazine blend. Pyrolytic graphite in the edge oriented configuration has very high thermal conductivity in the radial direction, so that the inside wall temperature of the 1K nozzle would require about 300 seconds to reach steady state temperatures.

The allowable erosion would probably not be limited by the thickness of the pyrolytic graphite, unlike the case of the pyrolytic graphite coating on Carb-I-tex. Nonetheless, the chemical erosion rates might be great enough to degrade performance. The weight of an edge oriented pyrolytic graphite nozzle of the size shown in Figure 61, a contraction ratio of 2.0, and an outside diameter of 8 inches, would be 32 pounds, an acceptable weight for a 1K engine.

5. Regenerative Cooling

The results of the heat transfer analysis (Figure 67) show that the inside wall temperature of a 1K thrust chamber could not be cooled below 4500°F by regenerative cooling with liquid B_2H_6 . Therefore, some composite design would be required which would use high temperature coatings or a high temperature inner wall with the proper thermal conductivity to transfer heat to a regeneratively cooled outer shell. Many problems arise with such concepts, including thermal stresses within the inner wall, heat storage within the wall, and selection of an inner wall material which would be resistant to chemical erosion.

6. Ablatives

Graphite phenolic ablatives would be subject to the same types of chemical attack by the combustion products of $\text{OF}_2/\text{B}_2\text{H}_6$ as graphite. Silica phenolic ablatives would probably also react rapidly with combustion species. Ablatives do not appear attractive for this application.

7. Radiation Cooling

A radiation cooled thrust chamber must have a thin, high conductivity, impervious wall. The chamber material must be resistant to thermal cyclic fatigue.

Tungsten might be considered for a radiation cooled thrust chamber. However, its resistance to thermal cycling and shock loading is questionable.

Wire wound tungsten has been tested with some success as a throat insert (Reference 19).

Its structural integrity as a free standing chamber is not known.

8. Transpiration Cooling

Transpiration cooling with liquid B_2H_6 would be difficult to achieve because of decomposition of the diborane. Furthermore, transpiration cooling with any liquid has the problem of controlling the liquid flow rate. Film cooling of the chamber wall from many closely spaced injection slots would avoid some of the disadvantages of transpiration cooling. However, neither scheme is particularly attractive.

9. Endothermic Cooling

Endothermic cooling of a rocket nozzle has been demonstrated recently at the 3000 pound thrust level by test firings at the AFRPL. The endothermic nozzles were fabricated by Marquardt using pyrolytic graphite washers, although the cooling concept is applicable to many other types of nozzle materials. Test results are presented in Reference 18.

The principal heat transfer mechanisms operative in an endothermically cooled nozzle are shown schematically in Figure 69. A material which will absorb heat by endothermic phase changes is packed into the coolant storage cavities within the pyrolytic graphite washers. The endothermic coolant ideally has gaseous reaction products which pass through exit slots and into the boundary layer, providing a film cooling effect.

The ultimate effect of the endothermic coolant is to keep the inside wall temperature at a lower temperature than it would be without the endothermic cooling. If the nozzle is cooler, chemical erosion of the nozzle by the combustion gas will be retarded or eliminated.

A preliminary analysis was made of the applicability of endothermic cooling to the $1K\ OF_2/B_2H_6$ engine. The results of the analysis were that pyrolytic graphite

washers could be cooled to 3500^oF in the combustion chamber. Maximum throat temperatures using NH₄Cl or Si₃N₄ coolants would be 4200^oF and 4500^oF, respectively. About 21 pounds of Si₃N₄ or 67 pounds of NH₄Cl would be consumed during a 1000 second firing.

The chemical erosion rates of pyrolytic graphite at the temperatures mentioned might be acceptable, although this could not be predicted without test firing data.

The preliminary design results were based on heat loads undiminished by film cooling. Hence, engine performance would not be penalized by the cooling system, unlike the situation encountered with film cooled engines.

10. Pyrolytic Boron Nitride

Boron nitride appears to be less reactive in the combustion products of OF₂/B₂H₆ than graphite to at least 4000^oR. Furthermore, it may be completely nonreactive with selected species such as B₂O₃ and boron which will be present in very large amounts along the chamber walls which are film cooled by B₂H₆. Boron nitride can be made as a pyrolytic deposit by Raytheon Co. with isotropic physical properties and in much greater thicknesses than anisotropic boron nitride or anisotropic pyrolytic graphite. However, it is unlikely that a combustion chamber could be made entirely of BN without excessive amounts of film cooling because of its relatively low sublimation temperature (5400^oF or less). Boron nitride might be valuable in constructing a composite thrust chamber, however. The boron nitride could be used in the chamber section adjacent to the injector which could be film cooled without excessive amounts of cooling. The boron nitride would be inert to deposits of boron or boron oxide in this region.

11. Composite Chamber

The results of the thermochemical and heat transfer analysis lead to the conclusion that a composite chamber design of the type shown in Figure 70 would be applicable to OF₂/B₂H₆. The boron nitride chamber liner would be kept below 4000^oF with B₂H₆ film cooling.

Pyrolytic boron nitride appears to be the best form for this application. The tungsten throat would be kept below 5500^oF by film cooling. The expansion nozzle could be made of a composite graphite, since the chemical erosion rates (proportional to static pressure) would be low in this region.

SECTION IX CONCLUSIONS

1. Fabrication techniques have been demonstrated for several different pyrolytic refractory composite thrust chamber components including:
 - a. PG vapor deposited on Carb-I-tex.
 - b. PG infiltrated carbon felt.
 - c. PG infiltrated high modulus carbon fiber (Thornel).
 - d. Multilamina pyrocarbide alloys.
 - e. Pyrocarbide infiltrated carbon felt.
 - f. Free standing PG filament wound with high modulus carbon fiber (Thornel) and infiltrated.
2. New material concepts which were explored for application to rocket thrust chambers, but require additional development, include:
 - a. Vitreous carbon reinforced with carbon fiber.
 - b. Copper impregnated isotropic graphite as a conduction cooled liner in a PG/Thornel structural shell.
 - c. Silicon nitride infiltrated carbon felt.
 - d. Metal/carbon joints formed by plasma spraying or electroforming nickel on carbon fiber composites.
3. Test firing of PG lined thrust chambers with FLOX/methane demonstrated the structural soundness of these pyrolytic refractory systems.
4. Pyrolytic graphite erosion rates in FLOX/methane were small but finite and sensitive to injector design and fuel film coolant distribution.
5. Thermal stress analytical studies provide an approach to optimizing wall thickness to handle cold, transient heating and steady state stress distribution in free standing composite thrust chambers.
6. Thermochemical analysis of materials for the $\text{OF}_2/\text{B}_2\text{H}_6$ propulsion system have indicated that two materials which may be more suitable for thrust chamber walls than graphite are tungsten and boron nitride. Both of these may be made by chemical vapor deposition and possibly incorporated into composite structures.

SECTION X
REFERENCES

1. Marquardt Report 5907, "Pyrolytic Graphite Rocket Thrust Chamber Development", Contract NAS 7-54, 31 July 1962.
2. Marquardt Report 5992, "Pyrolytic Refractory Thrust Chamber Development", Contract NAS 7-54, 20 May 1963.
3. Marquardt Report 6068, "Refractory Thrust Chambers for Spacecraft Engines", Contract NAS 7-262, 22 March 1965.
4. Marquardt Report 6115, "Pyrolytic Refractory Materials for Spacecraft Thrust Chambers", Contract NAS 7-373, 15 December 1966.
5. Marquardt Report 6142, "Pyrolytic Refractory Materials for Spacecraft Thrust Chambers", Contract NAS 7-555, 4 October 1968.
6. Marquardt Report 6147, "Space Storable Thrustor Investigation", Contract NAS 3-11215, 11 June 1969.
7. Contract No. 952290, California Institute of Technology, Jet Propulsion Laboratory.
8. Marquardt Report 6149, "Test and Evaluation of a Passively Cooled Thrust Chamber for Fluorinated Propellants (U)", Contract FO4611-68-C-0037, 19 December 1969, CONFIDENTIAL.
9. Leeds, D.H., Bauer, D.W., et al, "Orthogonally Isotropic Wool Base Versus Anisotropic Rayon Base Carbon and Graphite Composites", presented at Ninth Biennial Conference on Carbon, Boston, June 1969, Super Temp Co.

References (Continued)

10. Pierson, H.O., et al, "Effects of Deposition Temperature on Properties of Pyrolytic Carbon/Carbon Felt Composites", Sandia Laboratories, SC-DR-68-264, May 1968.
11. Goble, G.G. and Campbell, F.S., "Tension and Compression Test Devices for Filament-Wound Composite Rings", presented at S.E.S.A. Meeting, San Francisco, California, 28 October - 1 November 1968.
12. Lewis, J.C., "A Comparative Study of the Gaseous Oxidation of Vitreous Carbon and Various Graphites at 1500° to 3000°K", Report of the Plessey Co., Ltd., England, and the Beckwith Carbon Corp., Van Nuys, California, 1968.
13. ITRI-B6058-40, "Protective Coatings for Refractory Metals in Rocket Engines", Final Report, Contract No. NAS 7-431.
14. Marquardt Report 6118, "Free Standing Pyrolytic Graphite Thrust Chambers for Space Operation and Attitude Control, Phase II: Small Scale Testing (U)", Contract AF04(611)-10790, AD 382057, 29 May 1967, CONFIDENTIAL.
15. Aerojet-General Corporation Report 659-F, "FLOX-Diborane Technology-Boundary Reaction", NAS 7-659, September 1969.
16. Rogers and Sesonske, Los Alamos Scientific Laboratory Report LAMS-2896, VC-4, Chemistry, TID-4500 (19th Ed.), August 1962.
17. Marquardt Report 6149, "Test and Evaluation of a Passively Cooled Thrust Chamber for Fluorinated Propellants (U)", AFRPL-TR-69-232, December 1969, CONFIDENTIAL.
18. Marquardt Report 6150, "Test and Evaluation of Endothermically Cooled Pyrolytic Graphite Nozzles (U)", AFRPL-TR-69-233, December 1969, CONFIDENTIAL.
19. AFRPL-69-54, "High Chamber Pressure Test Firing of a Wire-Wound Tungsten Throat Insert Nozzle (Test Nozzle No. 5) (U)", March 1969, CONFIDENTIAL.

TABLE I

EXPLANATORY NOTES FOR FIGURE II-1

<u>Contract</u>	<u>Note</u>
NAS7-54	1. Pure boron nitride chambers fired as throat inserts with N_2O_4 /Hydrazine blend. Erosion greater than PG.
NAS7-54	2. Boron doped PG essentially the same erosion rate as PG in N_2O_4 /Hydrazine blend, 0.2 mil/sec.
NAS7-54	3. Pyroid was a 1/2-inch thick wall PG chamber with uncontrollable delaminations. Not considered a practical fabrication approach.
NAS7-54	4. The first 40:1 exit PG chamber made. PG quality and wall thickness control very good.
NAS7-555	5. Test firing with N_2O_4 /Hydrazine blend gave 1/3 PG erosion rate. One chamber fired 305 seconds.
NAS7-555	6. Test fired 300 seconds at 100 psia plus 18 seconds at 200 psi.
AFRPL (Ref. 14)	7. Fourteen chambers fired with N_2O_4 /HYZ, total run time 1022 sec. Fourteen chambers fired with LF_2 /BA1014, total run time 567 sec. Eleven chambers fired with LF_2 /GH ₂ , total run time 305 sec.
NAS7-555	8. Wall thickness 0.25 inches, five laminae, 20 wt % Zr in outer laminae with pure PG inside. Proof pressure failure by crack in inner lamina.
NAS7-555	9. Fired for 60 seconds with erosion at throat of 0.2 mil/sec.
Ref. 14	10. Three laminae, 0.125 wall thickness, fired 137 seconds.
AFRPL(Ref. 14)	11. Wall thickness \approx 0.050-in., failures during vibration tests.
IR&D	12. Filament wound carbitex 713 walls, 1/4-inch thickness, with several internal delaminations.
NAS7-555	13. Carbon felt impregnated with PG, machined to final shape with 0.10 wall, then recoated internally with 0.050 PG. Impregnated carbon felt cracked on cooling.

TABLE I (Continued)

EXPLANATORY NOTES FOR FIGURE II-1

<u>Contract</u>	<u>Note</u>
AF04(611)-10790	14. Four chambers fired total of 2000 seconds.
Ref. 17	15. Fired 300 Sec.
NAS3-11215	16. Maximum run time 322 seconds, throat erosion rate 0.12 mil/sec.
	17. Design goal, 1800 sec. firing at 100 psia.
Ref. 7	18. Scheduled for firing at 100 psia.
FO4(611)-70-C-0007	19. To be fired at 100 psia with ClF_5 /non-deposit fuel.
NAS7-555	20. PG impregnated carbon felt (RPG) machined to fit over free standing PG chamber and bonded pyrolytically.
NAS7-555	21. Thornel-50 (carbon yarn) wound over PG chamber and bonded by PG infiltration. Composite tensile strength over 50,000 psi.
NAS7-555	22. Thornel-50 (carbon yarn) wound over PG chamber and bonded by resin impregnation and pyrolyzed. Lower strength and higher external oxidation than 22 above.

TABLE II

THRUST CHAMBER PROCESS DATA

Run No.	Deposition Temperature (°C)	Pressure (mm Hg)	Gas Flow Rates (lpm)		
			CH ₄	A	Cl ₂
MRS-50	1850	10	2.4	0.5	0.15
MRS-51	1850	10	2.4	--	--
MRS-52*	1850	10	3.0	--	--
MRS-53*	1850	10	3.0	0.5	0.2
MRS-54	1850	10	2.4	0.5	0.15
MRS-55	1850	10	2.4	0.5	0.15
MRS-56	1825	7.5	2.4	0.5	0.15
MRS-57	1825	6.0	2.4	0.5	0.15
MRS-58	1825	6.0	2.4	0.5	0.15
MRS-59♦	1825	6.0	2.4	0.5	0.15
MRS-60♦	1825	6.0	2.4	0.5	0.15
MRS-61†	1825	6.0	2.4	0.5	0.15 to 0.05
MRS-62†	1825	6.0	2.4	0.5	0.15 to 0.05
MRS-63	1825	6.0	2.4	0.5	0.20
MRS-64	1825	6.0	2.4	0.5	0.15
MRS-65	1825	6.0	2.4	0.5	0.15
MRS-66♦	1825	6.0	2.4	0.5	0.15
MRS-67	1825	6.0	2.4	0.5	0.15

*Male Mandrel deposit

†Radially graded composition

♦Hafnium alloy

TABLE III

THRUST CHAMBER PHYSICAL PROPERTY DATA

Run No.	Position (in.)	Mandrel	Composition (wt % Zr)
MRS-50	0	ATJ	27.5
	12	ATJ	29.0
MRS-51	0	ATJ	0
	12	ATJ	0
			} PG
MRS-56	Bottom	ATJ	11.6
	Top	ATJ	14.5
MRS-57	Bottom	ATJ	11.8
	Top	ATJ	14.7
MRS-58	Bottom	ATJ	11.5
	Top	ATJ	14.4
MRS-62	Bottom	ATJ	8.0
	Top	ATJ	10.0
MRS-65	Bottom	ATJ	10.1
	Top	ATJ	10.6
MRS-67	Bottom	ATJ	12.1
	Top	ATJ	15.8

TABLE IV
THICKNESS PROFILES
(Inches)

MRS-50 (Throat Diameter = 0.770 Inches)

DISTANCE FROM INLET (BOTTOM) (Inches)	0°	90°	180°	270°
1	0.402	0.403	0.402	0.399
2	0.367	0.366	0.365	0.367
3	0.372	0.368	0.367	0.373
4	0.371	0.373	0.373	0.375
5	0.367	0.371	0.366	0.366
6	0.353	0.357	0.353	0.351
7	0.325	0.325	0.325	0.325
8 ← Throat	0.272	0.272	0.275	0.270
9	0.238	0.234	0.239	0.238
10	0.185	0.180	0.174	0.195
11	0.133	0.133	0.137	0.131
12 (Top)	0.113	0.114	0.114	0.110

MRS-51 (Throat Diameter = 0.950 Inches)

0 (Bottom)	0.260	0.265	0.260	0.285
1	0.295	0.320	0.300	0.275
2	0.350	0.310	0.350	0.325
3	0.330	0.280	0.345	0.345
4	0.295	0.245	0.300	0.310
5	0.245	0.210	0.245	0.255
6	0.210	0.180	0.210	0.215
7 ← Throat	0.195	0.180	0.200	0.205
8	0.165	0.150	0.170	0.175
9	0.135	0.130	0.150	0.145
10	0.120	0.110	0.130	0.125
11	0.095	0.090	0.100	0.100

	MRS-52	MRS-53	MRS-55
Bottom	~0.035	~0.040	~0.130
Throat	~0.040	~0.045	~0.075
Top	~0.035	~0.040	~0.030

TABLE IV (Continued)

THICKNESS PROFILES
(Inches ± 0.003)

MRS-56

DISTANCE FROM INLET (BOTTOM) (Inches)	0°	90°	180°	270°
0 (Bottom)	0.118	0.118	0.115	0.115
1	0.113	0.113	0.108	0.110
2	0.108	0.106	0.104	0.106
3	0.107	0.106	0.106	0.107
4	0.107	0.105	0.104	0.106
5	0.106	0.105	0.103	0.106
6	0.098	0.098	0.098	0.098
7 ← Throat	0.096	0.097	0.097	0.098
8	0.093	0.096	0.095	0.093
9	0.078	0.086	0.083	0.075
10	0.056	0.065	0.061	0.050
11	0.040	0.042	0.042	0.038

MRS-57

0 (Bottom)	0.176	0.177	0.176	0.177
1	0.168	0.172	0.167	0.172
2	0.148	0.148	0.148	0.147
3	0.147	0.148	0.147	0.146
4	0.149	0.150	0.147	0.149
5	0.152	0.152	0.149	0.150
6	0.149	0.149	0.147	0.146
7 ← Throat	0.144	0.144	0.142	0.141
8	0.140	0.138	0.140	0.141
9	0.125			
10	0.094	0.085	0.111	0.112
11	0.066	0.059	0.072	0.083

TABLE IV (Continued)

THICKNESS PROFILES

MRS-58

DISTANCE FROM INLET (BOTTOM) (Inches)	0°	90°	180°	270°
0 (Bottom)	0.190	0.183	0.178	0.181
1	0.173	0.171	0.165	0.171
2	0.156	0.150	0.150	0.152
3	0.154	0.151	0.150	0.148
4	0.154	0.151	0.151	0.150
5	0.155	0.153	0.151	0.150
6	0.151	0.150	0.149	0.147
7 ← Throat	0.148	0.146	0.143	0.145
8	0.143	0.146	0.143	0.142
9	0.119	0.133	0.140	0.121
10	0.087	0.105	0.116	0.090
11	0.060	0.070	0.068	0.060

MRS-62

0 (Bottom)	0.175	0.176	0.173	0.172
1	0.170	0.168	0.164	0.163
2	0.153	0.154	0.153	0.153
3	0.155	0.158	0.155	0.156
4	0.156	0.159	0.157	0.157
5	0.163	0.162	0.160	0.159
6	0.152	0.153	0.156	0.155
7 ← Throat	0.151	0.152	0.151	0.151
8	0.144	0.147	0.138	0.137
9	0.126	0.130	0.119	0.111

TABLE IV (Continued)

THICKNESS PROFILES
(Inches ± 0.001)

MRS-65

DISTANCE FROM INLET (BOTTOM) (Inches)	0°	180°
0 (Bottom)	0.208	0.208
1	0.175	0.179
2	0.156	0.158
3	0.156	0.158
4	0.155	0.158
5	0.155	0.158
6	0.150	0.150
7	0.144	0.146
8 ← Throat	0.138	0.136
9	0.109	0.108
10	0.067	0.064
Top	0.054	0.050

(Inches ± 0.002)

MRS-67

DISTANCE FROM INLET (BOTTOM) (Inches)	0°	90°	180°	270°
0 (Bottom)	0.171	0.170	0.169	0.169
1	0.150	0.152	0.152	0.152
2	0.147	0.149	0.148	0.146
3	0.148	0.147	0.148	0.148
4	0.148	0.148	0.148	0.148
5	0.145	0.146	0.145	0.145
6	0.139	0.138	0.136	0.139
7	0.137	0.138	0.136	0.137
8 ← Throat	0.134	0.137	0.134	0.136
9	0.130	0.131	0.129	0.132
10	0.101	0.103	0.102	0.105
Top	0.077	0.080	0.078	0.078

TABLE V
PROCESS DATA FOR FELT IMPREGNATION

RUN NO.	DEP. TEMP (°C)	DEP. TIME (hrs)	PRESSURE (mm Hg)	GAS FLOW RATES (lpm)			
				CH ₄	A	Cl ₂	H ₂
MQF-1	1200	- -	20.0	0.6	0.1	0.1	0.2
MQF-2	1100	- -	20.0	0.6	0.1	0.05	0.2
MQF-3	1100	- -	10.0	0.6	0.1	0.05	0.2
MQF-4	1500	20	10.0	1.0	0.5	0.05	- -
MQF-5	1500	40	10.0	2.0	0.5	0.05	- -
MQF-6	1500	28	5.0	2.0	0.5	0.05	- -
MQF-7	1350	40	5.0	3.0	0.5	0.25	1.0
MQF-8	1350	12	5.0	1.0	0.25	0.10	- -
MQF-9	1350	- -	10.0	1.0	0.25	0.25	- -
MQF-10	1350	12	10.0	1.0	0.25	0.25	- -

TABLE VI
AVERAGE PHYSICAL PROPERTIES

RUN NO.	DENSITY (gm/cc)		COMPOSITION (wt % Zr)	POSITION
	BULK	TOLUENE		
MQF-4	0.9	1.52	2.2	Middle
MQF-5	1.07	1.67	4.1	Middle
MQF-6	1.05	1.67	3.3	Middle
MQF-7	1.12	1.80	24.1	Middle
MQF-10	1.22	1.69	27.5	Middle

TABLE VII
LOCAL DENSITY OF RUN NO. MQF-5

RUN NO.	DENSITY (gm/cc)					
	BOTTOM POSITION		MIDDLE POSITION		TOP POSITION	
	BULK	TOLUENE	BULK	TOLUENE	BULK	TOLUENE
MQF-5 Inside Outside	1.13	1.42	1.12	1.67	1.23	1.99
	1.10		1.02		0.86	

TABLE VIII

FLEXURE STRENGTH

(4-point loading - 1 inch upper span, 2 inch lower span)

RUN NO.	TEMPERATURE (°C)	FLEXURE STRENGTH (psi)
MQF-6	20	3610
	20	4440
	20	3670
	20	3700
	20	4290
	20	3670
		<u>3900 Average</u>
MQF-10	20	5900
	20	4690
	20	7030
	20	4740
	20	6045
		<u>5700 Average</u>
	1800	5715
	1800	8205
	1800	7300
	1800	4730
	1800	6485
		<u>6490 Average</u>

TABLE IX

PROCESS DATA - MONOLITHIC DEPOSITS

RUN NO.	DEP. TEMP (°C)	DEP. TIME (hrs)	PRESSURE (mm Hg)	GAS FLOW RATES (lpm)						
				He	CH ₄	A	NH ₃	Cl ₂	BCl ₃	H ₂
MQP-106	1850	4	15.0	- -	4.5	0.5	- -	0.6	- -	4.5
MQP-107	1650	10	1.0	7.0	- -	- -	1.2	- -	0.8	- -
BN-794	1850	17	- -	- -	- -	- -	- -	- -	- -	- -

TABLE X

RESULTS OF NOL RING TENSILE TESTS OF PG/THORNEL-50 COMPOSITES

Spool No.	Description	Position and Thickness			
		A; 0.050 in.	B; 0.10 in.	C; 0.20 in.	D; 0.05 in. over 0.20 in felt
		Tensile Stress (Ksi); Two Specimens			
1	Standard composite	21.8 13.7	25.6 26.4	10.9 10.1	9.0 5.7
2	Chopped carbon fibers added	48.2 33.6	9.2 26.5	15.9 14.9	9.4 9.1
3	Yarn roughened during winding	7.6 22.2	10.8 15.8	8.2 11.1	8.9 5.9
4	Furfural and carbon black added	14.5 24.7	22.8 15.9	19.0 15.9	13.0 8.6

TABLE XI
SUMMARY OF THE TEST PERIOD II INJECTOR EVALUATION FIRINGS

Run No.	Date (1968)	Configuration			Injector S/N	Duration sec	Category*	t _{data} ** sec	O/F	P _c		F _N		η _{Ck}	Remarks
		Chamber	L*	Kistler Used						psia	N/cm ²	lbf	N		
			In.												
1	2 Aug.	Copper	18	45.72	No	4	1	~4	8.02	107	73.8	--	--	97	Facility shutdown and combustion performance. Instrumentation and propellant conditioning discrepancies resolved.
2	2 Aug.	Copper	18	45.72	No	4	1	~4	7.62	100	68.9	--	--	99	
3	6 Aug.	Copper	18	45.72	No	10	1	~4	6.26	102	70.3	59	262.4	98	
4	6 Aug.	Copper	18	45.72	No	10	1	~4	6.13	102	70.3	58	258.0	99	
5	6 Aug.	Copper	18	45.72	No	10	1	~4	4.36	88	60.7	48	213.5	100	
6	6 Aug.	Copper	18	45.72	No	10	1	~4	4.15	84	57.9	46	204.6	98	
7	8 Aug.	Copper	12	30.48	No	5	1	~4	5.40	88	60.7	49	218.0	90	
8	8 Aug.	Copper	12	30.48	No	5	1	~4	5.17	92	63.4	50	222.4	94	
9	8 Aug.	Copper	12	30.48	No	5	1	~4	6.57	102	70.3	56	249.1	93	
10	8 Aug.	Copper	12	30.48	No	5	1	~4	6.06	101	69.6	56	249.1	93	
11	13 Aug.	PG 001	18	45.72	No	Ign.	3	--	--	--	--	--	--	--	Chamber shattered, hard start
12	15 Aug.	PG 001	18	45.72	No	Ign.	3	--	--	--	--	--	--	--	
13	19 Aug.	Copper	18	45.72	Yes	0.5	2	Ignition data only							High response P _c instrumentation installed to monitor effect of ignition sequence and thermodynamic state.
14	20 Aug.	Copper	18	45.72	Yes	0.5	2								
15	20 Aug.	Copper	18	45.72	Yes	0.5	2								
16	20 Aug.	Copper	18	45.72	Yes	0.5	2								
17	20 Aug.	Copper	18	45.72	Yes	0.5	2								
18	20 Aug.	Copper	18	45.72	No	10.0	1, 2	5.3	5.3	80.4	55.4	40	177.9	84	Steady state run to evaluate effect of propellant thermodynamic state.
19	21 Aug.	Copper	18	45.72	Yes	0.5	2	Ignition data only							Ignition sequence and propellant thermodynamic state revised to achieve steady state transition.
20	22 Aug.	Copper	18	45.72	Yes	0.5	2								
21	22 Aug.	Copper	18	45.72	Yes	0.5	2								
22	22 Aug.	Copper	18	45.72	Yes	0.5	2								
23	22 Aug.	Copper	18	45.72	Yes	0.5	2								
24	22 Aug.	Copper	18	45.72	No	6.0	1, 2	5.8	6.1	95	65.5	54	240.2	95	Steady state run to evaluate effect of propellant thermodynamic state.
25	22 Aug.	PG 002	18	45.72	No	20.0	3	6.1	13.1	77.4	53.4	39	173.5	80	Oxidizer valve inadvertently closed during run.
26	26 Aug.	PG 005	18	45.72	No	Ign.	3	--	--	--	--	--	--	--	Chamber shattered at ignition, hard start, ignition marginal.
27	29 Aug.	PG 007	18	45.72	No	-3	3	Data not stabilized							Run cut prematurely, smooth start.
28	29 Aug.	PG 007	18	45.72	No	Ign.	3	--	--	--	--	--	--	--	Chamber failed at ignition, hard start, marginal ignition.

TABLE XI (Continued)
SUMMARY OF THE TEST PERIOD II INJECTOR EVALUATION FIRINGS

Run No.	DATE (1968)	Configuration			Injector S/N	Duration sec	Category*	t _{data} sec	O/F	P _c		F _M		η _C *	Remarks
		Chamber	L*	Kistler Used						psia	M/cm ²	lbf	N		
29	29 Aug.	Copper	18	45.72	No	5	1	5	5.6	87	60	--	--	100	GC ₂ system installed. Revised ignition sequence
30	29 Aug.	Copper	18	45.72	No	0.5	2	Ignition data only							Hard start
31	29 Aug.	Copper	18	45.72	No	0.5	2								Hard start
32	30 Aug.	Copper	18	45.72	Yes	0.76	2								Hard start
33	30 Aug.	Copper	18	45.72	Yes	1.76	2								Soft start
34	30 Aug.	Copper	18	45.72	Yes	1.65	2								Soft start
35	30 Aug.	Copper	18	45.72	Yes	2.3	2	Ignition data only							Soft start
36	30 Aug.	Copper	18	45.72	Yes	5.2	1								Hard start
37	30 Aug.	Copper	18	45.72	No	8.0	1								Hard start, ign. overpressure marginal
38	4 Sept.	Copper	18	45.72	Yes	0.5	2	Ignition data only							GC ₂ system installed. Revised ignition sequence. Soft starts.
39	4 Sept.	Copper	18	45.72	Yes	0.5	2								GC ₂ off prematurely. Steady state. Evaluate effect of propellant thermodynamic state. Good transition from ignition transient to steady state.
40	4 Sept.	Copper	18	45.72	Yes	0.5	2								
41	4 Sept.	Copper	18	45.72	No	4.0	2								
42	4 Sept.	Copper	18	45.72	No	9.7	1, 2								
43	4 Sept.	Copper	18	45.72	No	9.2	1, 2								
44	5 Sept.	PG 003	18	45.72	No	Ign.	3	--	--	--	--	--	--	--	Soft initial start. Hard restart. Fuel system start dynamics
45	5 Sept.	PG 006	18	45.72	No	23	3	2.5 12.4	3.8 5.1	92.4 87.4	63.7 60.3	53 43.5	238.8 193.5	100 99	Revised fuel start sequence--soft start Thermal performance and erosion -- Final data
46	9 Sept.	PG00	10.65	27.05	No	20	3	19.0	6.2	80.4	55.4	39.5	175.7	97.5	Pin hole in side of chamber
47	9 Sept.	PG 004	18	45.72	No	19	3	3.3 13.4 20.6	4.0 3.7 3.6	74.4 76.4 75.4	51.3 52.7 52.0	-- -- --	-- -- --	84 88 84	Thick wall graphite heat sink (PG00), minimum L*
								4.5 8.6 16.0	3.5 3.45 5.22	94.4 102.4 96.4	65.1 70.6 66.5	52 53 49	231.3 235.8 218.0	97 100 100	Thin wall PG chamber, maximum L*

* Category:
1. Combustion performance
2. Ignition compatibility
3. Thermal and erosion characteristics
** t_{data} = Time (sec) from both propellants on to performance point
PG = Pyrolytic graphite

OXIDIZER:
FLOX -- 82.5% LF₂/17.5% LO₂ Mixture (by weight)

FUEL:
Liquified natural gas (weight %)
Methane 87.5
Ethane 11.6
Propane 0.5
Nitrogen 0.4

TABLE XII
SUMMARY OF EROSION OF THREE FREE STANDING PG CHAMBERS AND ONE POCO GRAPHITE CHAMBER

PG Chamber Erosion														
Run No.	Run Time (sec)	Chamber and Injector Face						Mid-Chamber			Throat			
		Initial		Final Wall Thickness		Initial		Final		Initial		Final		
		ID (in.)	Wall Thick. (in.)	Between Film Orifices (in.)	In-Line Film Orifices (in.)	ID (in.)	Wall Thick. (in.)	ID (in.)	Wall Thick. (in.)	ID (in.)	Wall Thick. (in.)	OD (in.)	Wall Thick. (in.)	Internal Erosion Rate (in./sec)
25	21.1	1.396	0.066	0.029 to 0.041	0.050 to 0.053	1.396	0.066	0.042 to Deposit	0.814	0.931	0.057	0.928	0.043 to 0.052	0.00060 to 0.00016
45	19	1.396	0.066	<0.000 to 0.026	0.034 to 0.048	1.396	0.066	0.043 to Deposit	0.826	0.929	0.053	0.926	0.044 to Deposit	0.00040 to 0.0
47	16	1.407	0.062	0.047 to 0.050	0.056 to 0.062	1.407	0.062	0.041 to Deposit	0.827	0.931	0.052	0.925 to 0.928	0.038 to Deposit	0.00074 to 0.0
POCO Chamber**														
46	19.6	Initial ID (in.)	Final ID (in.)	Throat Internal Erosion Rate (in./sec)										
				0.00005 to 0.001										

* No measureable erosion at injector region

TABLE XIII
TEST PERIOD II SUMMARY OF AMBIENT THRUST CHAMBER FIRING TESTS
IN MAGIC MOUNTAIN CELL M-2

28 December 1968 to 11 February 1969, M-2 Test No. 6060

Run No.	Date	Configuration		Duration (sec)	O/F Ratio	P _c (psia)	C* (ft/sec)	η_c (%)	Run Objectives (Note 1)	Remarks
		Chamber	Injector							
1.	28 Dec. 1968	Cu L* = 18 in.	X29401, S/N 001 18 weep holes (12 Hi Angle 6 Lo Angle)	7.52	5.07	98.3	6340	92	(2), (4)	GF ₂ /LCH ₄ ignition
2.	28 Dec.	Cu L* = 18 in.	X29401, S/N 001 18 weep holes (12 Hi Angle 6 Lo Angle)	12.18	4.98	100.4	6460	93	(2), (4)	GF ₂ /LCH ₄ ignition
3.	28 Dec.	Cu L* = 18 in.	X29401, S/N 001 18 weep holes (12 Hi Angle 6 Lo Angle)	10.5	3.55	88.4	6620	98	(2), (4)	FLOX flow decay due to tank near empty
4.	28 Dec.	Cu L* = 18 in.	X29401, S/N 001 18 weep holes (12 Hi Angle 6 Lo Angle)	10.13	2.48	66.4	6450	99	(2), (4)	FLOX flow decay due to tank near empty
5.	31 Dec.	PG, SL-6	X29401, S/N 001 18 weep holes (12 Hi Angle 6 Lo Angle)	--	--	--	--	--	(3)	Chamber shattered at ignition
6.	6 Jan. 1969	Cu L* = 18 in. Kistler P _c	X29401, S/N 001 18 weep holes (12 Hi Angle 6 Lo Angle)	0.5	--	--	--	--	(1)	Ambient purge prior to ignition GF ₂ /LCH ₄ Max. P _c spike = 75 psia
7.	6 Jan.	Cu L* = 18 in. Kistler P _c	X29401, S/N 001 18 weep holes (12 Hi Angle 6 Lo Angle)	0.5	--	--	--	--	(1)	Ambient purge prior to ignition GF ₂ /LCH ₄ Max. P _c spike = 75 psia

TABLE XIII (Continued)
TEST PERIOD II SUMMARY OF AMBIENT THRUST CHAMBER FIRING TESTS
IN MAGIC MOUNTAIN CELL M-2
28 December 1968 to 11 February 1969, M-2 Test No. 6060

Run No.	Date	Configuration		Duration (sec)	O/F Ratio	P _c (psia)	C* (ft/sec)	η_c (%)	Run Objectives (Note 1)	Remarks
		Chamber	Injector							
8.	6 Jan.	Cu L* = 18 in. Kistler P _c	X29401, S/N 001 18 weep holes (12 Hi Angle 6 Lo Angle)	0.5	--	--	--	--	(1)	Max. P _c spike = 100 psia
9.	6 Jan.	Cu L* = 18 in. without Kistler	X29401, S/N 001 18 weep holes (12 Hi Angle 6 Lo Angle)	7.02	4.12	99.4	6100	90	(1), (2)	Data not stabilized
10.	7 Jan.	P0C0 No. 2 L* = 14 in.	X29401, S/N 001 18 weep holes (12 Hi Angle 6 Lo Angle)	31.52	4.5	99.9	6260	91	(2), (3)	Erosion nil
11.	7 Jan.	P0C0 No. 2 L* = 14 in.	X29401, S/N 001 18 weep holes (12 Hi Angle 6 Lo Angle)	65.0	4.27	97.4	6000	88	(2), (3)	Erosion nil
12.	8 Jan.	PG, SL-7 L* = 14 in.	X29401, S/N 001 18 weep holes (12 Hi Angle 6 Lo Angle)	--	--	--	--	--	(1), (3)	Chamber shattered at ignition
13.	8 Jan.	PG, SL-11 L* = 14 in.	X29401, S/N 001 18 weep holes (12 Hi Angle 6 Lo Angle)	22.9	4.18	97.4	6550	95	(3)	GF ₂ /GCH ₄ Ignition procedure Upstream chamber erosion
14.	13 Jan.	PG, SL-1 L* = 14 in.	X24401, S/N 001 12 weep holes (Hi Angle) Long splash ring	20.9	4.56	95.9	6400	93	(3)	Upstream erosion nil Erosion at mid-chamber in line with oxidizer doublets
15.	14 Jan.	PG, SL-9 L* = 14 in.	Same, with short splash ring	15.5	3.9	93.4	6080	90	(3)	Upstream erosion nil Erosion at mid-chamber in line with oxidizer doublets

TABLE XIII (Continued)
TEST PERIOD II SUMMARY OF AMBIENT THRUST CHAMBER FIRING TESTS
IN MAGIC MOUNTAIN CELL M-2

28 December 1968 to 11 February 1969, M-2 Test No. 6060

Run No.	Date	Configuration		Duration (sec)	O/F Ratio	P _c (psia)	C* (ft/sec)	η_c (%)	Run Objectives (Note 1)	Remarks
		Chamber	Injector							
16.	15 Jan.	PG, SL-2 L* = 14 in.	X24401, S/N 002 18 weep holes Short splash ring. Biprop valve modified with blank plate	--	--	--	--	--	--	Hard start caused by defective Teflon seal at biprop blank plate
17.	16 Jan.	MRS-58 Pyrocarbide multilaminar L* = 14 in.	X24401, S/N 001 with 18 weep holes Short splash ring	60	4.27	106.9	6400	94	(3)	One axial streak in line with fuel doublet (Note 2)
18.	23 Jan.	POCO No. 2 L* = 14 in.	X24401, S/N 001 with 18 weep holes Short splash ring	81.1	4.29	100.9	6300	92.5	(3)	Erosion nil
19.	23 Jan.	POCO No. 2 L* = 14 in.	X24401, S/N 001 with 18 weep holes Short splash ring	6.1	--	32.4	--	--	(3)	Restart without engine disassembly after Run 18. Facility FLOX valve did not open.
20.	1 Feb.	Cu L* = 12	X24401, S/N 001 Short splash 18 weep	63.7	4.10	96.4	6100	89.5	(6)	Good run Throat dia. change 0.8232 to 0.8480 in.
21.	1 Feb.	Cu L* = 12	X24401, S/N 001 Short splash 18 weep	67.5	4.43	94.9	6000	87	(6)	Good run Throat dia. change 0.8480 to 0.8880 in.
22.	1 Feb.	PG/Carbitex SL-1	X24401, S/N 001 Short splash 18 weep	36.7	4.42	101.4	6850	99	(3)	Good run Erosion nil

TABLE XIII (Continued)
TEST PERIOD II SUMMARY OF AMBIENT THRUST CHAMBER FIRING TESTS
IN MAGIC MOUNTAIN CELL M-2
28 December 1968 to 11 February 1969, M-2 Test No. 6060

Run No.	Date	Configuration		Duration (sec)	O/F Ratio	P _c (psia)	C* (ft/sec)	η_c (%)	Run Objectives (Note 1)	Remarks
		Chamber	Injector							
23.	4 Feb.	P0C0 No. 2	X24401, S/N 002 Biprop valve blank plate	10.7	--	--	--	--	(2)	P _c tap failure
24.	6 Feb.	Cu Ch L* = 12 ϵ = 12	X24401, S/N 001 Short splash 18 weep	10.2	4.27	101.9	6400	93	(5)	Good run Cell transient ~ 20 sec
25.	7 Feb.	PG/Carbiter SL-3 ϵ = 12	X24401, S/N 001 Short splash 18 weep	59.8	4.22	107.4	6470	94.4	(5)	Good run Min. P _{cell} = 3.12 psia Chamber bell failure at ~ 12 sec
26.	10 Feb.	Same without nozzle expansion	X24401, S/N 001 Short splash 18 weep	47.5	4.18	97.4	6350	92.6	(3)	Good run Throat erosion rate 0.221 mil/sec
27.	10 Feb.	Same without nozzle expansion	X24401, S/N 001 Short splash 18 weep	59.5	4.23	96.4	6500	94.9	(3)	Good run
28.	11 Feb.	Same without nozzle expansion	X24401, S/N 001 Short splash 18 weep	71.3	4.67	98.4	6690	96.5	(3)	Good run Throat erosion rate 0.129 mil/sec
29.	11 Feb.	Same without nozzle expansion	X24401, S/N 001 Short splash 18 weep	68.2	4.50	92.4	6500	94.3	(3)	Good run
30.	11 Feb.	Same without nozzle expansion	X24401, S/N 001 Short splash 18 weep	15.7	--	--	--	--	(3)	Chamber failed at throat

TABLE XIII (Continued)

TEST PERIOD II SUMMARY OF AMBIENT THRUST CHAMBER FIRING TESTS
IN MAGIC MOUNTAIN CELL M-2

28 December 1968 to 11 February 1969, M-2 Test No. 6060

TOTAL ACCUMULATED RUN TIME:

1. Test Phase I	213.4 sec
2. Test Phase II	862.7 sec
3. Total Time on One Injector (Phase II)	852.0 sec
4. Total Time on One Chamber (Phase II) (PG/Carbitex SL-3)	322.0 sec

Notes:

1. Run objectives: (1) = Ignition, (2) = Performance, (3) = Streaking and life, (4) = Facility check, (5) Altitude test, (6) Film conduction cooling investigation
2. Caused by misaligned film jet, which occurred when low angle weeper jets were reopened from 12 weeper configuration.
3. All data points taken at stabilized conditions 6 to 16 seconds from engine ignition
4. Oxidizer: FLOX - 82.5% LF₂/17.5% LO₂ (by weight)
Fuel: Methane (LCH₄)

TABLE XIV

SUMMARY OF AVERAGE THRUST CHAMBER THROAT EROSION DATA,
TEST PERIOD II -- DECEMBER 1968 TO FEBRUARY 1969

Chamber Type	Chamber Number	Run Number	Run Duration sec	Throat Diameter Before Run in. (cm)	Throat Diameter After Run in. (cm)	Erosion Rate mil/sec (cm/sec)
Copper, L* = 12 in. = 30.48 cm	--	20	63.7	0.8232 (2.0909)	0.8428 (2.1407)	0.154 (0.000391)
Copper, L* = 12 in. = 30.48 cm	--	21	67.5	0.8428 (2.1407)	0.8845 (2.2466)	0.309 (0.000785)
POCO Graphite	POCO 2	10, 11, 18	180 ⁽¹⁾	0.8188 (2.0798)	0.8150 (2.0701)	0 (0)
PG Streak	SL 11	13	22.9	0.8258 (2.0975)	0.8278 (2.1026)	0.044 (0.000712)
PG Streak	SL 1	14	20.	0.8345 (2.1196)	0.8440 (2.1428)	0.238 (0.000605)
PG Streak	SL 9	15	15.	0.8277 (2.1024)	0.8365 (2.1247)	0.25 (0.000635)
Multilamina	MRS 58	17	60.	0.7907 (2.0084)	0.8135 (2.0663)	0.19 (0.000482)
PG/Carbitex	Carbitex SL-1	22	40.	0.8553 (2.1724)	0.8572 (2.1773)	0.024 (0.000061)
PG/Carbitex/ RPG Altitude	Carbitex SL-3	25	59.8	0.8042 (2.0427)	0.8333 (2.1166)	0.243 (0.000617)
PG/Carbitex/ RPG Altitude	Carbitex SL-3	26, 27	107. ⁽²⁾	0.8333 (2.1166)	0.8609 (2.1867)	0.129 (0.000328)
PG/Carbitex/ RPG Altitude	Carbitex SL-3	28, 29, 30	155.2 ⁽³⁾	0.8609 (2.1867)	0.906 ⁽⁴⁾ (2.3012)	0.145 ⁽⁴⁾ (0.000368)

NOTES:

- (1) Run 10 (30 sec), Run 11 (60 sec), Run 18 (90 sec)
- (2) Run 26 (47.5 sec), Run 27 (59.5 sec)
- (3) Run 28 (71.3 sec), Run 29 (68.2 sec), Run 30 (15.7 sec)
- (4) Hole burned in vicinity of throat

TABLE XV

EXTENDED RANGE FILM TEMPERATURE DATA, TEST PERIOD II TESTS

Run No.	Max. Temp.		Run Duration sec	Chamber	Remarks
	°F	(°K)			
11	2760	(1789)	65	POCO No. 2	Measurement taken at internal surface of exit
13	2730	(1772)	22.9	PG SL-11	External surface at throat
14	2880	(1855)	20.9	PG SL-1	External surface at throat
17	3150	(2005)	60	Pyrocarbide Multilaminar MRS-58	External surface at throat (See Note 1)
18	2700	(1755)	81.1	POCO No. 2	Same as Run 11

NOTES:

1. Temperature measurement questionable due to fogging of camera window.
2. Tests of the 100-pound FLOX/Methane engine.

TABLE XVI
TEST PERIOD III - 100 LB THRUST FLOX/METHANE ENGINE TEST DATA

RUN NO.	DATE	CONFIGURATION		RUN DURATION SEC	THROAT EROSION RATE MIL/SEC	O/F (NOM)	P _C (NOM) PSIA	C* FT/SEC	C* %	F _n LBS	REMARKS
		CHAMBER	INJECTOR								
1	7/9/69	Poco No. 1 I* = 14 in.	X24401 S/N 001	20.0	N.A.*	4.40	110.4	6651	96.7	64.0	Performance and facility check. Throat carbon deposits.
2	7/9/69	"	"	23.0	0.15	4.30	107.4	6631	96.6	63.0	Repeat Run 1 Oxidizer flow decay
3	7/9/69	"	"	26.1	N.A.	4.39	106.4	6593	95.9	63.0	P _C increase to 164.4 psia from nominal. Heavy throat deposits.
4	7/10/69	Poco No. 2 I* = 10 in.	X24401 S/N 002	10.0	N.A.	- -	- -	- -	- -	- -	Oxidizer leak at injector plate. Data invalid. Throat deposits.
5	7/11/69	PG/TH/resin No. 1	X24401 S/N 001	20.0	0.067	6.72	77.4	6319	94.4	43.0	O/F Survey
6	7/11/69	"	"	10.0	- -	- -	- -	- -	- -	- -	P _C monitor inoperative
7	7/11/69	"	"	20.0	- -	8.66	52.4	4520	73.0	30.5	High O/F due to fuel freezing. Transient data
8	7/11/69	"	"	60.1	- -	4.20	82.4	6804	99.7	52.0	Duration run. P _C steady
9	7/11/69	PG/TH/resin No. 2	X24401 S/N 001	82.0	0.14	4.58	96.4	6765	98.2	52.0	Duration run. P _C increased to 126.4 psia from nominal.
10	7/15/69	Poco No. 2 I* = 10 in.	X24401 S/N 002	5.0	- -	- -	- -	- -	- -	- -	Oxidizer leak at injector plate. Run terminated. Slight throat deposit.
11	7/16/69	PB/Carbitex SL-1	X24401 S/N 001	40.0	0	6.00	100.4	7190	104.0	50.0	O/F variation due to oxidizer two phasing.
12	7/16/69	"	"	105.0	0.15	5.20	85.4	6681	96.0	50.5	Duration run. P _C increased to 131 psia then dropped back to nominal.
13	7/16/69	Poco No. 2 I* = 10 in.	X24401 S/N 001	30.0	0.28	5.62	83.4	5739	83.1	50.0	O/F - Deposition survey

* Not Available

TABLE XVI (Continued)
TEST PERIOD III - 100 LB THRUST FLOX/METHANE ENGINE TEST DATA

RUN NO.	DATE	CONFIGURATION		RUN DURATION SEC	THROAT EROSION RATE MIL/SEC	O/F (NOM)	P _c (NOM) PSIA	C* FT/SEC	C* %	F _n LBS	REMARKS
		CHAMBER	INJECTOR								
14	7/16/69	Poco No. 2 I* = 10 in.	X24401 S/N 001	30.0	0.12	5.69	80.4	5627	81.7	51.5	Repeat Run 13
15	7/16/69	"	"	60.0	0.32	4.98	66.4	5949	86.1	43.0	O/F, F _n survey
16	7/18/69	Carbiter SL-2	X24401 S/N 002	7.0	1.14	- -	- -	- -	- -	- -	Oxidizer leak at injector plate. Run terminated
17	7/23/69	"	"	20.0	0.04	5.67	52.4	4631	67.6	32.5	Injector fuel/oxidizer momentum angle change performance check
18	7/23/69	"	"	15.0	0	- -	- -	- -	- -	- -	Run aborted due to photographic difficulty
19	7/23/69	"	"	61.0	0.41	5.62	52.4	5006	73.0	37.5	Minor throat deposits.
20	7/23/69	Poco No. 3 I* = 14 in.	X24401 S/N 002	20.0	0	4.54	72.4	4483	65.4	40.0	Injector performance check. Deep erosion streak in throat.
21	7/23/69	"	X24401 S/N 001	60.0	0.22	6.2	101.2	6873	100.0	56.0	O/F deposition
22	7/24/69	3-piece chamber	X24401 S/N 001	10.0	0.19	10.15	67.4	4757	80.0	26.0	Propellant flows not stabilized. Two phasing.
23	7/24/69	"	"	15.0	0.26	7.57	81.4	5668	87.0	38.0	Same
24	7/24/69	"	"	35.0	0.14	6.22	93.4	6584	96.6	44.5	Materials test
25	7/25/69	FG/TH/FG No. 1	X24401 S/N 002	20.0	0.06	6.0	87.4	6004	87.6	49.0	Injector fuel/oxidizer momentum angle change performance check
26	7/25/69	"	"	45.0	0.18	5.97	89.4	6101	88.9	52.0	Same
27	7/25/69	Tantalum-Tungsten/ HFC coating	X24401	10.0	5.0	7.79	63.4	5019	78.0	29.5	Coating removed at throat but intact in chamber.

TABLE XVII

SUMMARY OF STRESSES IN ZrC/PG COMPOSITE THRUST CHAMBERS

Zr-C Distribution	Temperature Distribution	ID (in.)	t (in.)	Circumferential Stress (psi)	
				Inside	Outside
0% inside 30% outside linear	Transient at 300 seconds into run 5280°F - in 2350°F - out	1.4	0.24	-10,000	28,500
30% inside 0% outside linear	Transient at 300 seconds into run 5280°F - in 2350°F - out	1.4	0.24	-80,500	39,200
30% constant	Transient at 300 seconds into run 5280°F - in 2350°F - out	1.4	0.24	-71,200	59,300
0% constant (Pure PG)	Transient at 300 seconds into run 5280°F - in 2350°F - out	1.4	0.24	-27,300	22,200
0% inside 12% middle 0% outside	Transient at 300 seconds into run 5280°F - in 2350°F - out	1.4	0.24	-20,800	26,700
0% inside 30% outside linear	4500°F - in 2250°F - out linear	1.4	0.24	-15,800	22,900
0% inside 30% outside linear	4500°F - in 2800°F - out linear	1.4	0.12	- 2,700	8,300
0% inside 30% outside linear	4000°F - in 2500°F - out linear	2.8	0.24	- 3,500	8,400

TABLE XVIII

HEAT TRANSFER AT THROAT FOR $OF_2/B_2/H_2$

$P_c = 100$ PSIA $D_t = 2.6$ INCH

	HEAT TRANSFER COEFFICIENT BTU/IN ² SEC °F	HEAT FLUX TO 1000°F WALL BTU/IN ² /SEC	BOUNDARY TEMPERATURE °F
RMD REPORT 6039-F, 1966 TEST DATA: $P_c = 150$ PSIA $D_t = 3.32$ INCH $L^* = 30$ $O/F = 2.6$ TO 3.2 $CR = 2.75$ $C^*_{eff} = 89\%$ TO 96% MARQUARDT ANALYSIS (BARTZ EQ.) $D_t = 2.6$ INCH $O/F = 3.0$	0.90×10^{-3}	NOT REPORTED	NOT REPORTED
AEROJET REPORT 659-F, 1969 TEST DATA: $P_c = 110$ PSIA $D_t = 2.67$	1.0×10^{-3}	5.0	6000
TEST 007 - BARRIER COOLING - 1.5:1 O/F (BARRIER) = 1.4 T_c (BARRIER) = 4600°F (THEOR.) O/F (ENGINE) = 4.73 $I_{sp} = 87\%$	1.6×10^{-3}	6 TO 9	5600-6400
TEST 015 - BARRIER COOLING - 1.5:1 O/F (BARRIER) = 0.68 T_c (BARRIER) = 3300°F (THEOR.) $I_{sp} = 87\%$	2.2×10^{-3}	5.3	3400
TEST 006 - FILM COOLING - 8:1 ROCKETDYNE - AIAA PAPER 69-505 NO FILM COOLING	2.48×10^{-3}	6.2	3400-3600
TEST DATA: $P_c = 100$ PSIA $D_t = 4.2$ INCH $O/F = 3.5$ $I_{sp} = 93\%$	4.7×10^{-3}	5.7	UNSATISFACTORY (1766)
	0.7 TO 1.4×10^{-3}	5.4	6200
	NOT REPORTED	6.4	NOT REPORTED (≈ 6000)

TABLE XIX
COMBUSTION PRODUCTS OF $\text{OF}_2/\text{B}_2\text{H}_6$
 $\text{O/F} = 3.0$
 $P_c = 100$ PSIA

SPECIES	MOLE FRACTIONS									
	7000°R	6000°R	5000°R	4000°R	3000°R	2000°R	1000°R			
B	0.00058	0.00010	0.00001	0.00000	0.0	0.0	0.0	0.0		
BF	0.06708	0.06171	0.03243	0.00301	0.00000	0.0	0.0	0.0		
BF2	0.00764	0.01023	0.00873	0.00161	0.00002	0.0	0.0	0.0		
BF3	0.00216	0.00918	0.03873	0.07778	0.16267	0.19666	0.22549	0.0		
BH	0.00004	0.00002	0.00000	0.00000	0.0	0.0	0.0	0.0		
BHF2	0.00061	0.00267	0.00983	0.01464	0.00624	0.00015	0.0	0.0		
BH2	0.00008	0.00013	0.00012	0.00002	0.00000	0.0	0.0	0.0		
BH303	0.00000	0.00000	0.00000	0.00000	0.00001	0.00005	0.00010	0.0		
BO	0.06440	0.02757	0.00626	0.00055	0.00000	0.0	0.0	0.0		
BOF	0.16129	0.23008	0.27560	0.28941	0.05696	0.00008	0.0	0.0		
BOF2	0.00004	0.00003	0.00001	0.00000	0.00000	0.0	0.0	0.0		
BO2	0.00069	0.00016	0.00002	0.00000	0.0	0.0	0.0	0.0		
B2O	0.00003	0.00002	0.00001	0.00000	0.0	0.0	0.0	0.0		
B2O2	0.00047	0.00076	0.00087	0.00074	0.00000	0.0	0.0	0.0		
B2O3(L)	0.0	0.0	0.0	0.0	0.05941	0.08328	0.0	0.0		
B2O3(S)	0.0	0.0	0.0	0.0	0.0	0.0	0.10845	0.0		
B2O3	0.00016	0.00024	0.00030	0.00096	0.00007	0.0	0.0	0.0		
B3O3F3	0.0	0.00000	0.00000	0.00025	0.03290	0.03015	0.00007	0.0		
F	0.00506	0.00052	0.00002	0.00000	0.0	0.0	0.0	0.0		
H	0.23706	0.09199	0.01995	0.00179	0.00003	0.00000	0.0	0.0		
HBO	0.00048	0.00038	0.00017	0.00004	0.00000	0.0	0.0	0.0		
HBO2	0.00098	0.00126	0.00133	0.00338	0.00240	0.00001	0.0	0.0		
HF	0.21602	0.18553	0.11600	0.04761	0.02939	0.01732	0.00395	0.0		
H2	0.22985	0.37496	0.48831	0.55675	0.64603	0.66407	0.64756	0.0		
H2O	0.00273	0.00220	0.00130	0.00144	0.00386	0.00820	0.01438	0.0		
H3B3O6	0.0	0.0	0.0	0.0	0.00000	0.00005	0.00001	0.0		
O	0.00095	0.00003	0.00000	0.0	0.0	0.0	0.0	0.0		
OH	0.00161	0.00023	0.00001	0.00000	0.00000	0.0	0.0	0.0		

ADDITIONAL PRODUCTS WHICH WERE CONSIDERED BUT WHOSE MOLE FRACTIONS WERE LESS THAN 0.000005:

B(L) B(S) B(L) B2 F02 H02
BH3 O2 BH3 F0 F2 H02

O/F = 3.0
P_c = 100 PSIA
Weight Ratio = 20:1
TABLE XX
GRAPHITE EQUILIBRIUM WITH OF₂/B₂H₆

SPECIES	MOLE FRACTIONS									
	7000°R	6000°R	5000°R	4000°R	3000°R	2000°R	1000°R			
B	0.00012	0.00002	0.00000	0.00000	0.0	0.0	0.0			0.0
BF	0.00959	0.00890	0.00315	0.00087	0.00000	0.0	0.0			0.0
BF ₂	0.00077	0.00090	0.00069	0.00017	0.00000	0.0	0.0			0.0
BF ₃	0.00015	0.00049	0.00245	0.00308	0.00361	0.00465	0.00548			
BH	0.00001	0.00000	0.00000	0.00000	0.0	0.0	0.0			0.0
BH ₂ F	0.00004	0.00020	0.00071	0.00150	0.00092	0.00000	0.0			0.0
BH ₂	0.00001	0.00002	0.00001	0.00001	0.00000	0.0	0.0			0.0
BO	0.00000	0.00001	0.00001	0.00001	0.00000	0.0	0.0			0.0
BOF	0.00001	0.00004	0.00022	0.00233	0.00134	0.00000	0.0			0.0
B ₂ O ₂	0.0	0.00000	0.00000	0.00001	0.00000	0.0	0.0			0.0
B ₂ O ₃ (L)	0.0	0.0	0.0	0.0	0.00126	0.00192	0.0			0.0
B ₂ O ₃ (S)	0.0	0.0	0.0	0.0	0.0	0.0	0.00264			0.00000
B ₃ O ₃ F ₃	0.0	0.0	0.0	0.00000	0.00073	0.00071	0.00000			0.00000
C(S)	0.95405	0.96179	0.96678	0.97019	0.97592	0.97815	0.98347			
C	0.00024	0.00001	0.00000	0.0	0.0	0.0	0.0			0.0
CB ₄ (L)	0.0	0.0	0.00084	0.0	0.0	0.0	0.0			0.0
CR ₄ (S)	0.0	0.0	0.0	0.00065	0.0	0.0	0.0			0.0
CF	0.00010	0.00000	0.00000	0.0	0.0	0.0	0.0			0.0
CH	0.00003	0.00000	0.00000	0.0	0.0	0.0	0.0			0.0
CH ₃	0.00000	0.00001	0.00000	0.00000	0.00000	0.00000	0.0			0.0
CH ₄	0.00000	0.00000	0.00000	0.00001	0.00008	0.00172	0.00777			0.00000
CO	0.00820	0.00808	0.00792	0.00577	0.00079	0.00020	0.00000			0.0
C ₂	0.00034	0.00000	0.00000	0.0	0.0	0.0	0.0			0.0
C ₂ H	0.00682	0.00089	0.00003	0.00000	0.0	0.0	0.0			0.0
C ₂ HF	0.00001	0.00000	0.00000	0.0	0.0	0.0	0.0			0.0
C ₂ H ₂	0.00240	0.00179	0.00048	0.00005	0.00000	0.00000	0.0			0.0
C ₃	0.00101	0.00002	0.00000	0.0	0.0	0.0	0.0			0.0
F	0.00016	0.00001	0.00000	0.00000	0.0	0.0	0.0			0.0
H	0.00704	0.00297	0.00059	0.00005	0.00000	0.00000	0.0			0.0
HBO ₂	0.0	0.00000	0.00000	0.00000	0.00001	0.00000	0.0			0.0
HF	0.00449	0.00364	0.00278	0.00049	0.00010	0.00024	0.00009			0.00000
H ₂	0.00441	0.01020	0.01334	0.01479	0.01522	0.01233	0.00020			0.00000
H ₂ O	0.00000	0.00000	0.00000	0.00000	0.00000	0.00007	0.00034			0.00000
ADDITIONAL PRODUCTS WHICH WERE CONSIDERED BUT WHOSE MOLE FRACTIONS WERE LESS THAN 0.000005:										
	B(S)	B(L)	BH ₃	RH ₃ O ₃	BOF ₂	B ₂ O ₂	B ₂ O ₃	C ₂ F ₂	C ₂ F ₄	R ₂ O
	CF ₂	CF ₃	CF ₄	CH ₂	COF	COF ₂	CO ₂	HCO	H ₂ O	
	C ₂ O	C ₃ O ₂	FO	F ₂ O	F ₂	HBO	HCO	H ₂ O		
	H ₃ B ₃ O ₆	O	OH	O ₂						

TABLE XXI
B₄C EQUILIBRIUM WITH OF₂/B₂H₆
O/F = 3.0
P_c = 100 PSIA
Weight Ratio = 20:1

SPECIES	MOLE FRACTIONS									
	7000°R	6000°R	5000°R	4000°R	3000°R	2000°R	1000°R			
B(S)	0.0	0.0	0.0	0.03431	0.0	0.0	0.08707			
B	0.00796	0.00052	0.00001	0.00000	0.0	0.0	0.0			
BF	0.05774	0.04617	0.01952	0.00403	0.00003	0.00000	0.0			
BF2	0.00041	0.00108	0.00179	0.00061	0.00002	0.00000	0.0			
BF3	0.00001	0.00014	0.00269	0.00844	0.01450	0.01803	0.02180			
BH	0.00053	0.00008	0.00000	0.00000	0.0	0.0	0.0			
BHF2	0.00003	0.00028	0.00199	0.00547	0.00548	0.00342	0.00028			
BH2	0.00097	0.00066	0.00020	0.00009	0.00000	0.00000	0.0			
BH3	0.00000	0.00001	0.00000	0.00001	0.00000	0.00000	0.0			
BO	0.01651	0.01052	0.00181	0.00015	0.00000	0.0	0.0			
BOF	0.00258	0.01240	0.02713	0.02301	0.00547	0.00001	0.0			
B2	0.00002	0.00000	0.00000	0.0	0.0	0.0	0.0			
B2O	0.00054	0.00030	0.00003	0.00000	0.00000	0.0	0.0			
B2O2	0.00017	0.00072	0.00057	0.00051	0.00002	0.0	0.0			
B2O3(L)	0.0	0.0	0.0	0.0	0.00655	0.00877	0.0			
B2O3(S)	0.0	0.0	0.0	0.0	0.0	0.0	0.01099			
B2O3	0.00000	0.00002	0.00003	0.00004	0.00001	0.0	0.0			
B3O3F3	0.0	0.0	0.00000	0.00001	0.00293	0.00276	0.00001			
C	0.00001	0.00000	0.0	0.0	0.0	0.0	0.0			
CB4(L)	0.81782	0.84716	0.87282	0.0	0.0	0.0	0.0			
CB4(S)	0.0	0.0	0.0	0.85223	0.89973	0.90169	0.83765			
CH4	0.00000	0.00000	0.00000	0.00001	0.00012	0.00056	0.02205			
CO	0.01171	0.00785	0.00319	0.00856	0.00051	0.00000	0.0			
C2H2	0.00000	0.00000	0.00000	0.00001	0.00000	0.0	0.0			
F	0.00006	0.00001	0.00000	0.00000	0.0	0.0	0.0			
H	0.04159	0.01368	0.00251	0.00020	0.00000	0.00000	0.0			
HBO	0.00012	0.00014	0.00005	0.00001	0.00000	0.0	0.0			
HBO2	0.00000	0.00003	0.00006	0.00005	0.00003	0.00000	0.0			
HF	0.00237	0.00390	0.00495	0.00151	0.00030	0.00001	0.0			
H2	0.03883	0.05430	0.06061	0.06073	0.06430	0.06476	0.02016			
H2O	0.00001	0.00002	0.00003	0.00001	0.00000	0.00000	0.0			
OH	0.00001	0.00000	0.00000	0.00000	0.0	0.0	0.0			
ADDITIONAL PRODUCTS WHICH WERE CONSIDERED BUT WHOSE MOLE FRACTIONS WERE LESS THAN 0.000005:										
	B(L)	B(L)	BH3O3	BHF2	B2	C(S)	CB	CF	CF2	
	CH	CH	CH2	CH3	COF	COF2	CO2	C2	C2F2	
	C2HF	C2HF	C2H4	C2O	C3	C3O2	FO	F02	F2	
	H2O(S)	H2O(S)	H2O(L)	H3B3O6	O	O2				

O/F = 3.0
P_c = 100 PSIA
Weight Ratio = 20:1

TABLE XXII

BORON NITRIDE EQUILIBRIUM WITH OF₂/B₂H₆

SPECIES	MOLE FRACTIONS									
	7000°R	6000°R	5000°R	4000°R	3000°R	2000°R	1000°R			
B(L)	0.55277	0.61682	0.00085	0.0	0.0	0.0	0.0	0.0	0.0	
B	0.05478	0.0336	0.00001	0.00000	0.0	0.0	0.0	0.0	0.0	
BF	0.02180	0.02099	0.01497	0.00061	0.00000	0.0	0.0	0.0	0.0	
BF ₂	0.00001	0.00003	0.00064	0.00016	0.00000	0.0	0.0	0.0	0.0	
BF ₃	0.00000	0.00000	0.00045	0.00395	0.00783	0.00937	0.01093	0.0	0.0	
BH	0.00098	0.00018	0.00001	0.00000	0.0	0.0	0.0	0.0	0.0	
BHF ₂	0.00000	0.00000	0.00067	0.00148	0.00048	0.00001	0.0	0.0	0.0	
BH ₂	0.00048	0.00047	0.00029	0.00001	0.00000	0.0	0.0	0.0	0.0	
BH ₃	0.00000	0.00000	0.00001	0.00000	0.00000	0.0	0.0	0.0	0.0	
BN(S)	0.0	0.0	0.92817	0.94556	0.95203	0.95275	0.95175	0.0	0.0	
BN	0.00897	0.00092	0.00000	0.00000	0.0	0.0	0.0	0.0	0.0	
B ₂	0.00994	0.00913	0.00175	0.00006	0.00000	0.0	0.0	0.0	0.0	
B ₂ O	0.00009	0.00076	0.01227	0.01553	0.00273	0.00000	0.0	0.0	0.0	
B ₂ O ₂	0.00039	0.00001	0.00000	0.0	0.0	0.0	0.0	0.0	0.0	
B ₂ O ₃ (L)	0.00090	0.00066	0.00009	0.00000	0.0	0.0	0.0	0.0	0.0	
B ₂ O ₃ (S)	0.00002	0.00022	0.00095	0.00016	0.00000	0.0	0.0	0.0	0.0	
B ₂ O ₃	0.0	0.0	0.0	0.0	0.00290	0.00400	0.0	0.0	0.0	
B ₃ O ₃ F ₃	0.0	0.0	0.00003	0.00005	0.00000	0.0	0.0	0.0	0.0	
F	0.00001	0.00000	0.00000	0.00001	0.00158	0.00144	0.00000	0.0	0.0	
H	0.02728	0.01143	0.00131	0.00010	0.00000	0.0	0.0	0.0	0.0	
H ₂ O	0.00002	0.00004	0.00004	0.00000	0.00000	0.0	0.0	0.0	0.0	
H ₂	0.00000	0.00000	0.00003	0.00010	0.00007	0.00000	0.0	0.0	0.0	
HF	0.00009	0.00023	0.00121	0.00130	0.00088	0.00041	0.00002	0.0	0.0	
H ₂	0.00680	0.01512	0.02972	0.03033	0.03125	0.03175	0.03135	0.0	0.0	
H ₂ O	0.00000	0.00000	0.00001	0.00002	0.00007	0.00010	0.00001	0.0	0.0	
N	0.00016	0.00001	0.00000	0.0	0.0	0.0	0.0	0.0	0.0	
NH	0.00001	0.00000	0.00000	0.0	0.0	0.0	0.0	0.0	0.0	
NH ₃	0.00000	0.00000	0.00000	0.00000	0.00000	0.00000	0.00045	0.0	0.0	
N ₂	0.31450	0.31960	0.00651	0.00056	0.00016	0.00016	0.00003	0.0	0.0	

ADDITIONAL PRODUCTS WHICH WERE CONSIDERED BUT WHOSE MOLE FRACTIONS WERE LESS THAN 0.000005:

B(S)	BH ₃ O ₃	BOF ₂	BO ₂	FO	FO ₂	F ₂	HO ₂
H ₃ B ₃ O ₃	NF	NF ₂	NF ₃	NH ₂	NO	NOF	NO ₂
N ₂ O	N ₂ O ₄	O	OH	O ₂			

TABLE XXIII

TUNGSTEN EQUILIBRIUM WITH $\text{OF}_2/\text{B}_2\text{H}_6$

$\text{O/F} = 3.0$ $P_c = 100$ PSIA $T = 6500^\circ\text{R}$ Weight Ratio = 20:1

SPECIES	MOLE FRACTION
H2	0.303943
BlF101	0.196605
BlF1	0.672809E-01
F1H1	0.206151
W	0.493160E-05
H2O1	0.261625E-02
BlF3	0.427957E-02
BlF2	0.903003E-02
BlH1	0.287915E-04
BlH101	0.456680E-03
BlH102	0.117679E-02
BlH2	0.108439E-03
BlH202	0.130790E-06
BlH3	0.719595E-06
BlH303	0.172300E-08
Bl02	0.349316E-03
B201	0.274693E-04
B0	0.457590E-01
B2	0.884583E-08
B2H6	0.282430E-15
B202	0.635878E-03
B203	0.208589E-03
B3F303	0.180200E-08
B3H306	0.642487E-15
B5H9	0.242782E-32

SPECIES	MOLE FRACTION
BlOH14	0.0
F1H101	0.341074E-08
F101	0.825796E-09
F2	0.103262E-08
F1	0.177728E-02
F201	0.420241E-14
H1	0.158610
H102	0.131397E-08
H101	0.700285E-03
H202	0.187245E-09
O1	0.206367E-03
O2	0.701233E-06
O3	0.397906E-14
WF	0.907279E-05
WF6	0.818037E-15
W0	0.284071E-04
W02	0.453357E-05
W03	0.309831E-07
W206	0.884190E-12
W308	0.602580E-17
W309	0.215580E-19
W4012	0.477467E-27
B203*	0.238419E-06
W*	0.491960
W02*	-0.108033E-06

* Solid

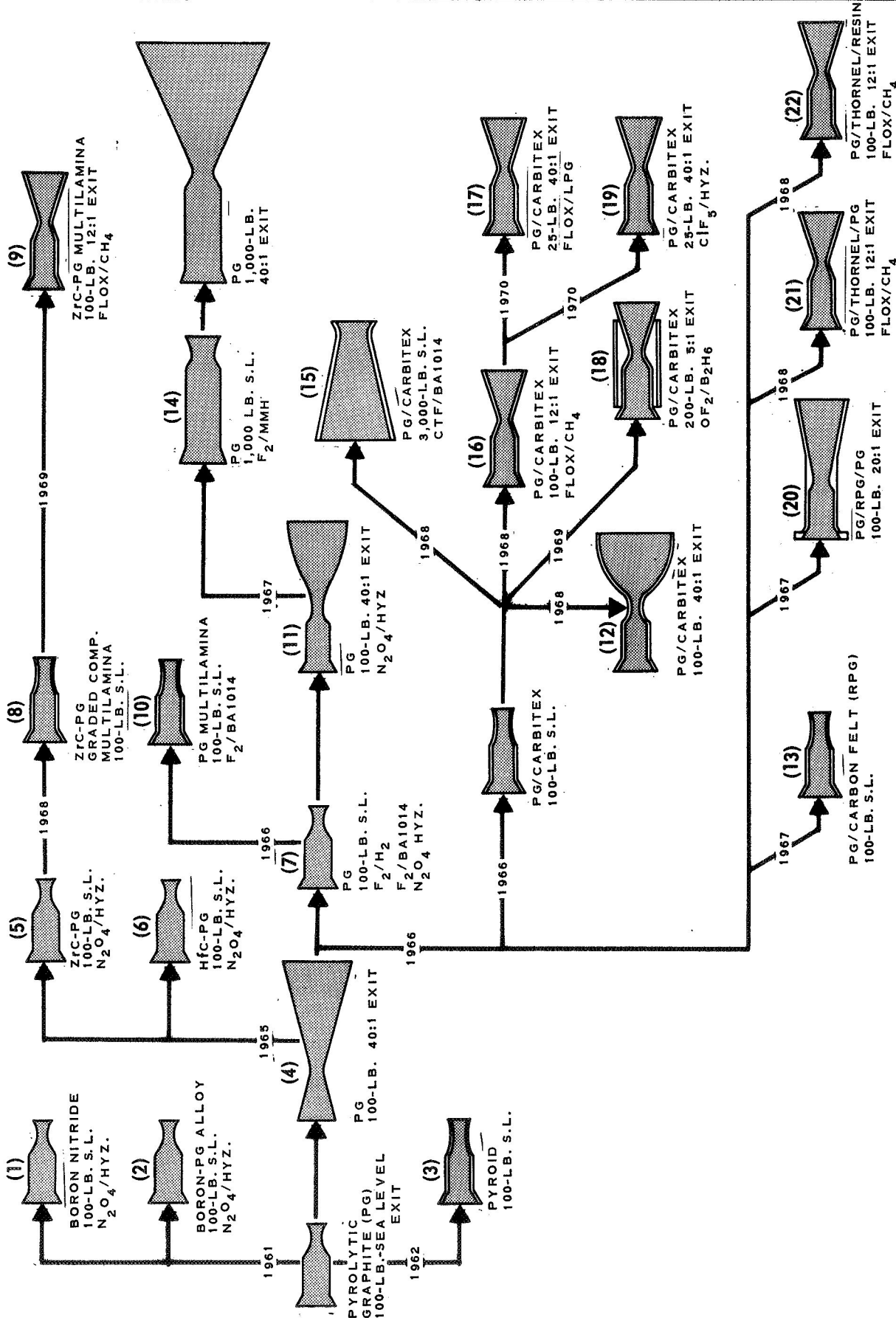
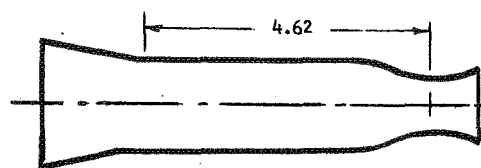
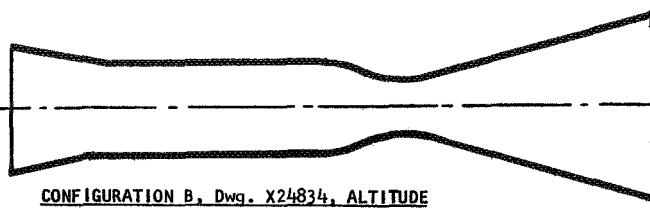


FIGURE 1. Free Standing Pyrolytic Chamber History at the Marquardt Company Under NASA and AFRL Contracts.



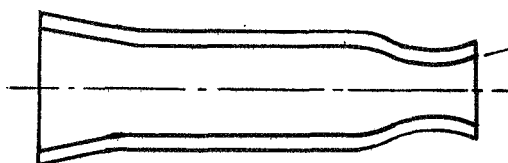
CONFIGURATION A, Dwg. X24396, SEA LEVEL

Throat ID	0.823 in.
Chamber ID	1.420 in.
Wall Thickness	0.050 in.
Exit Expansion	1.66:1



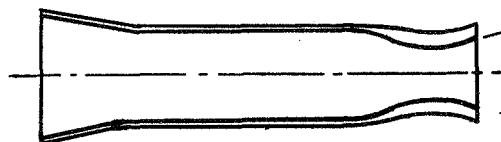
CONFIGURATION B, Dwg. X24834, ALTITUDE

Throat ID	0.823 in.
Chamber ID	1.420 in.
Wall Thickness	0.050 in.
Exit Expansion	12:1



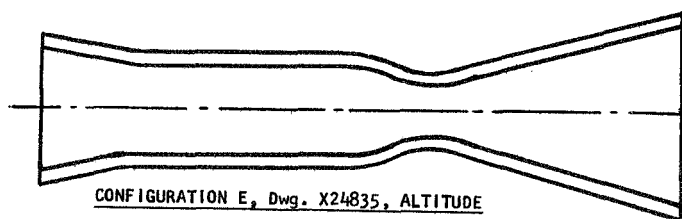
CONFIGURATION C, Dwg. X24397, SEA LEVEL

Throat ID	0.823 in.
Chamber ID	1.420 in.
Wall Thickness	0.250 in.
Exit Expansion	1.66:1



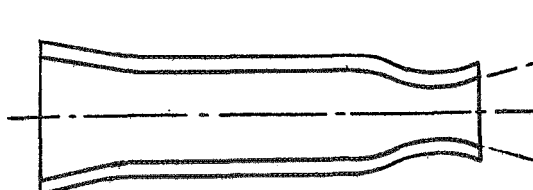
CONFIGURATION D, Dwg. X24836, SEA LEVEL

Throat ID	0.823 in.
Chamber ID	1.420 in.
Wall Thickness	0.125 in.
Throat	0.250 in.
Exit Expansion	1.66:1



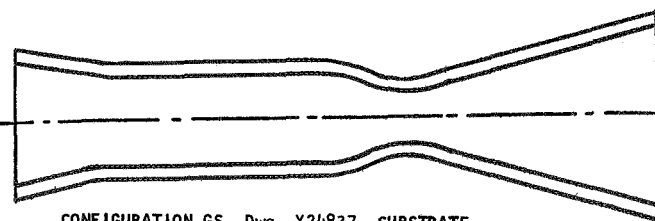
CONFIGURATION E, Dwg. X24835, ALTITUDE

Throat ID	0.823 in.
Chamber ID	1.420 in.
Wall Thickness	0.250 in.
Exit Expansion	12:1



CONFIGURATION FS, Dwg. X24487, SUBSTRATE

Throat ID	0.90 in.
Chamber ID	1.50 in.
Wall Thickness	0.250 in.
Exit Expansion	3.1:1



CONFIGURATION GS, Dwg. X24837, SUBSTRATE

Throat ID	0.90 in.
Chamber ID	1.50 in.
Wall Thickness	0.250 in.
Exit Expansion	13:1

FIGURE 2. Layouts of Structural Thrust Chambers for Pyrobond Fabrication Studies



FIGURE 3. Raytheon Multilamina Chambers

NEG. 9424-1

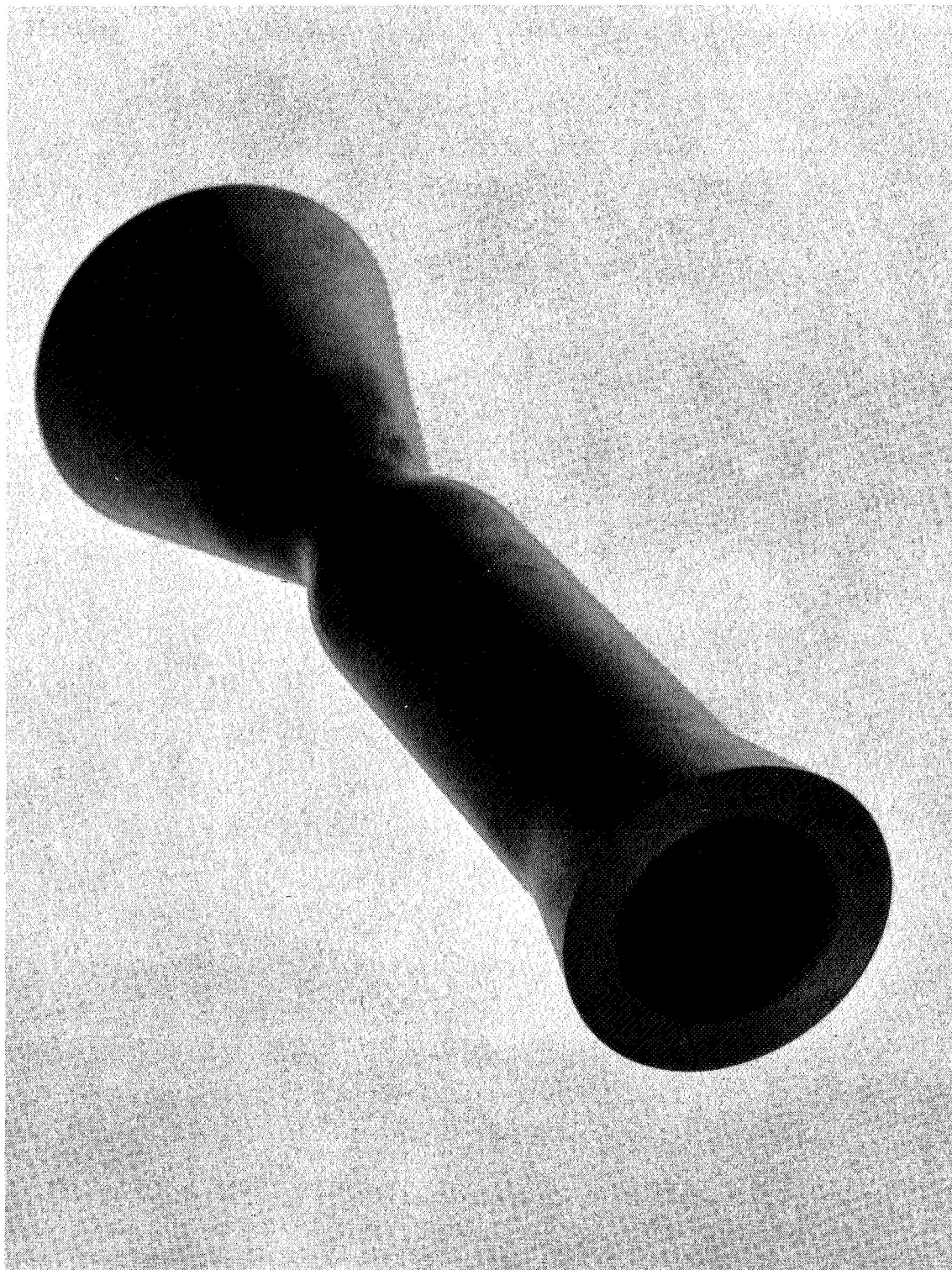


FIGURE 4. Chamber MRS-50

NEG. 9311-2

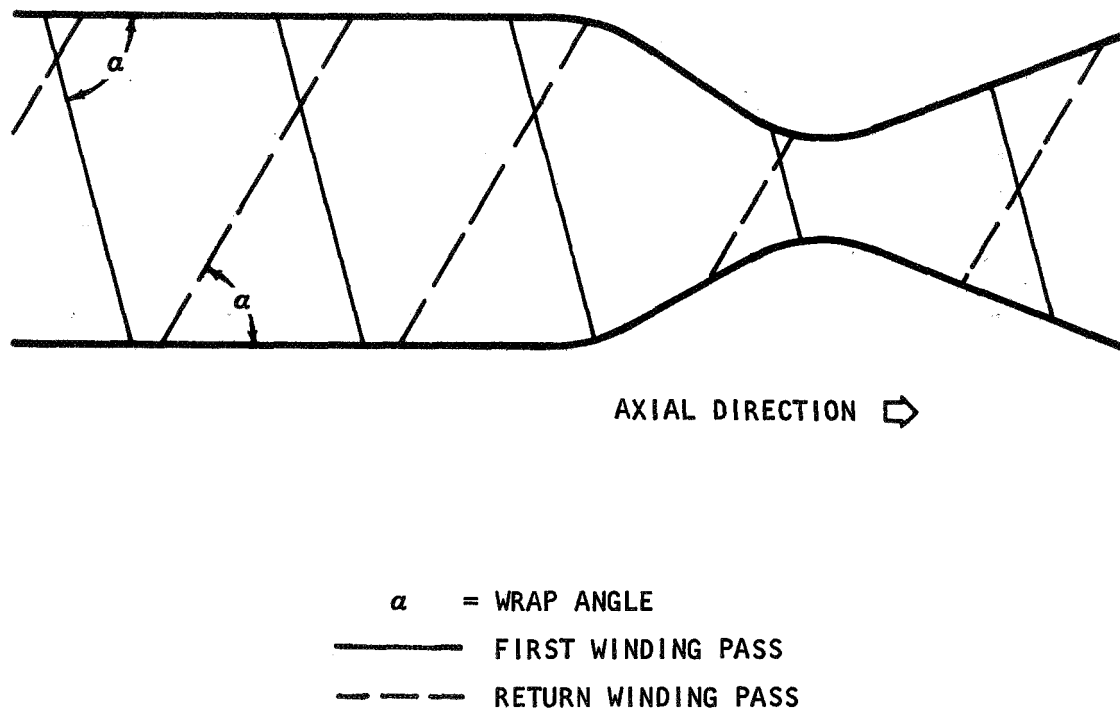


FIGURE 5. Schematic Diagram of Filament Orientation in a Carbitex Thrust Chamber

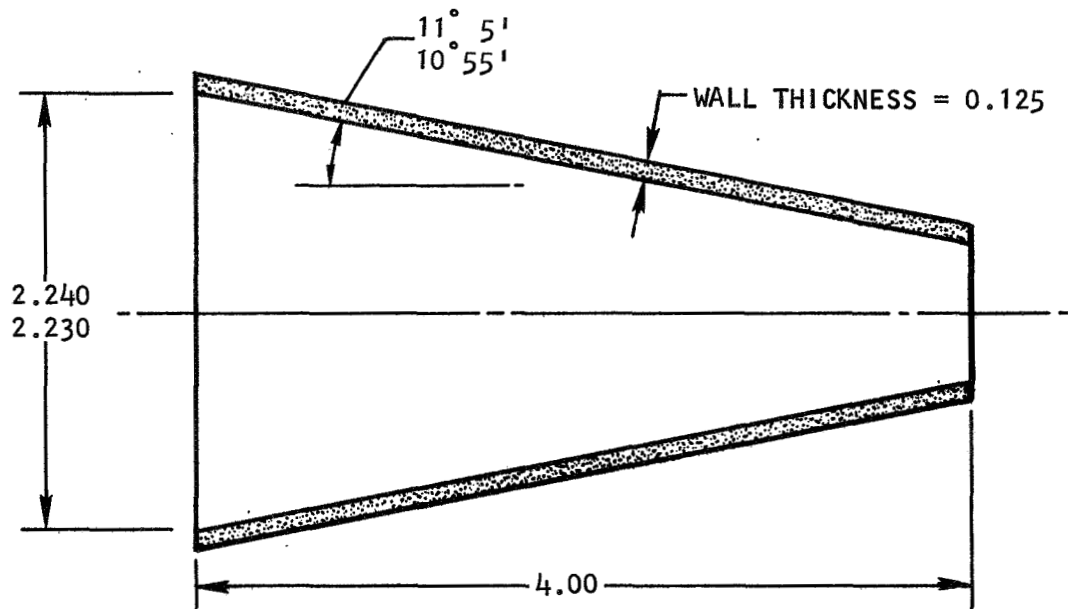


FIGURE 6. Dimensions of Pyrolytic Graphite/Carbitex Composite Test Cones



FIGURE 7. Pyrolytic Graphite/Carbitex Test Cones

NEG. 9312-1

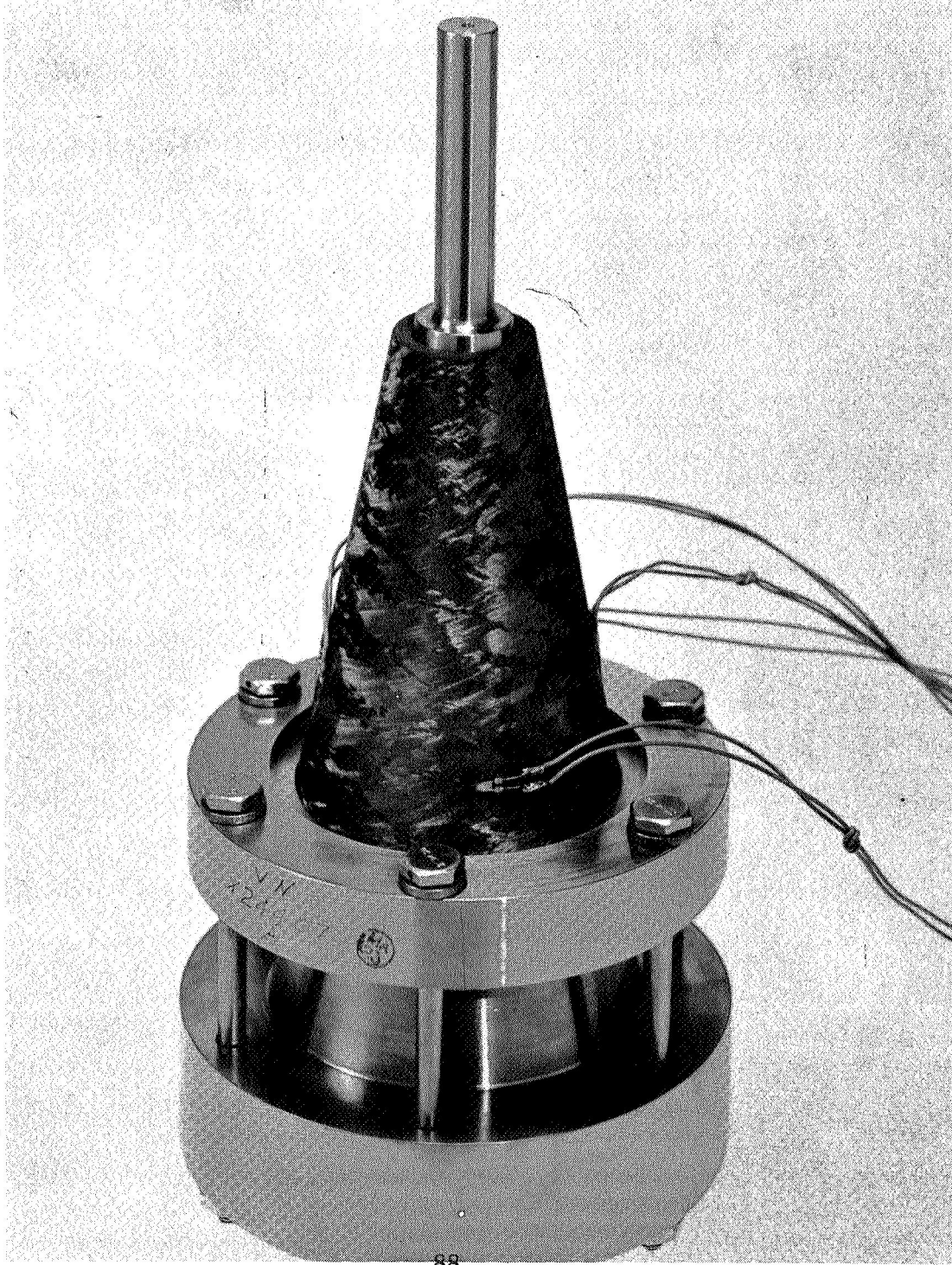


FIGURE 8. Fixture for Pressurization of Test Cones

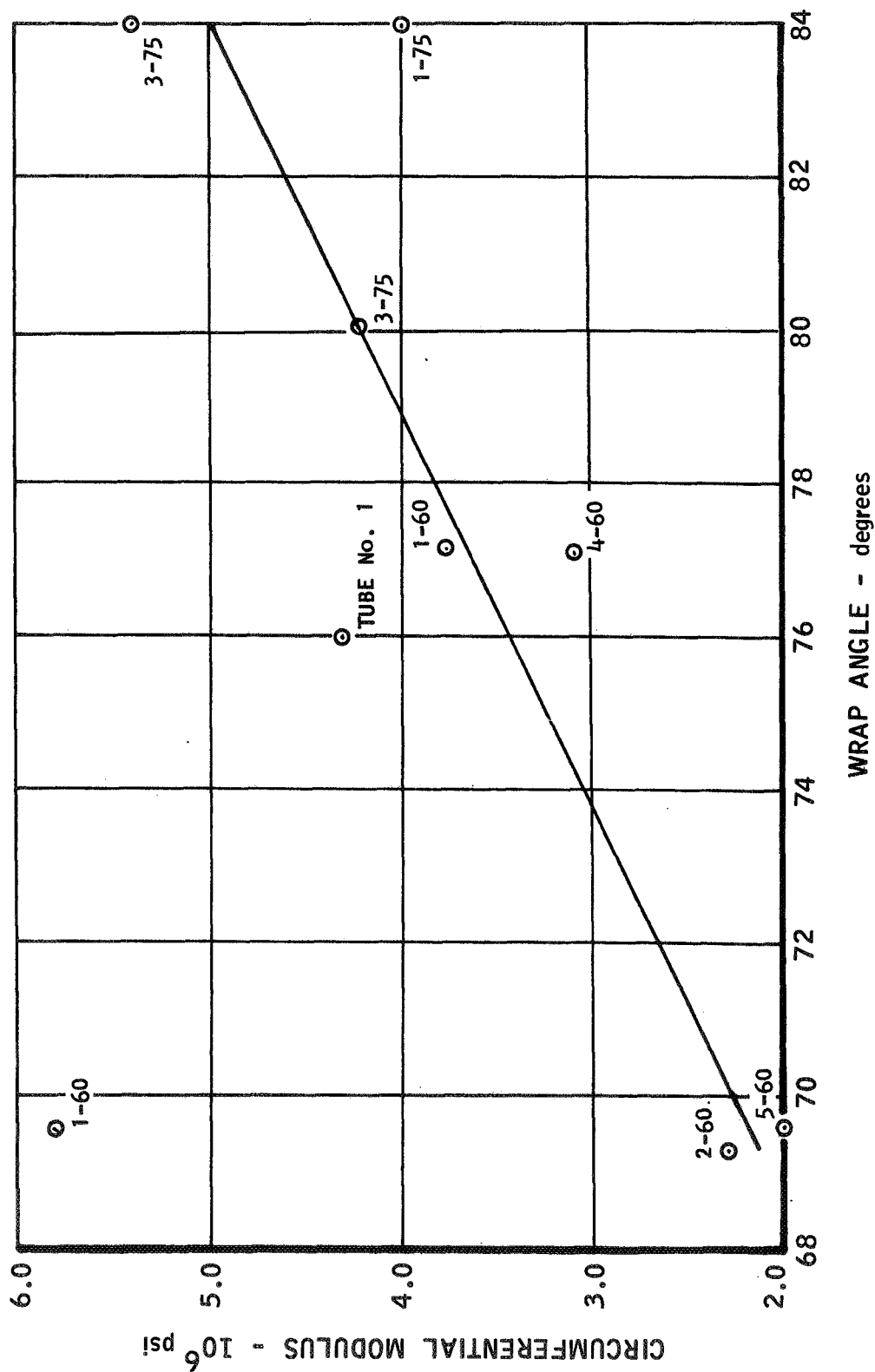


FIGURE 9. Variation of Circumferential Modulus of Elasticity of Carbitex with Wrap Angle

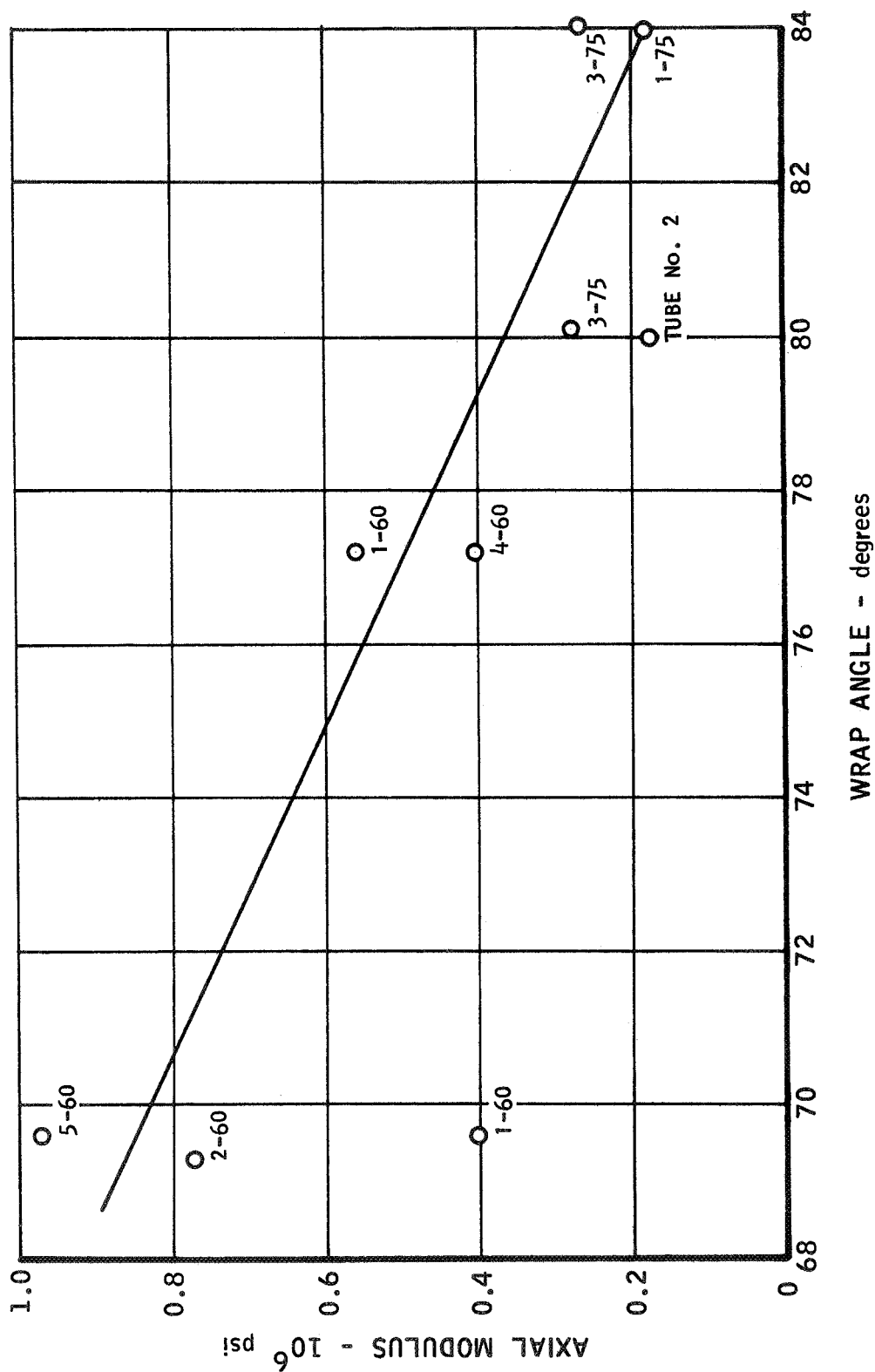


FIGURE 10. Variation of Axial Modulus of Elasticity of Carbitex with Wrap Angle

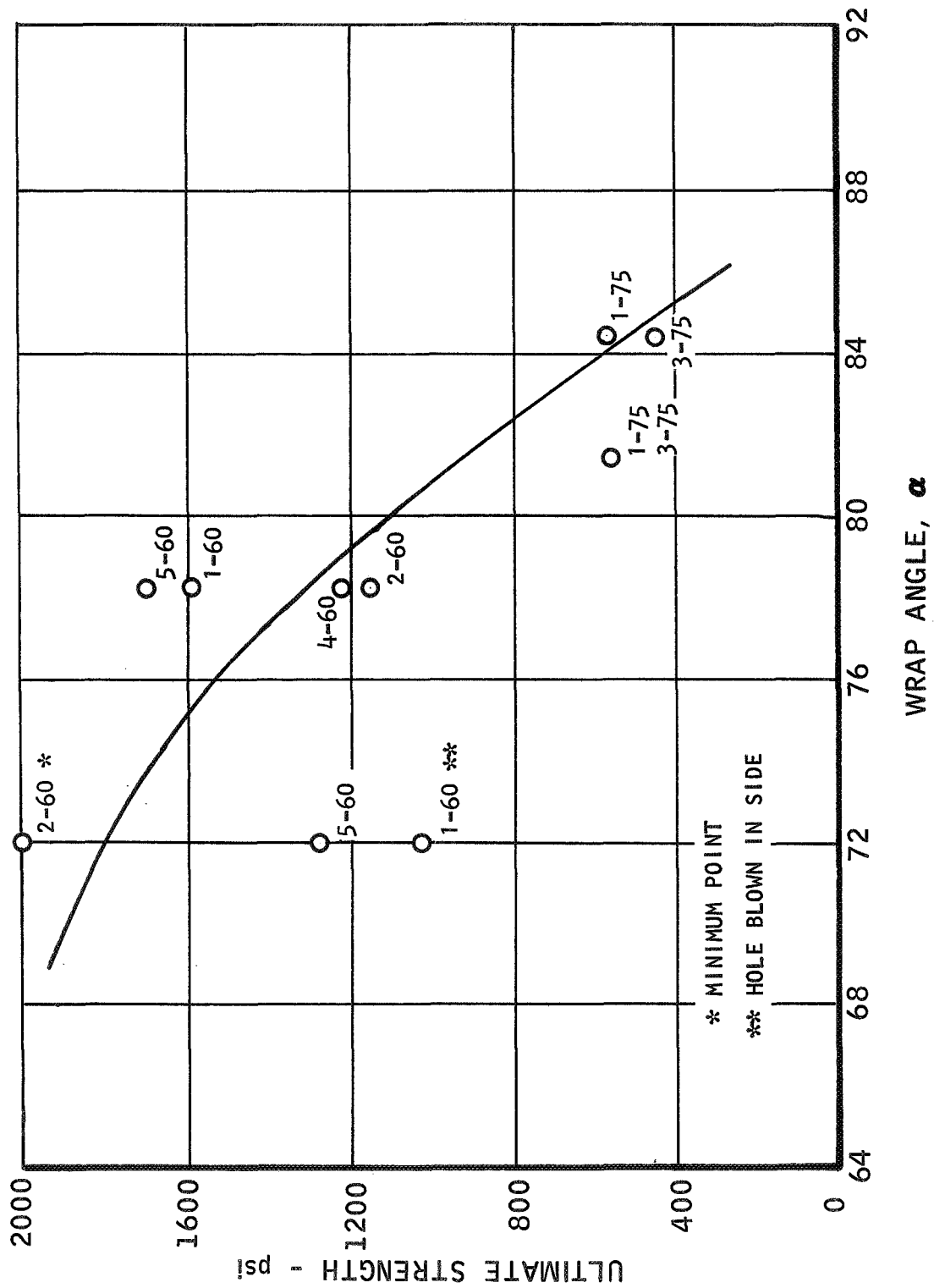


FIGURE 11. Variation of Axial Strength of Carbitex Cones with Wrap Angle

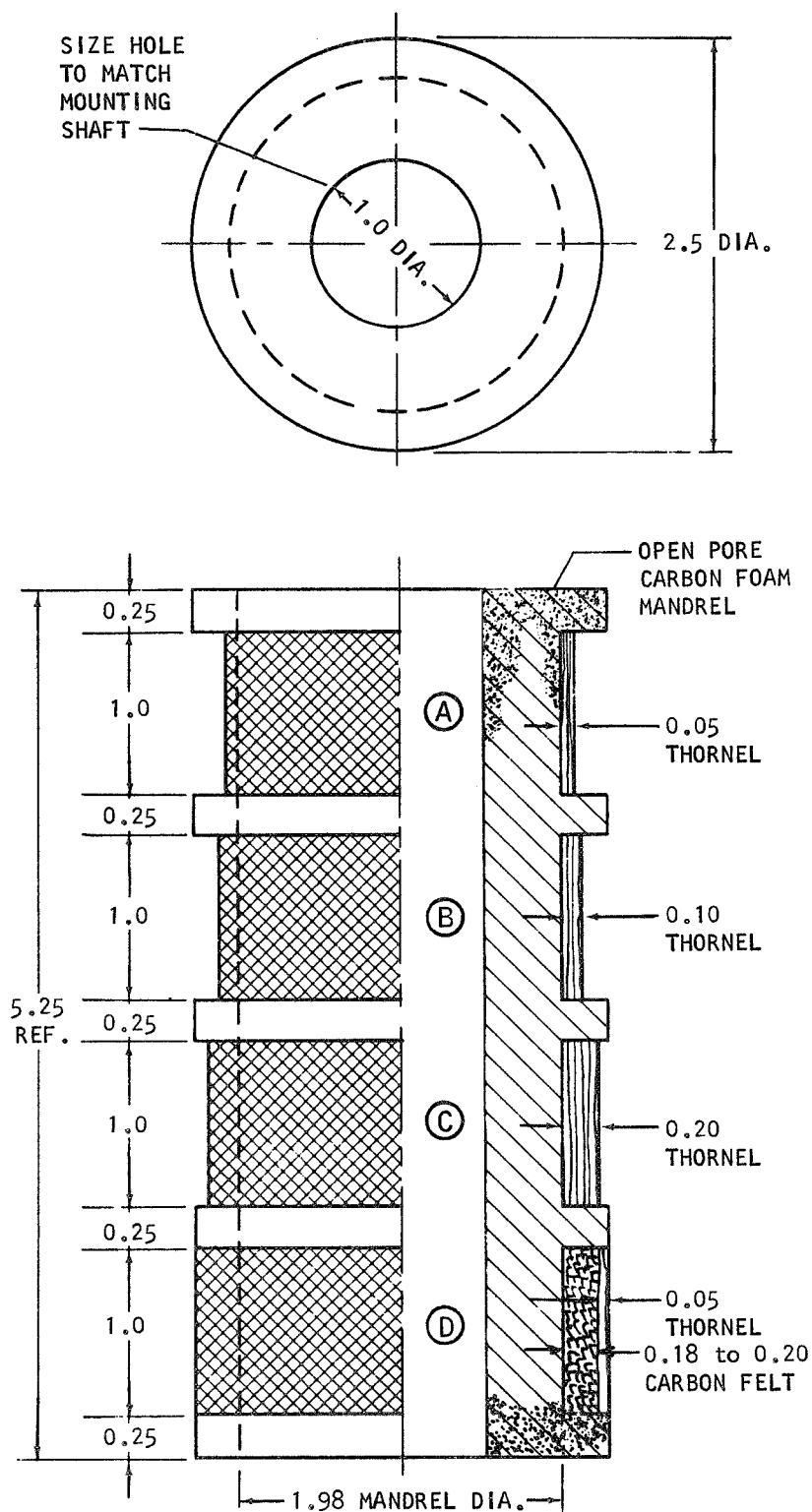


FIGURE 12. Dimensions of PG/Thornel Test Sample Spool

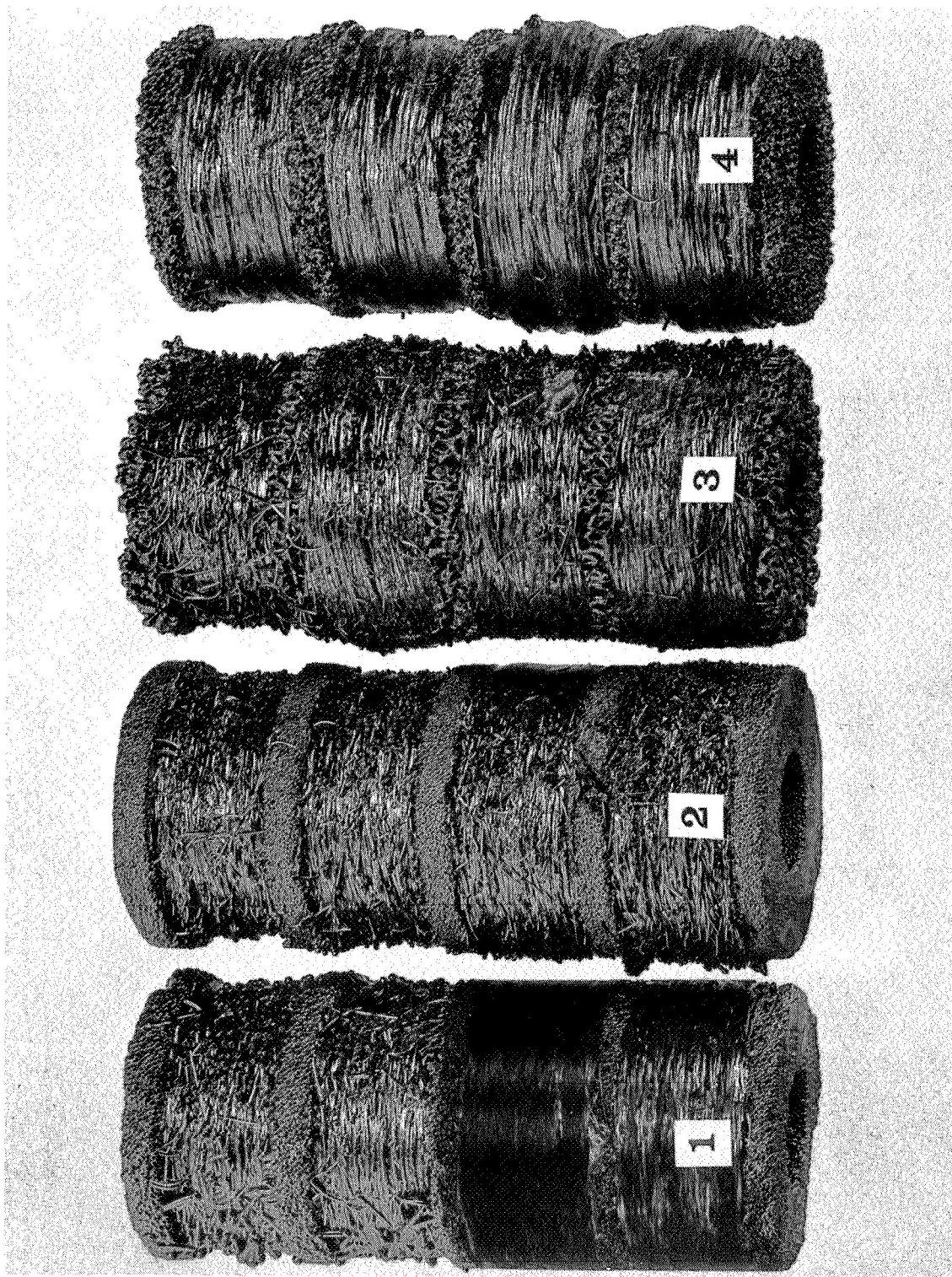


FIGURE 13. PG/Thornel Test Sample Spools

NEG. 9217-1

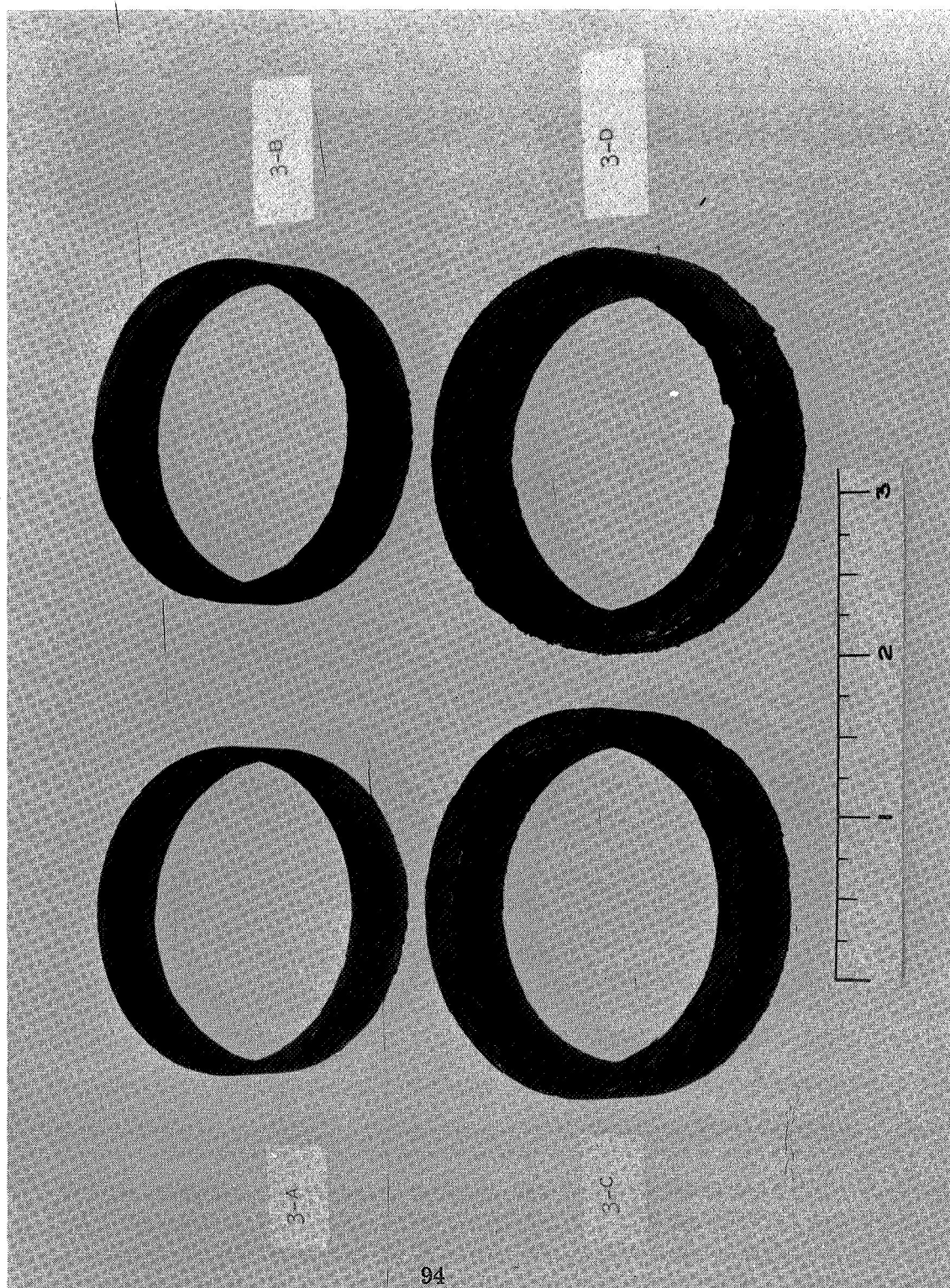


FIGURE 14. PG/Thornel NOL Ring Specimens for Tensile Tests

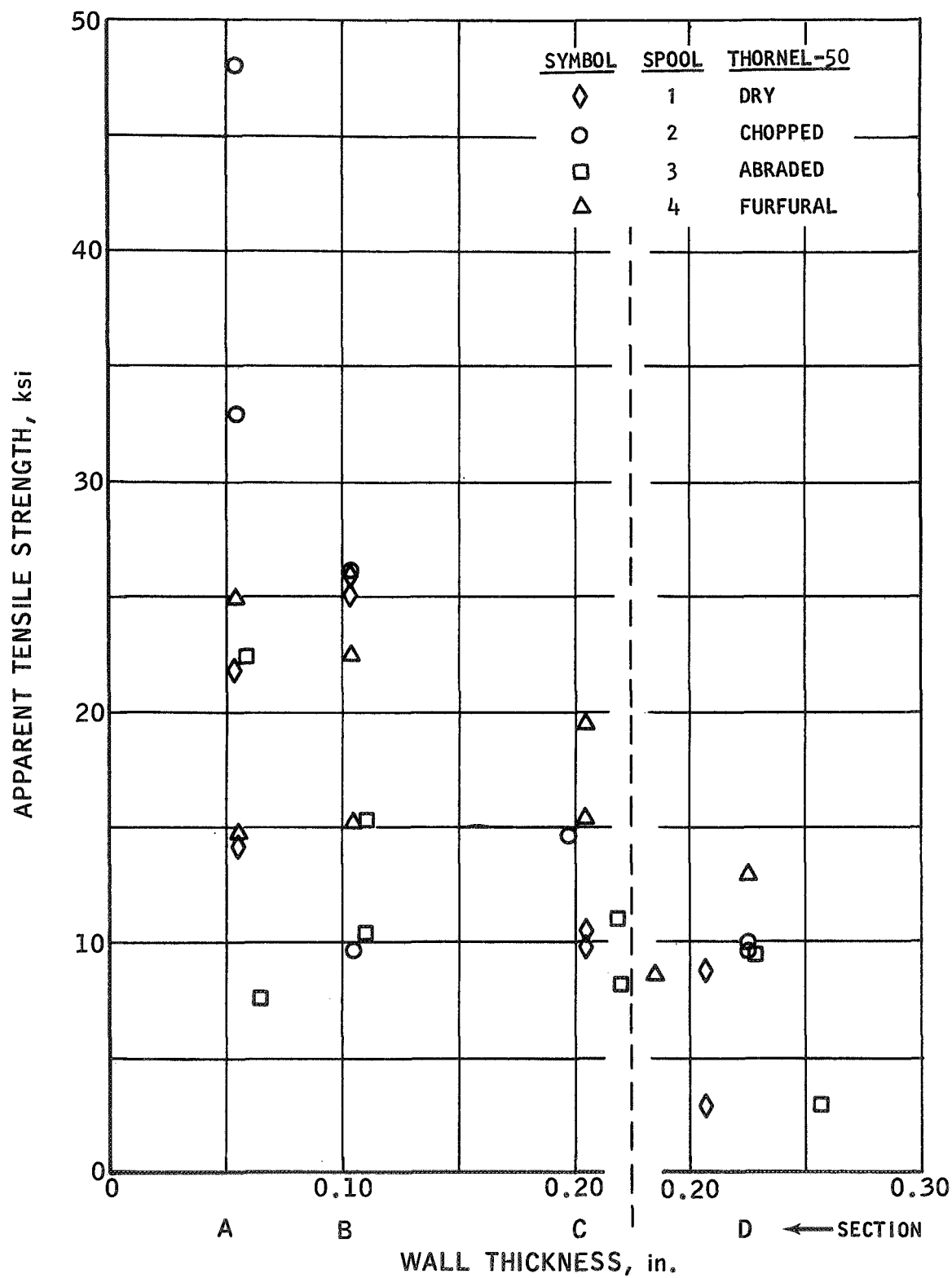
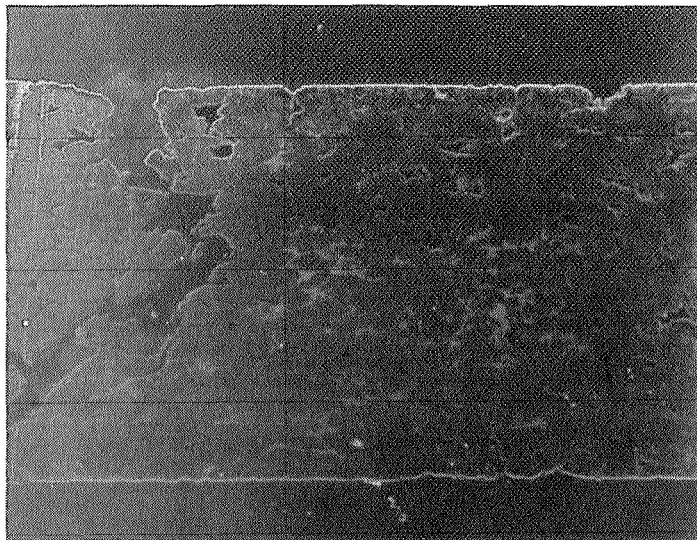
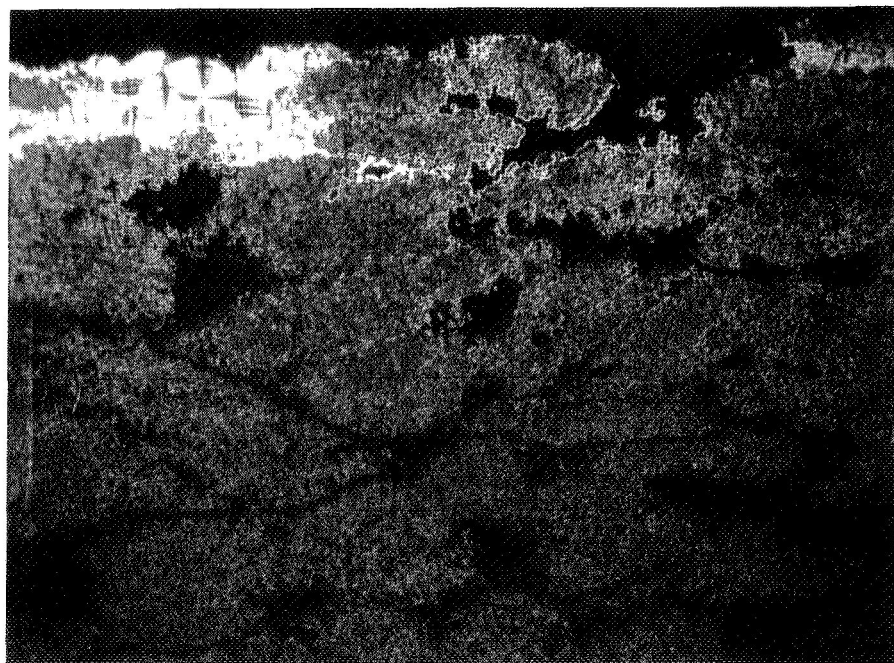


FIGURE 15. Results of Tensile Tests of PG/Thornel NOL Ring Specimens

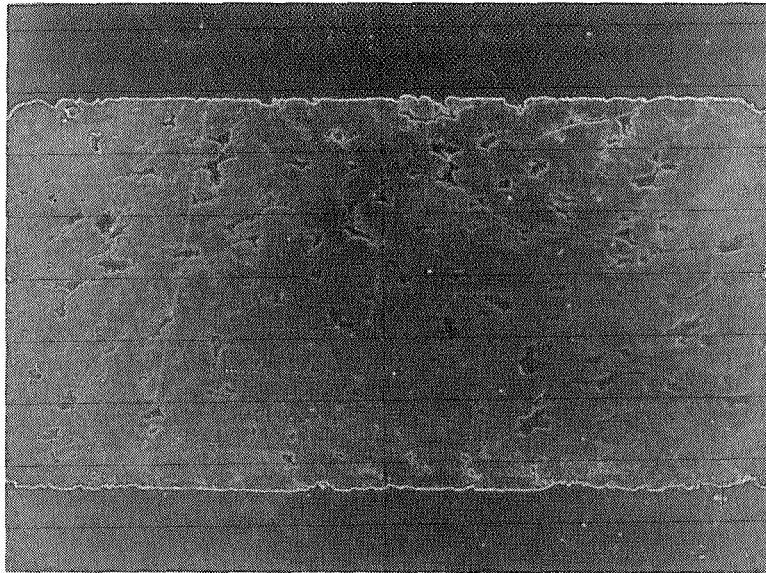


A. Full Cross Section (10X)

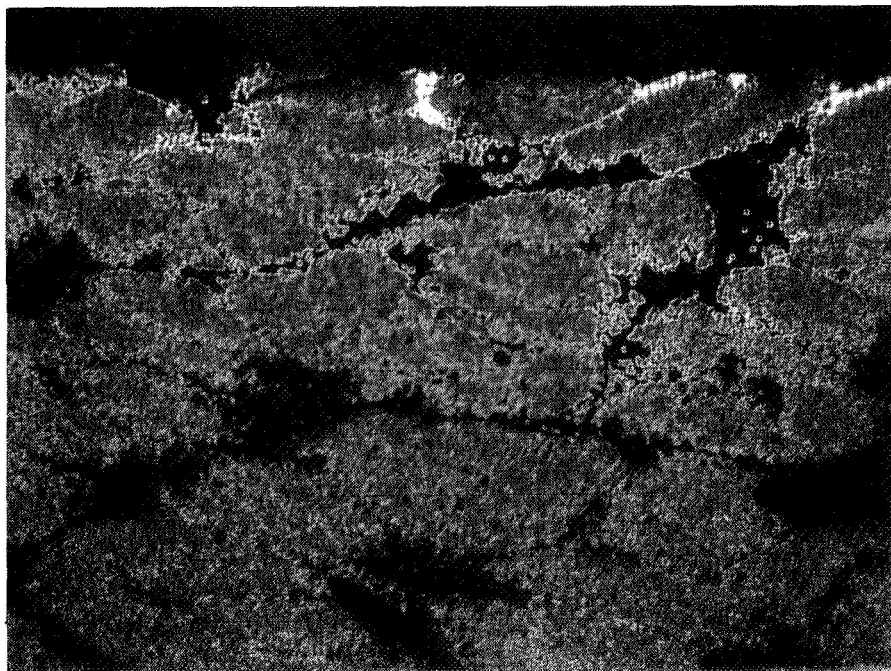


B. Polarized Light (50X)

FIGURE 16. Microstructure of PG/Thornel Ring Specimen 1C



A. Full Cross Section (10X)

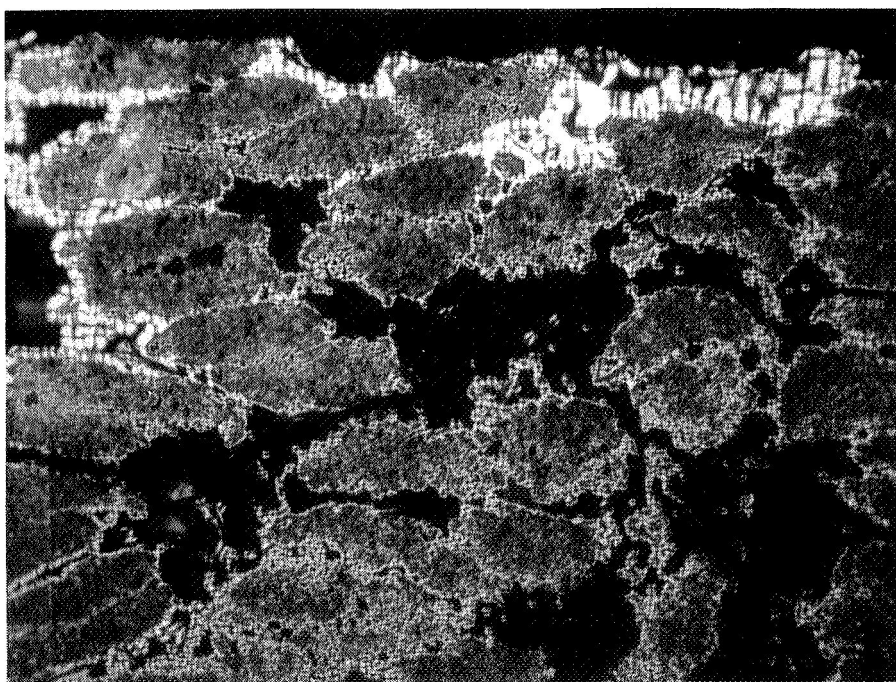


B. Polarized Light (50X)

FIGURE 17. Microstructure of PG/Thornel Ring Specimen 2C

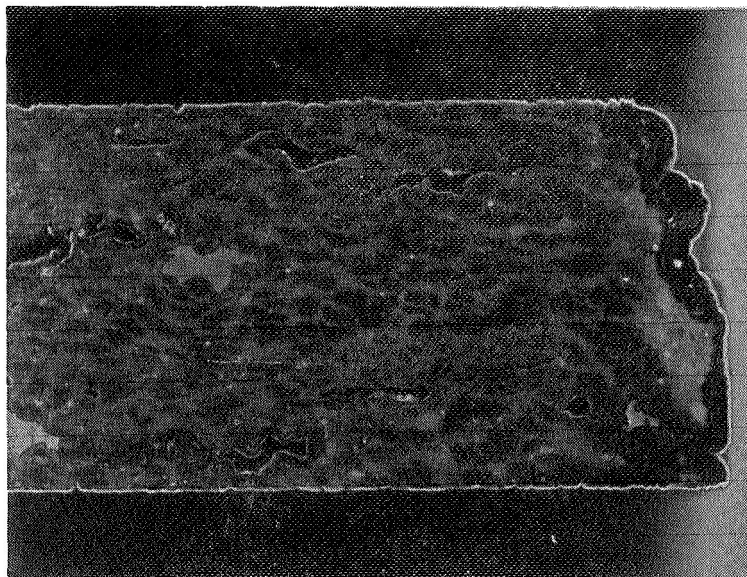


A. Full Cross Section (10X)

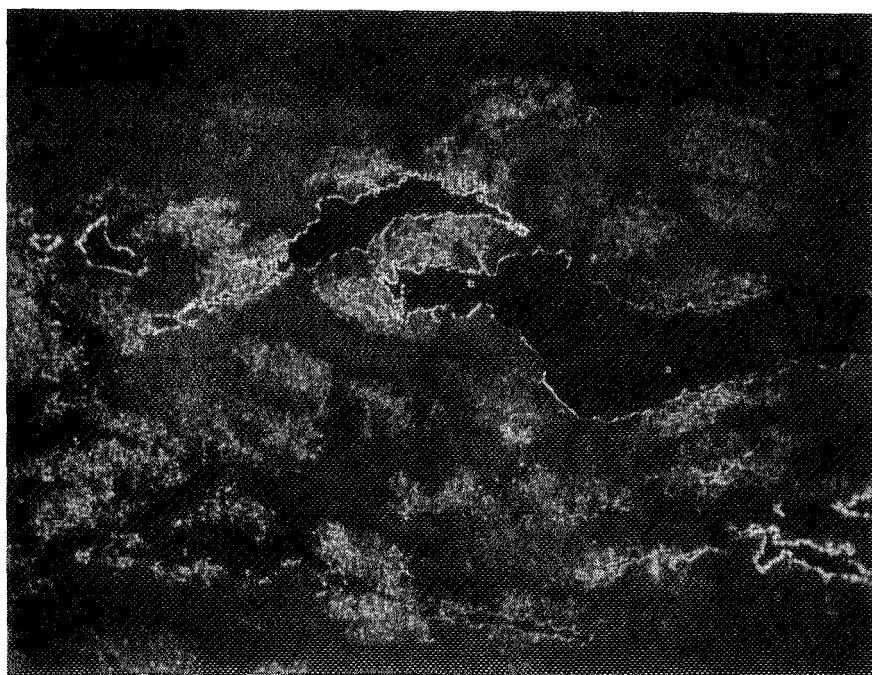


B. Polarized Light (50X)

FIGURE 18. Microstructure of PG/Thornel Ring Specimen 3C

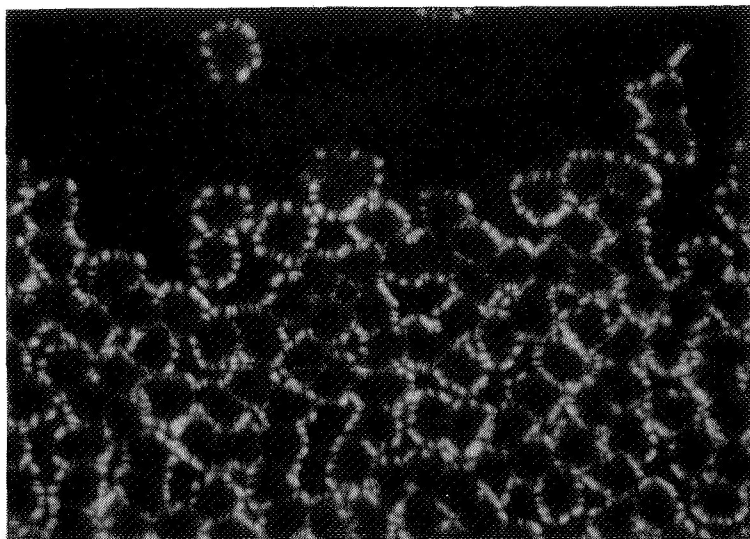


A. Full Cross Section (10X)



B. Polarized Light (50X)

FIGURE 19. Microstructure of PG/Thornel Ring Specimen 4C

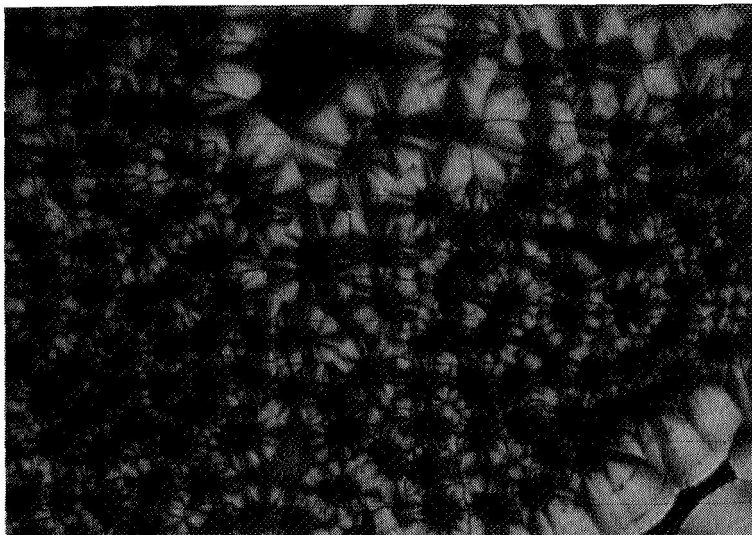


A. Spool No. 1, Polarized Light (750X)

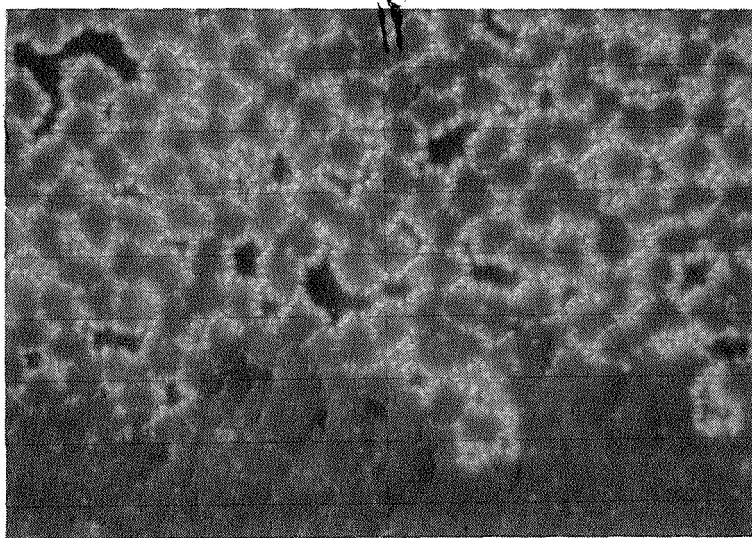


B. Spool No. 2, Polarized Light (750X)

FIGURE 20. Photomicrographs of Representative Sections of
PG Infiltrated Thornel, Spools Nos. 1 and 2



A. Spool No. 3, Polarized Light (750X)



B. Spool No. 4, Polarized Light (750X)

FIGURE 21. Photomicrographs of Representative Sections of PG Infiltrated Thornel, Spools Nos. 3 and 4

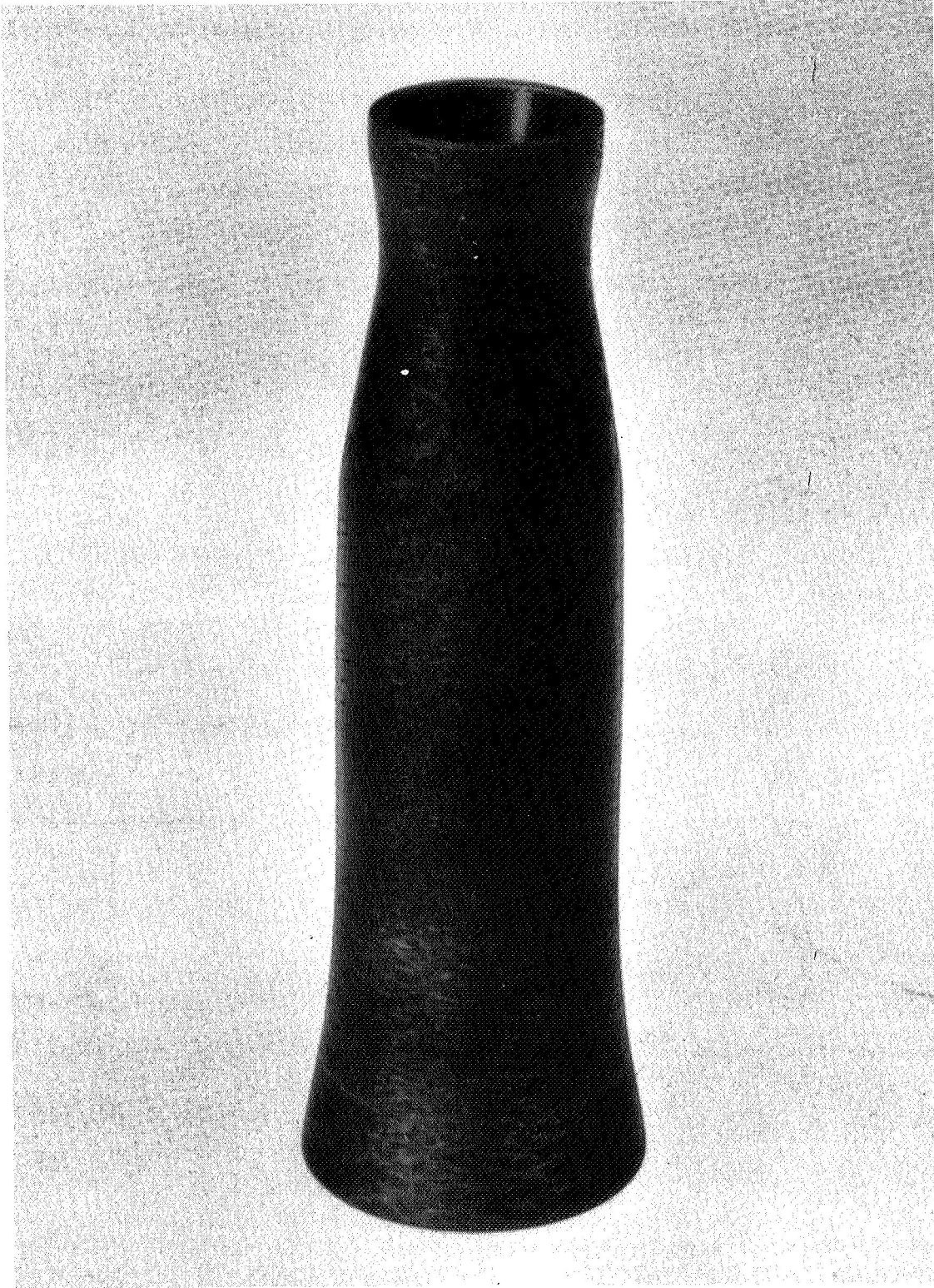
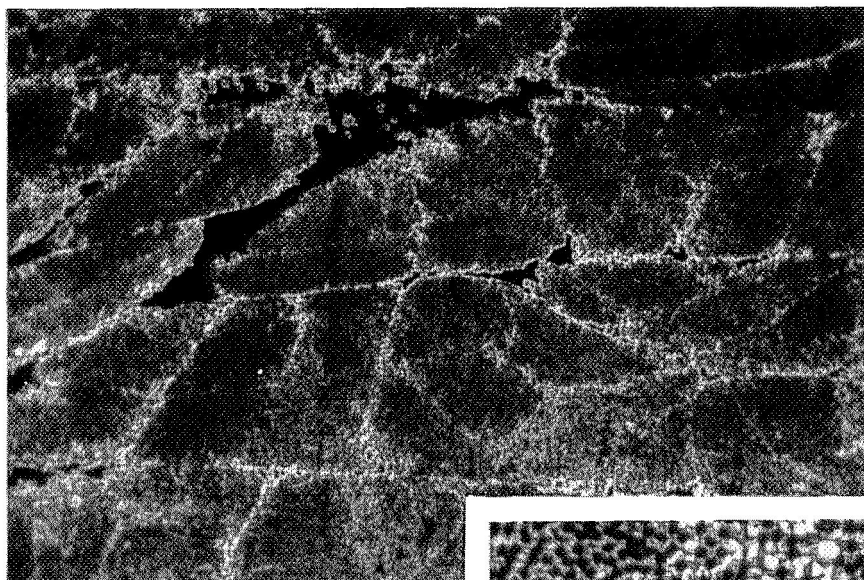


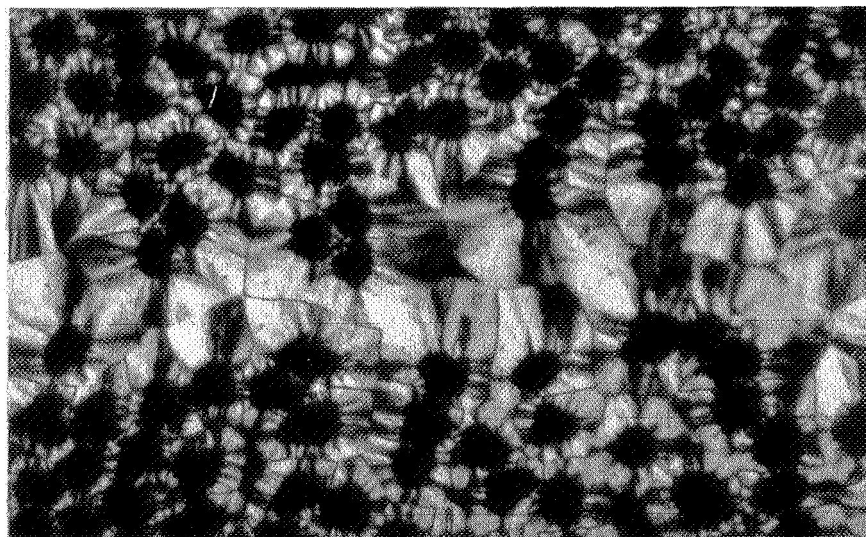
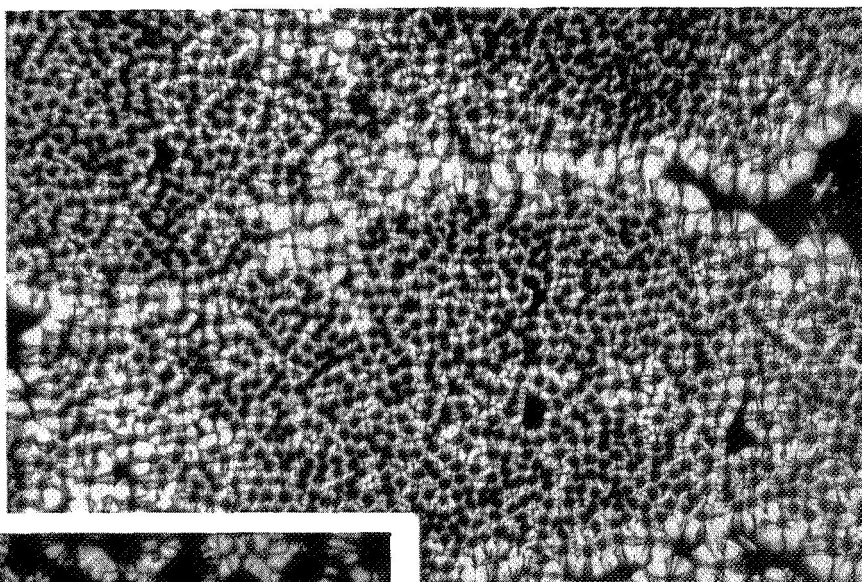
FIGURE 22. PG/Thornel/PG Chamber

NEG. 9605-4



X50

X200



X750

FIGURE 23. PG Infiltrated Thornel-50 Carbon Yarn

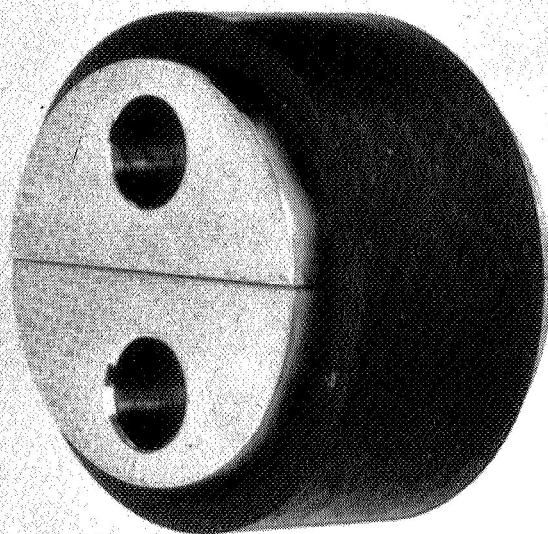


FIGURE 24. PG/Thornel/PG Tensile Test Apparatus

NEG. 9617-4

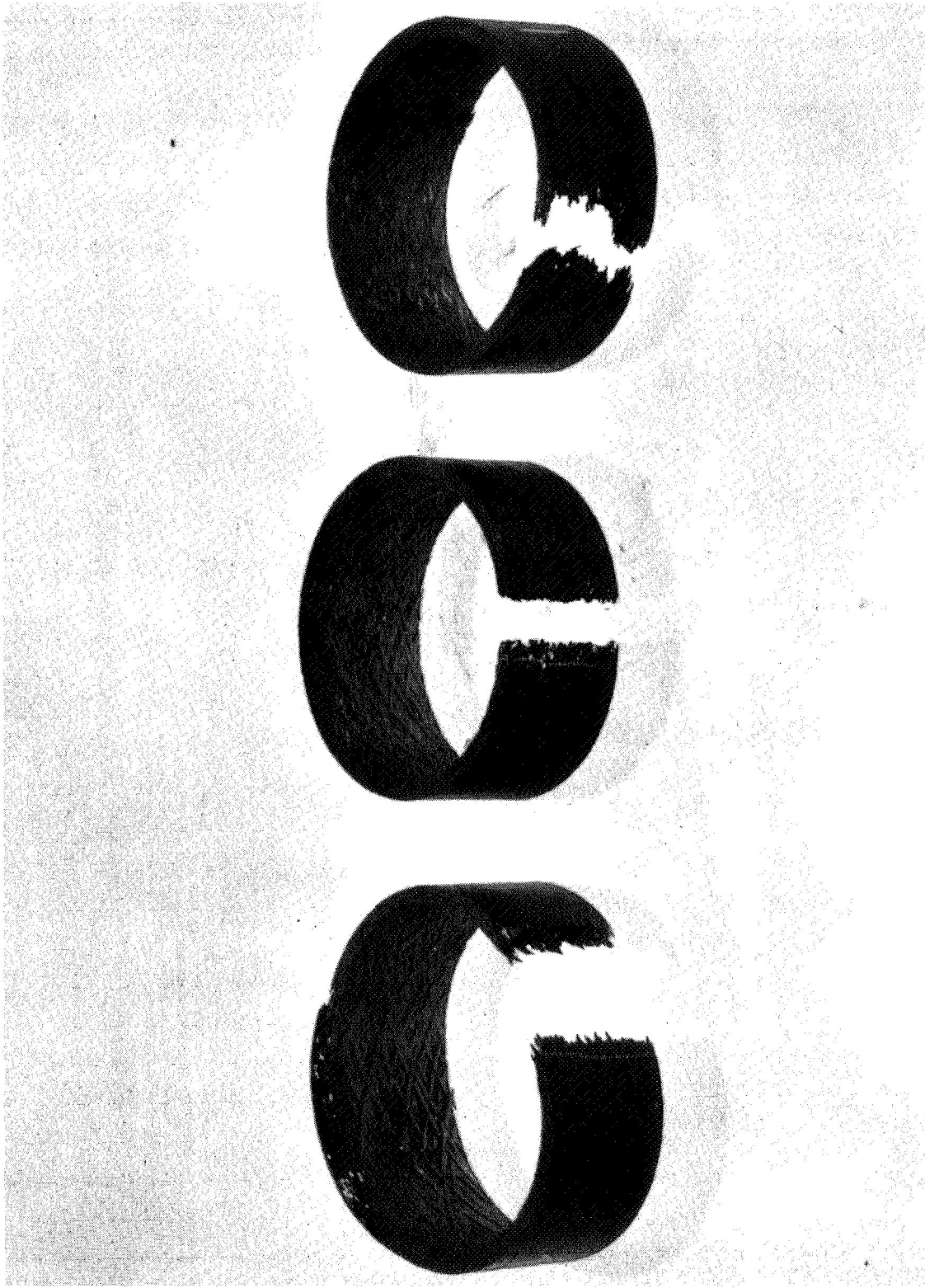


FIGURE 25. PG/Thornel/PG Tensile Test Rings after Failure

NEG. 9636-10

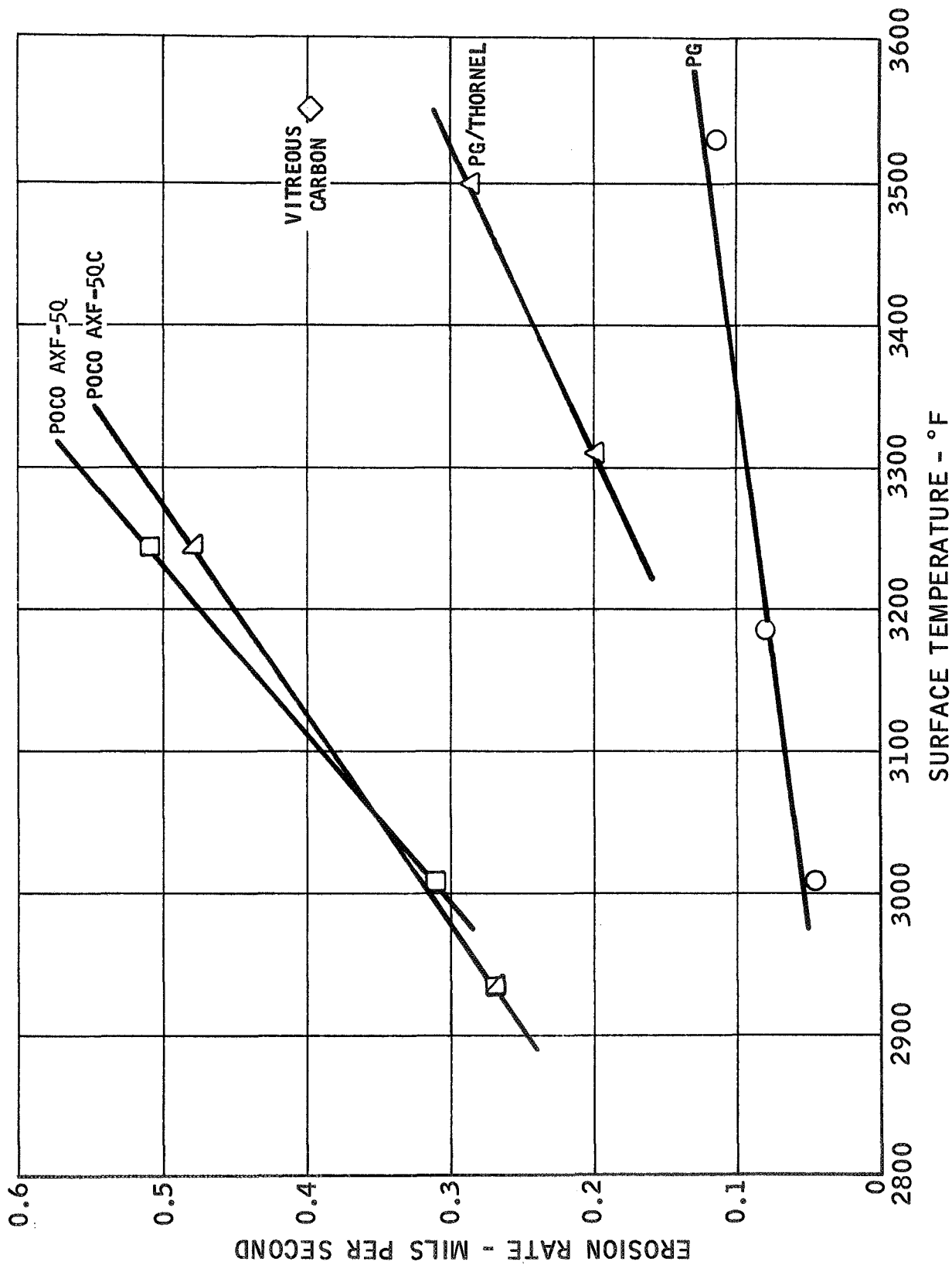


FIGURE 26. Carbon Materials Erosion Rate - Oxyacetylene Flame in Air

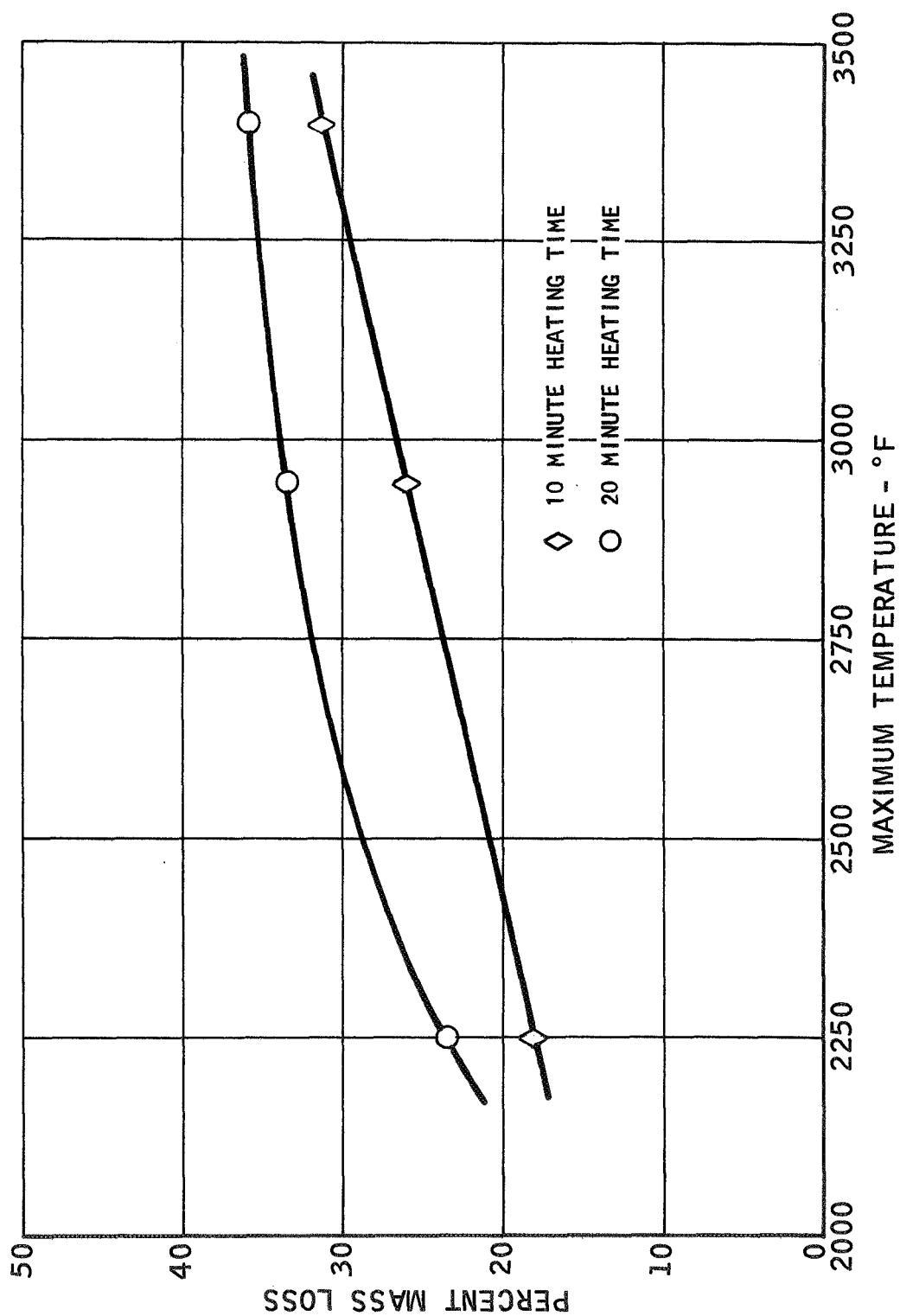


FIGURE 27. Loss of Copper from AXF-5QC

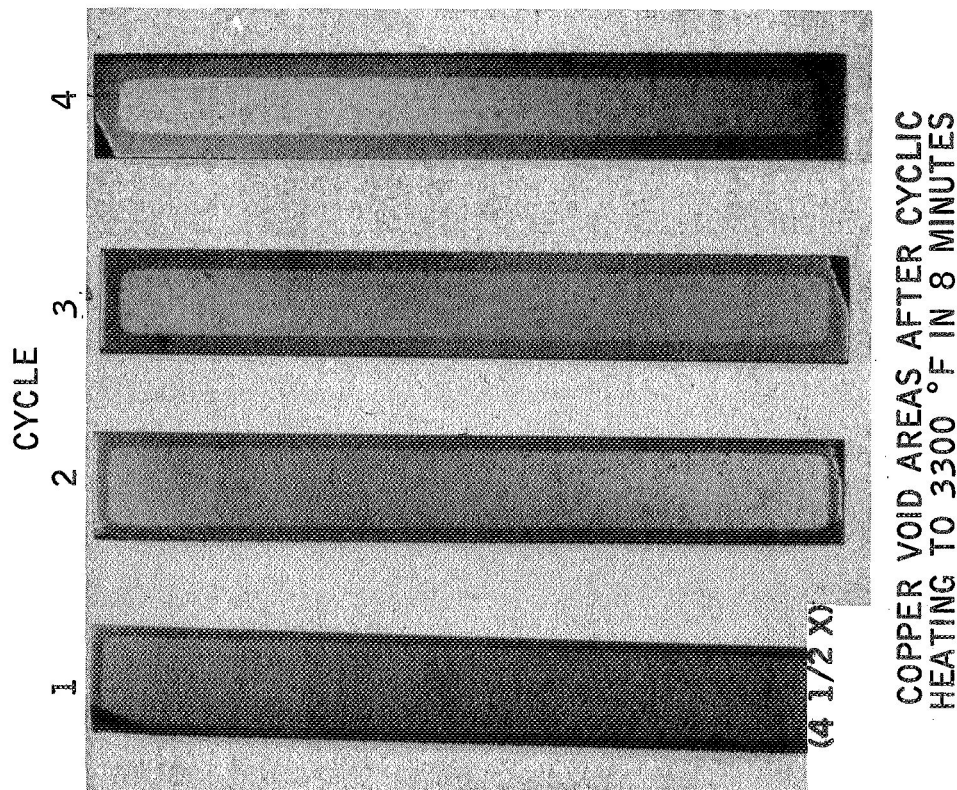
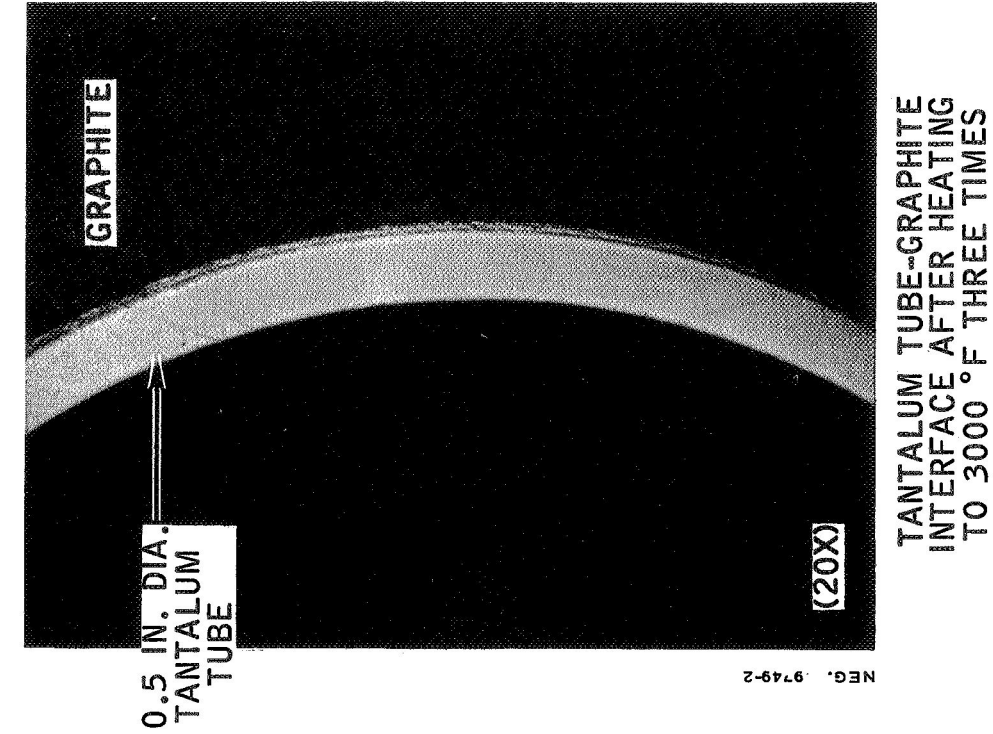


FIGURE 28. Copper Impregnated Graphite after Cyclic Heating

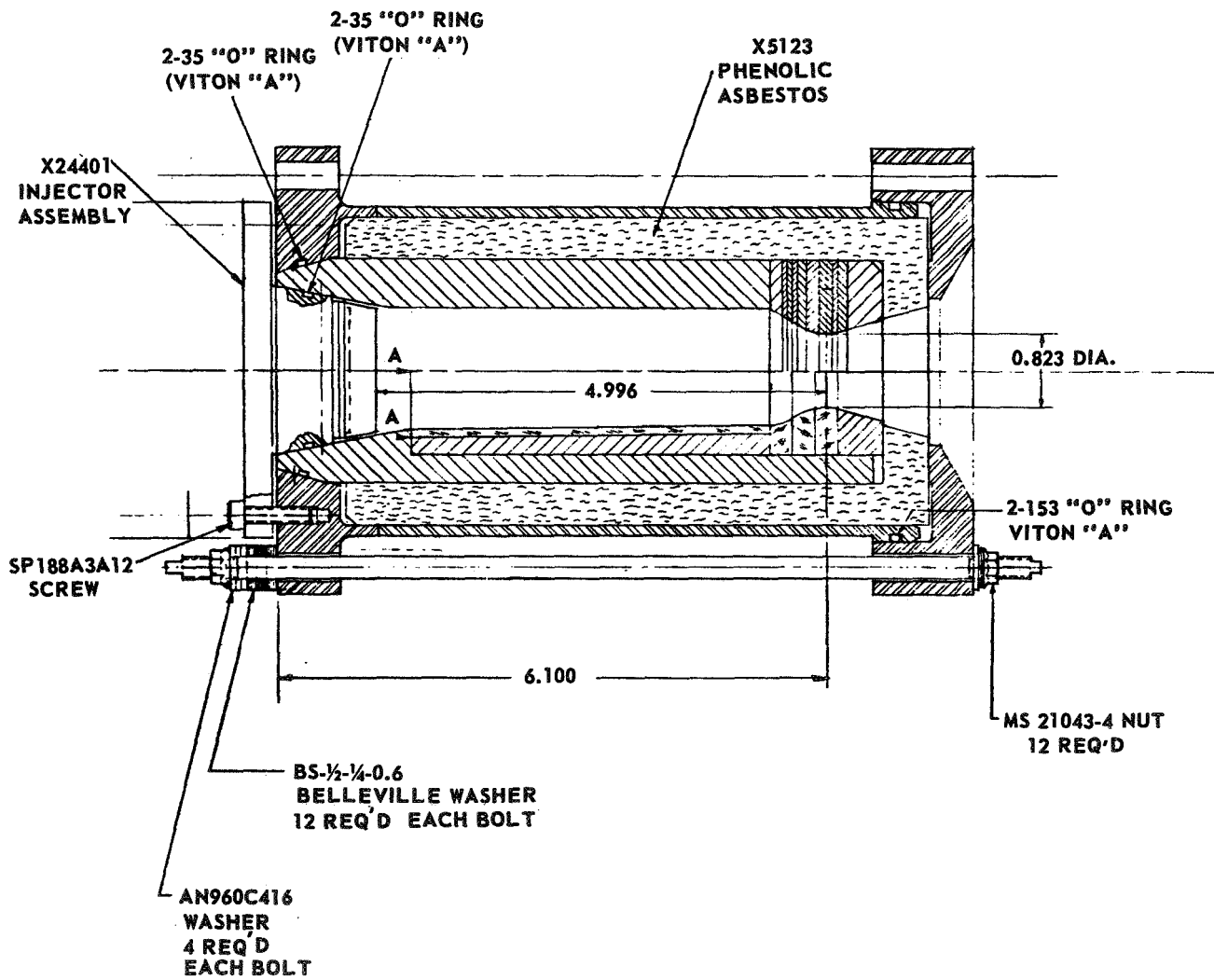


FIGURE 29. Composite Chamber FLOX/LPG

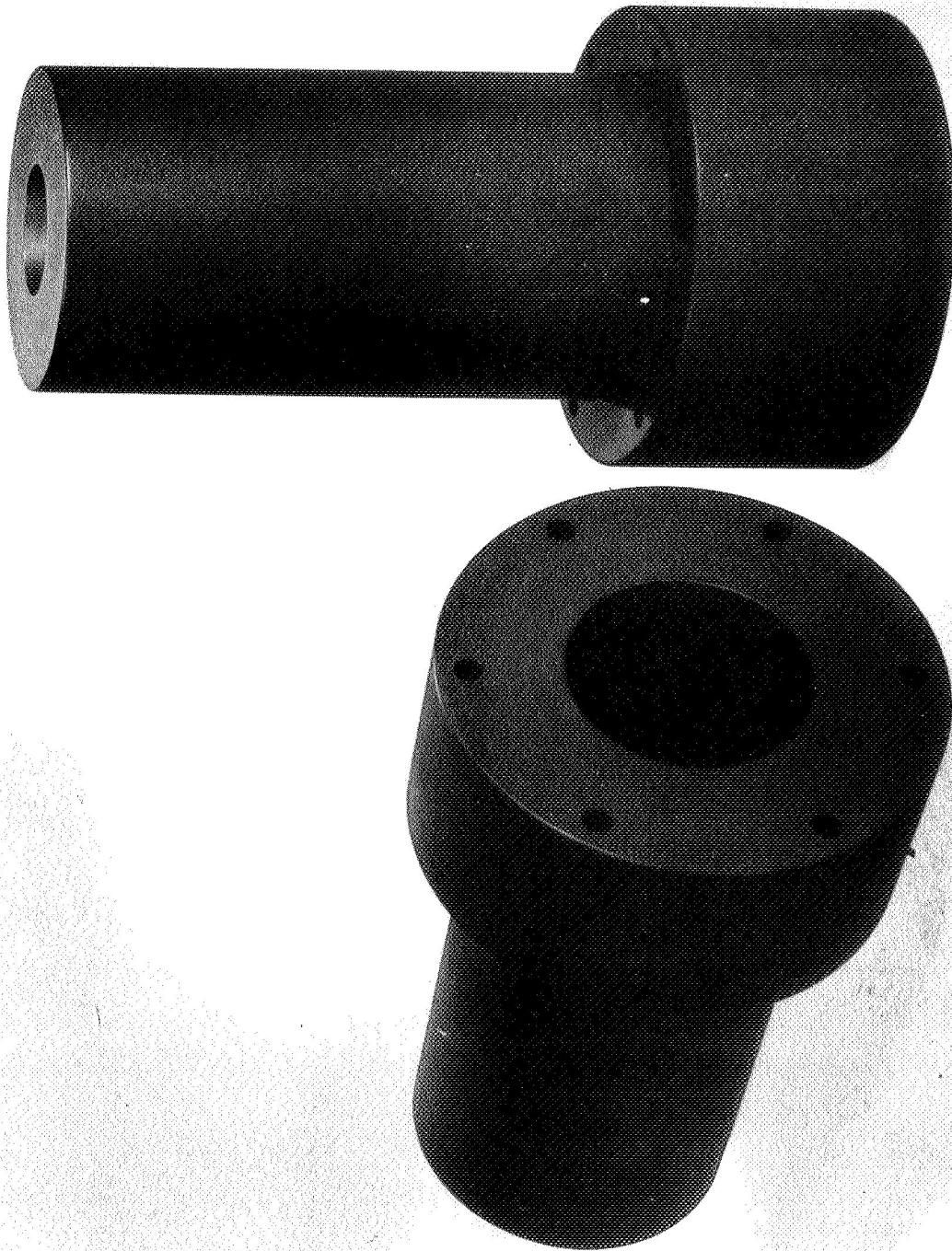


FIGURE 30. POCO Graphite Heat Sink Thrust Chambers

NEG. 9392-1

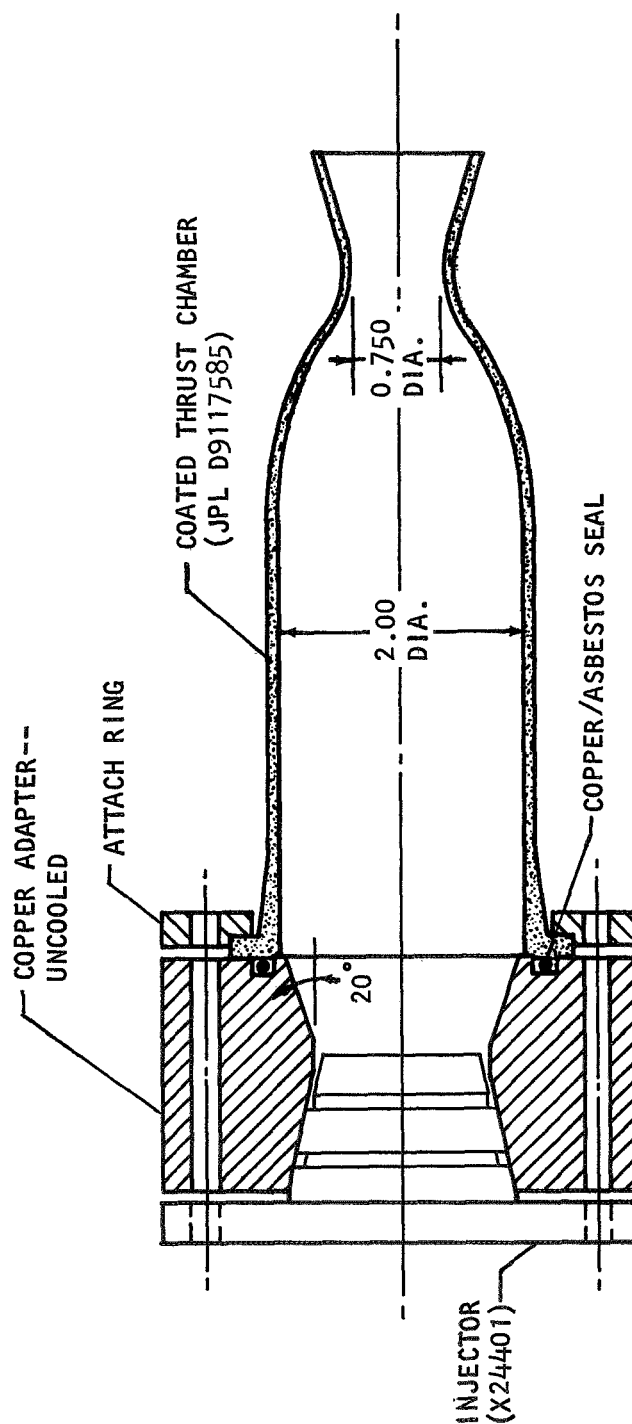


FIGURE 31. Uncooled Copper Adapter Section for Testing Coated Tantalum-Tungsten Chambers

NEG. 9617-3

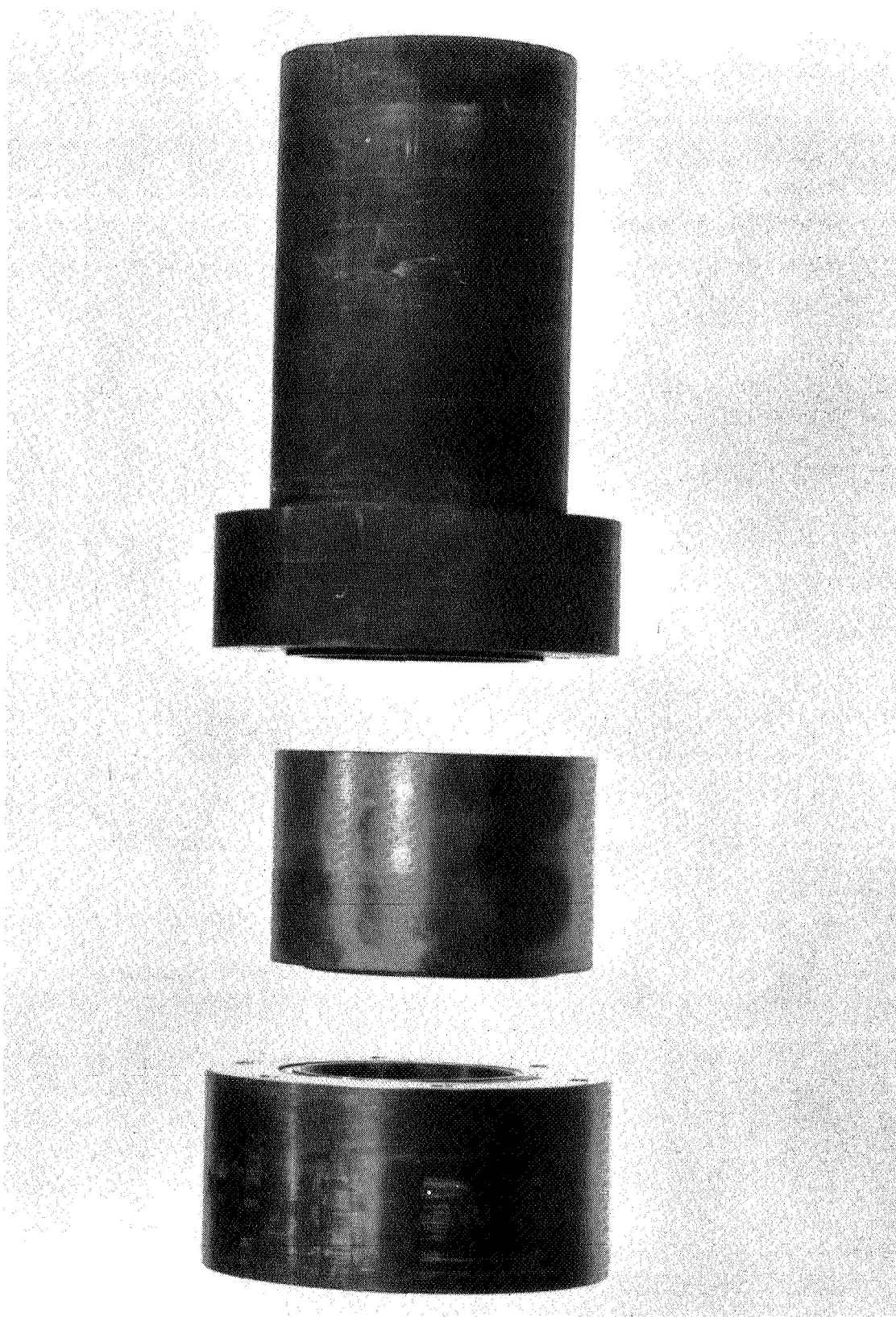


FIGURE 32. Copper Impregnated POCO Chamber Segment



NEG. 9302-1

FIGURE 33. 100-pound Thrust Carbitex 713 Chambers



NEG. 9424-2

FIGURE 34. PG/Carbitex Thrust Chamber with RPG Nozzle Extension

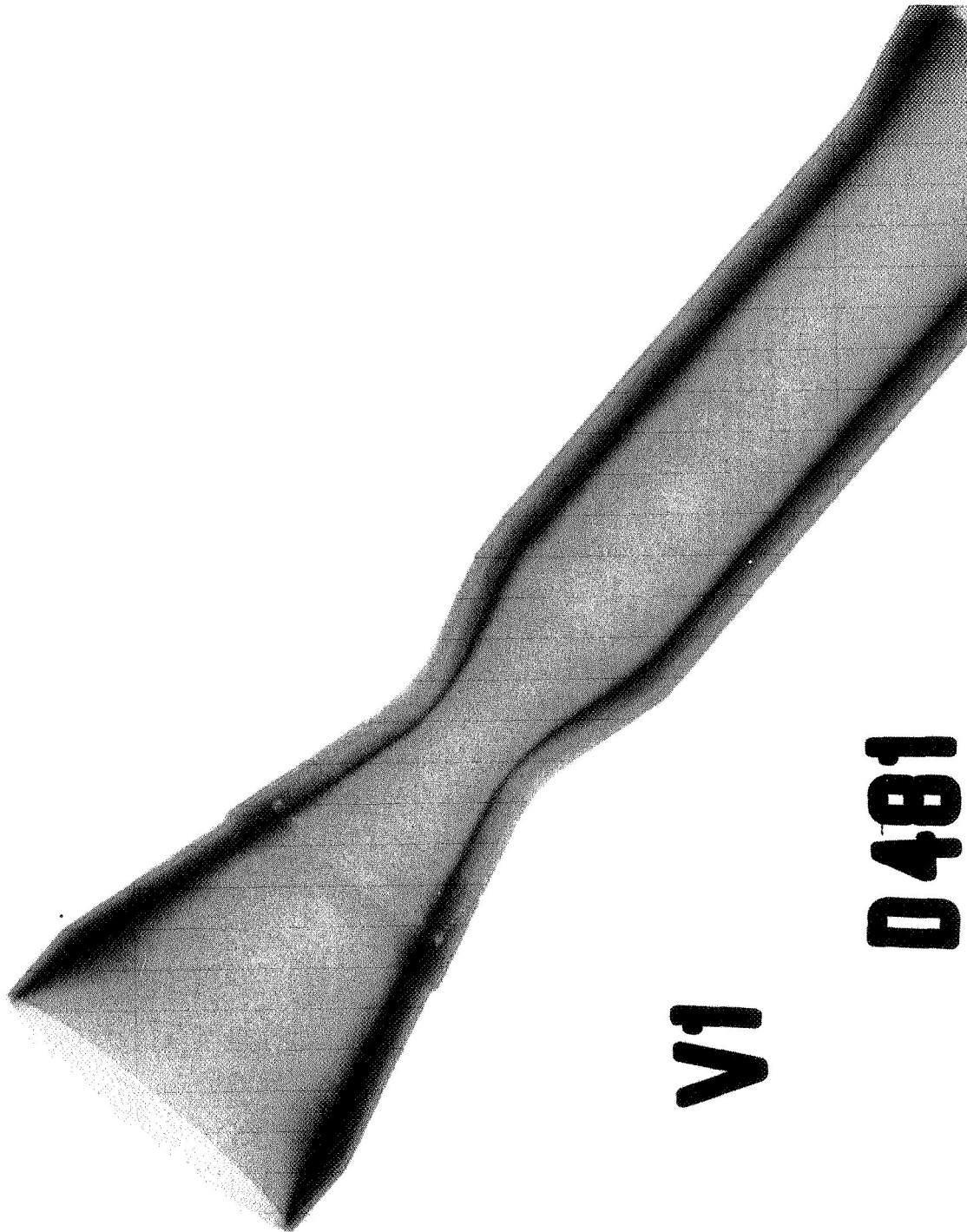


FIGURE 35. X-Ray Photograph of PG/Carbitex Thrust Chamber with RPG Nozzle Extension

NEG. 9432-2

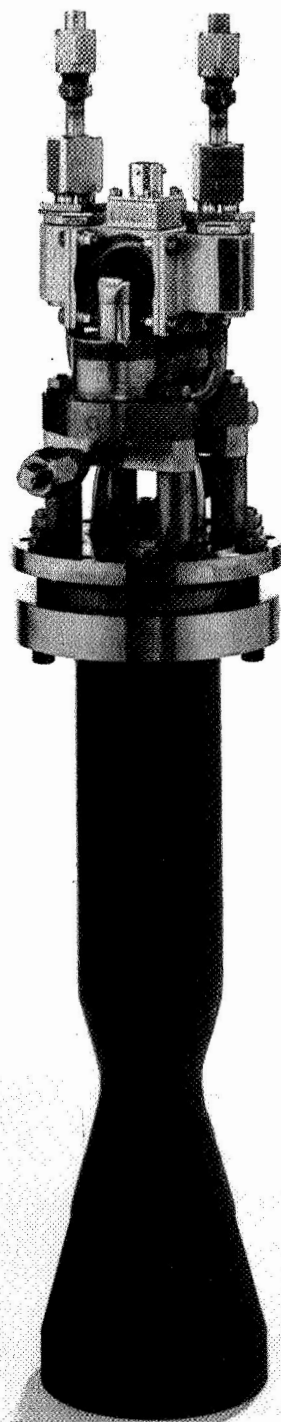


FIGURE 36. 100-pound Thrust FLOX/LPG Engine Assembly



FIGURE 37. PG/Carbitex 100-pound Thrust Sea Level Chamber with Coating on the Inside Only

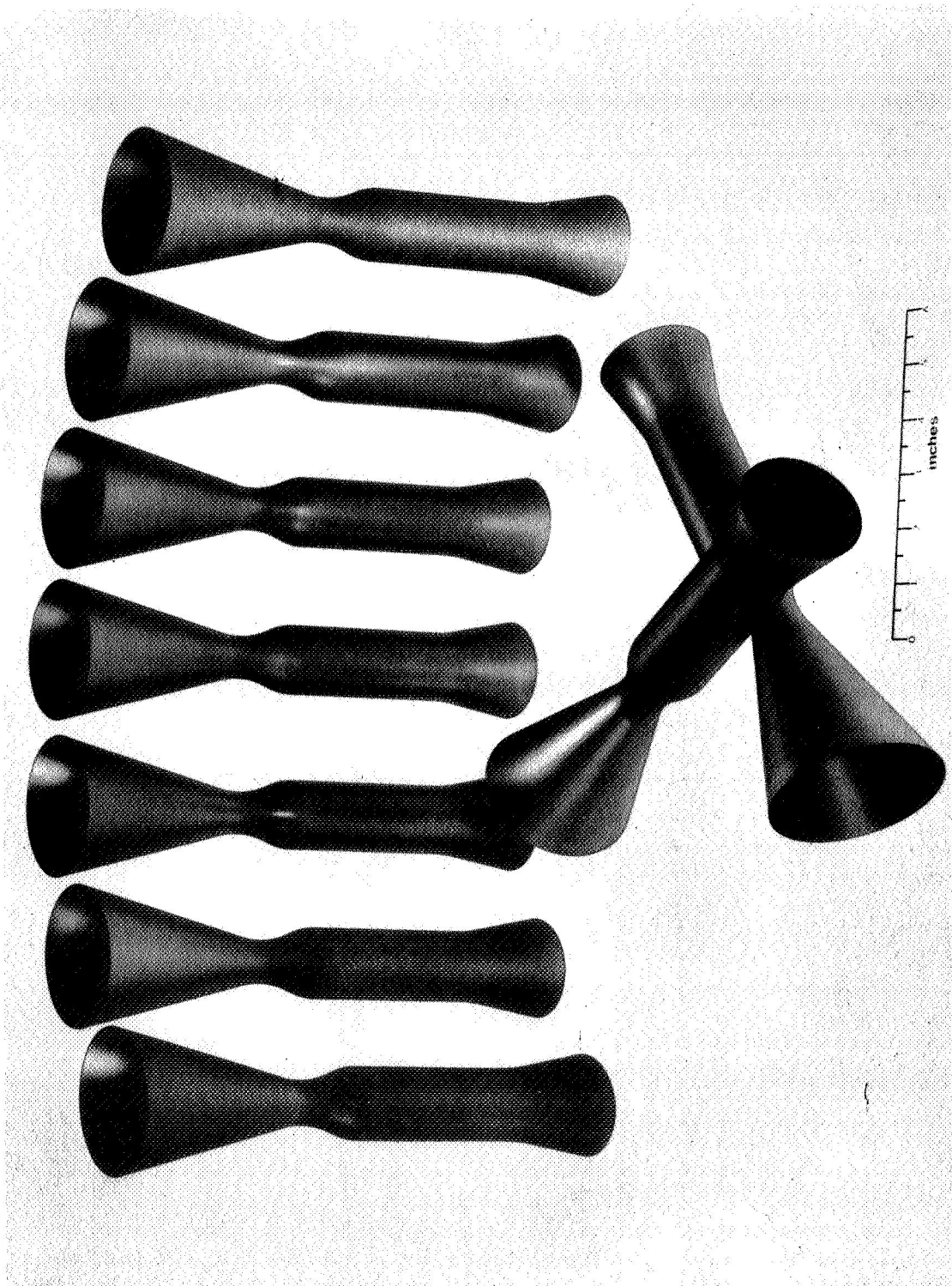


FIGURE 38. PG Liners Used for PG/Thornel Composite Altitude Thrust Chambers

NEG. 9337-1



FIGURE 39. ThorneL Wound Sea Level Chamber before PG Infiltration

NEG. 9424-3



FIGURE 40. Thornel Wound Altitude Chamber before PG Infiltration

NEG. 9428-1

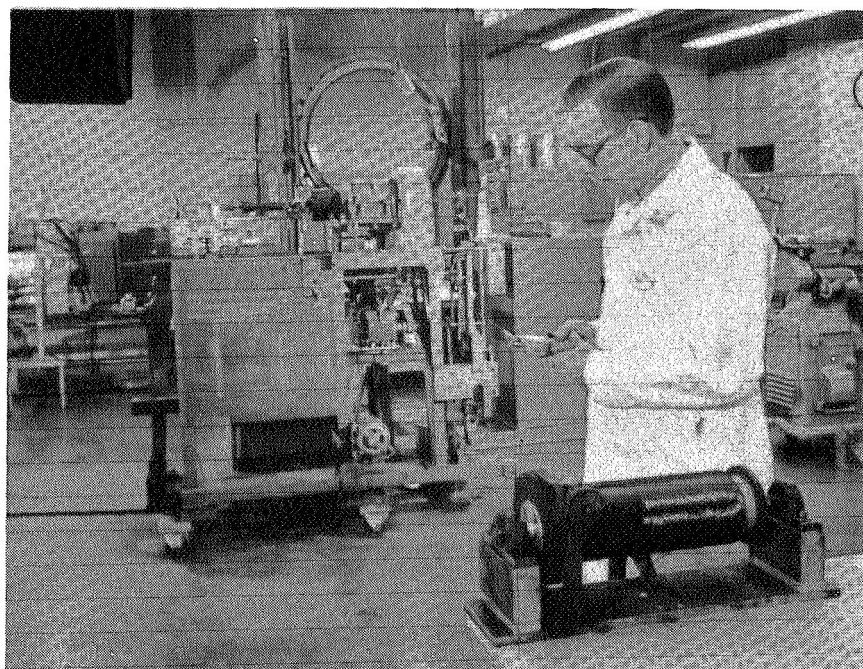
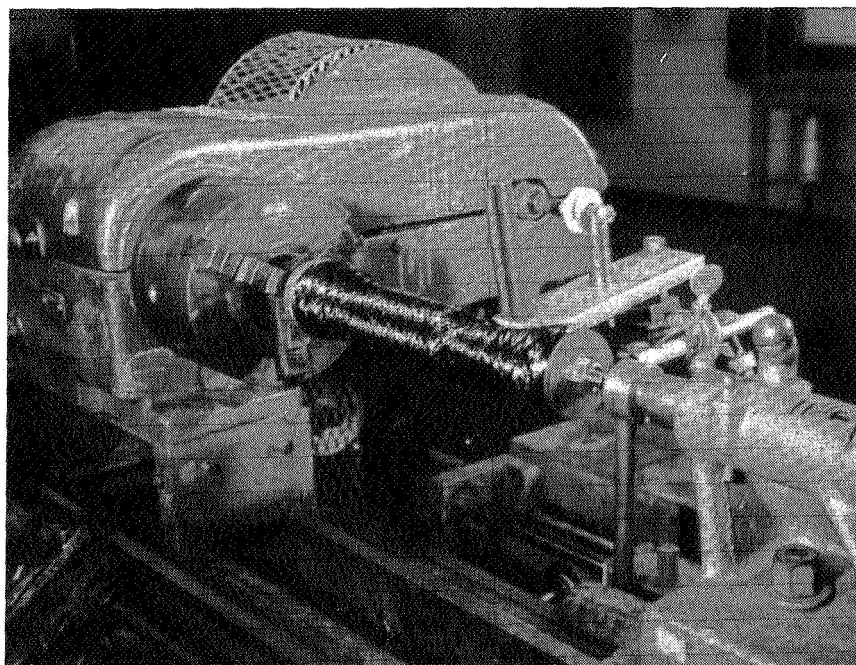
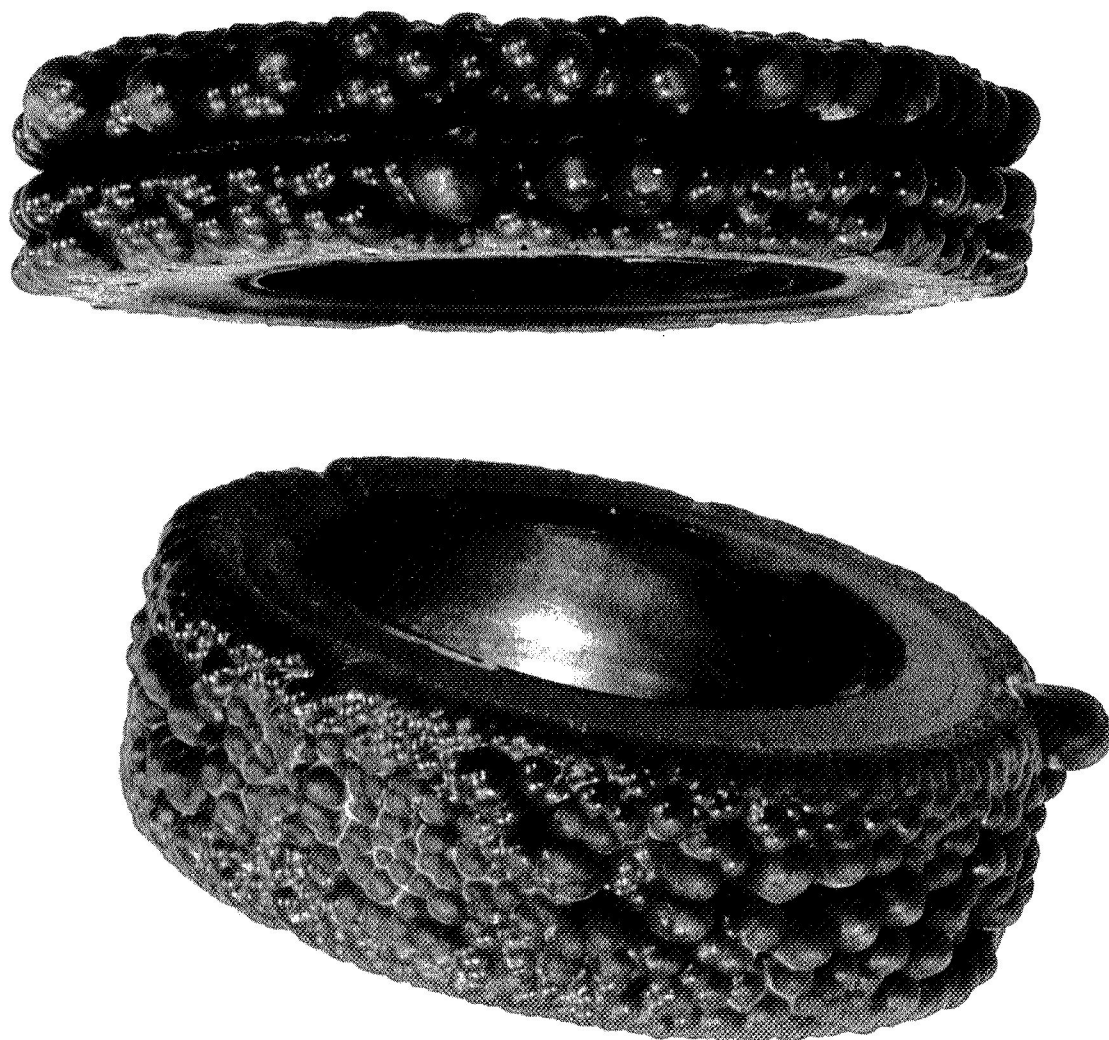
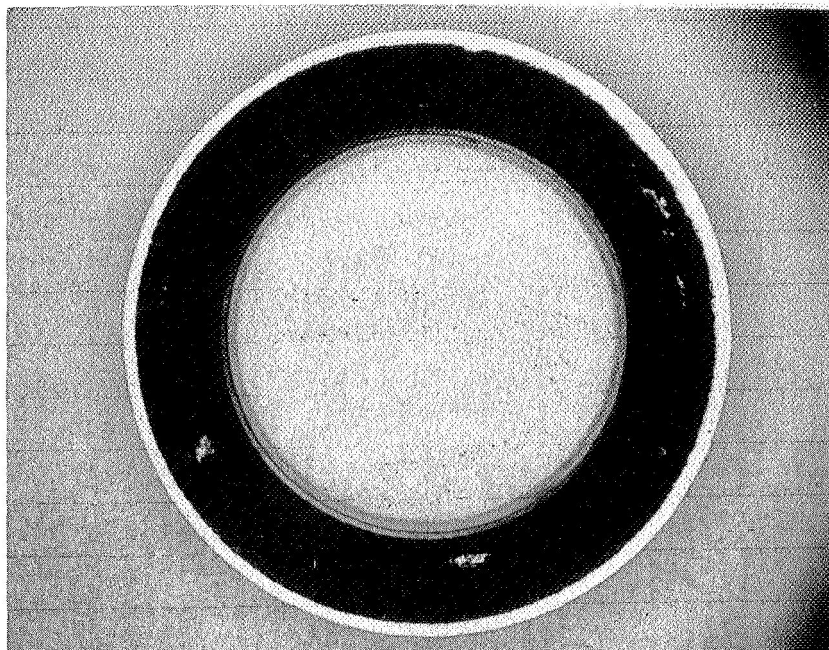


FIGURE 41. Filament Winding Setup for PGI Thornel Thrust Chambers

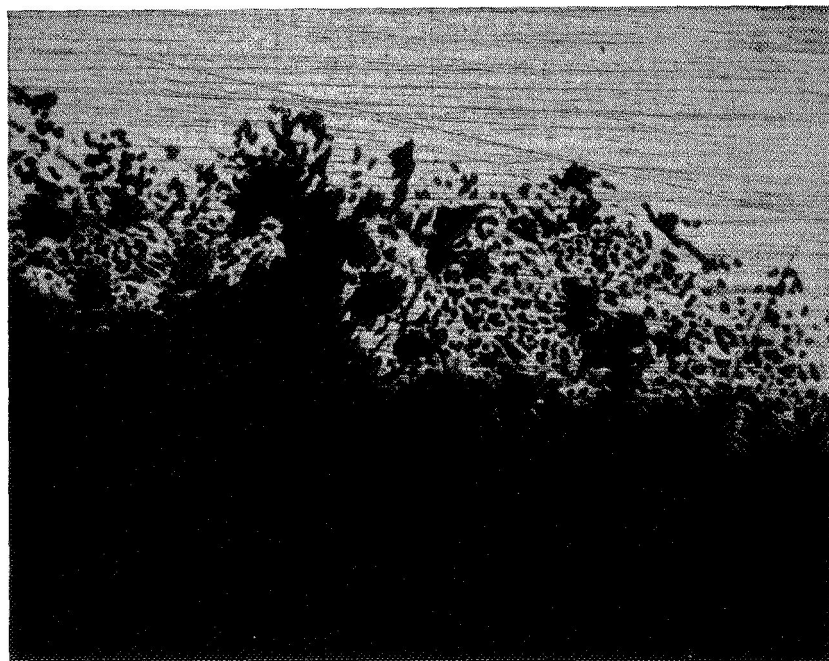


NEG. 9368-1

FIGURE 42. Electrodeposited Nickel on RPG/PG Cylinders before Machining

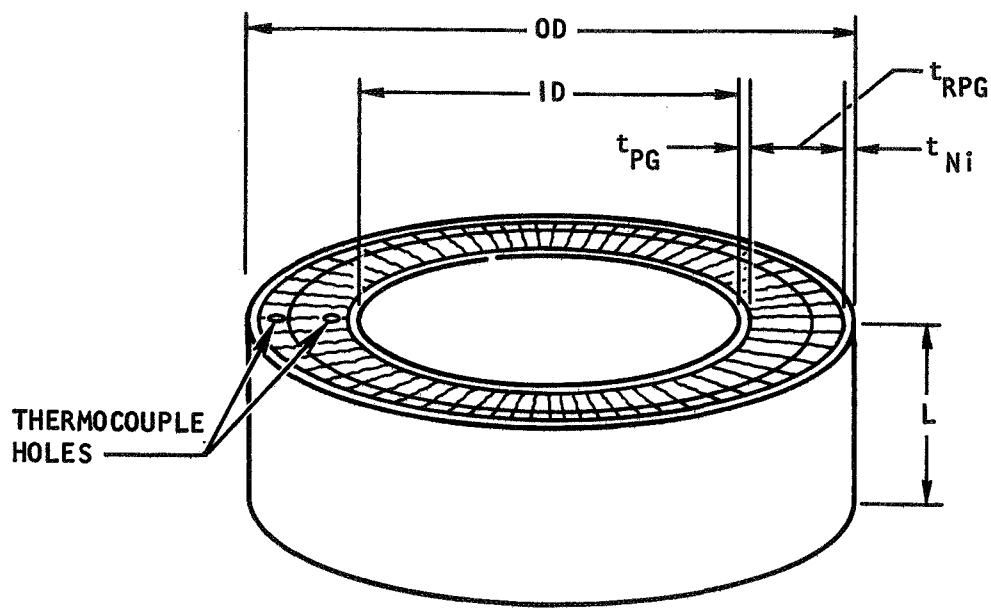


A. Electrodeposited Nickel Layer on RPG
after Machining (Full Size)



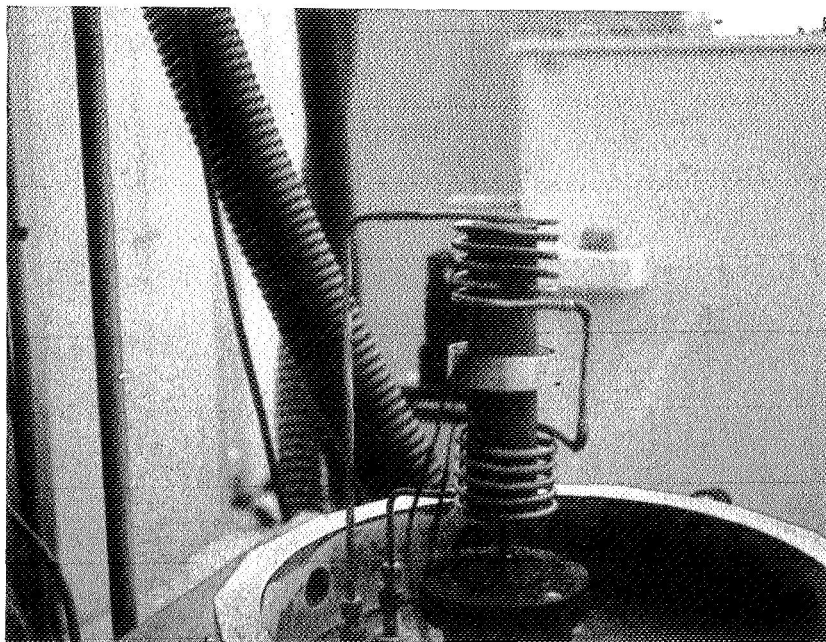
B. Interface between Nickel and RPG (50 X)

FIGURE 43. Electrodeposited Nickel on RPG/PG Cylinder after Machining

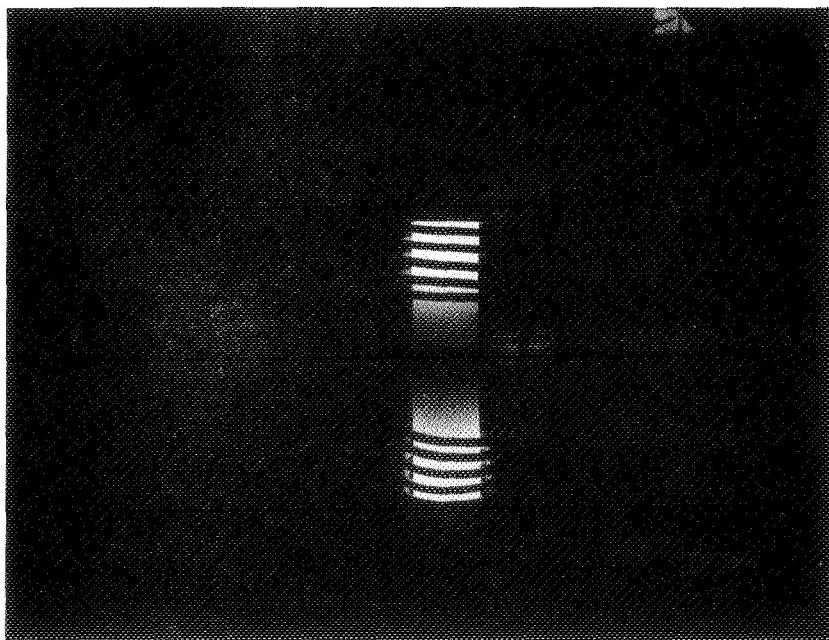


$OD = 3.15 \text{ in.}$
 $ID = 2.15 \text{ to } 2.35 \text{ in.}$
 $L = 0.94 \text{ in.}$
 $t_{PG} = 0.04 \text{ in.}$
 $t_{RPG} = 0.45 \text{ in.}$
 $t_{Ni} = 0.04 \text{ to } 0.08 \text{ in.}$

FIGURE 44. Test Specimen Used for Thermal Cycling Test of Bond of Electrodeposited Nickel on RPG



A. Experimental Arrangement for
Thermal Cycling Tests



B. Thermal Cycling Test in Progress

FIGURE 45. Setup for Thermal Cycling Test of Electrodeposited
Nickel on RPG

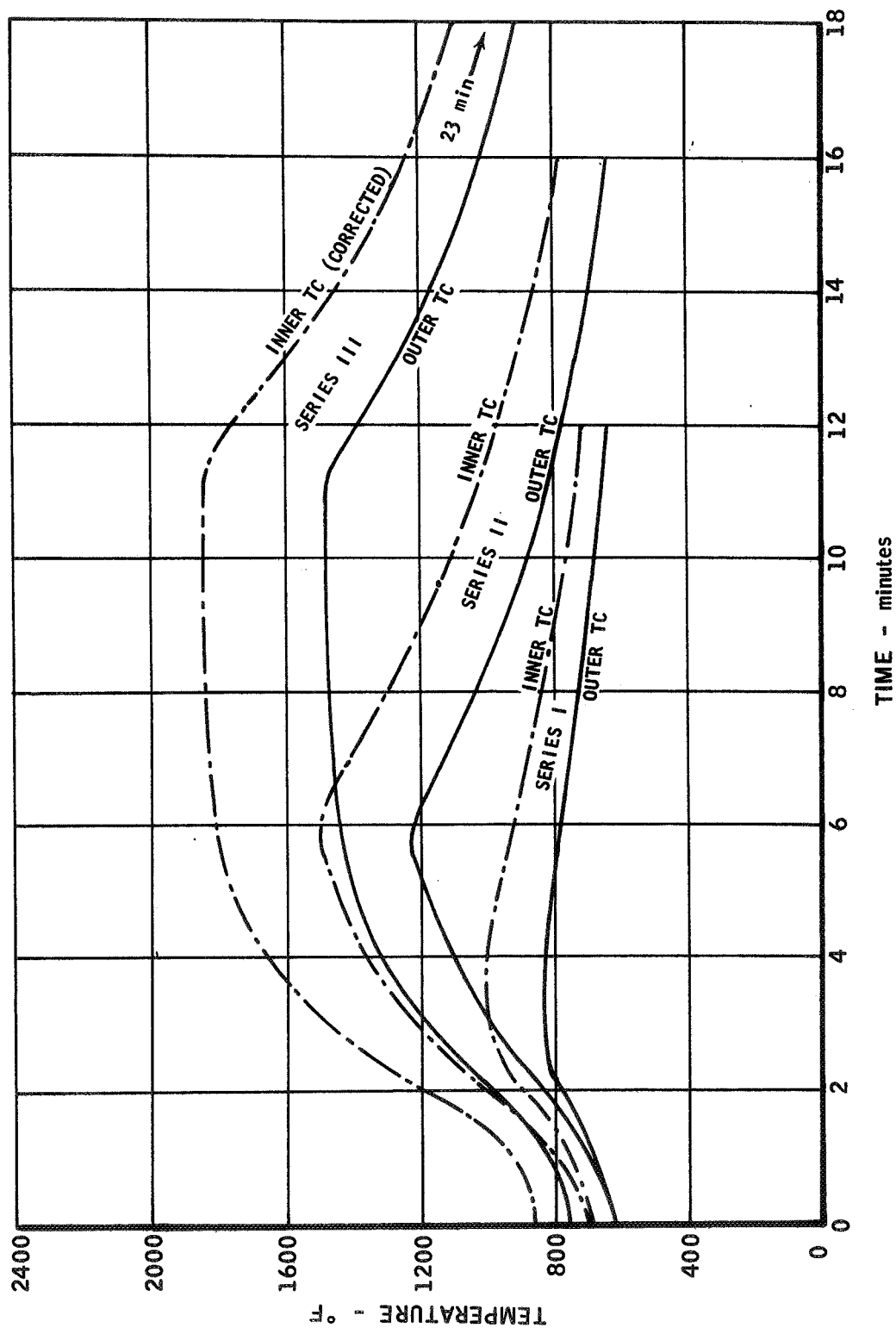
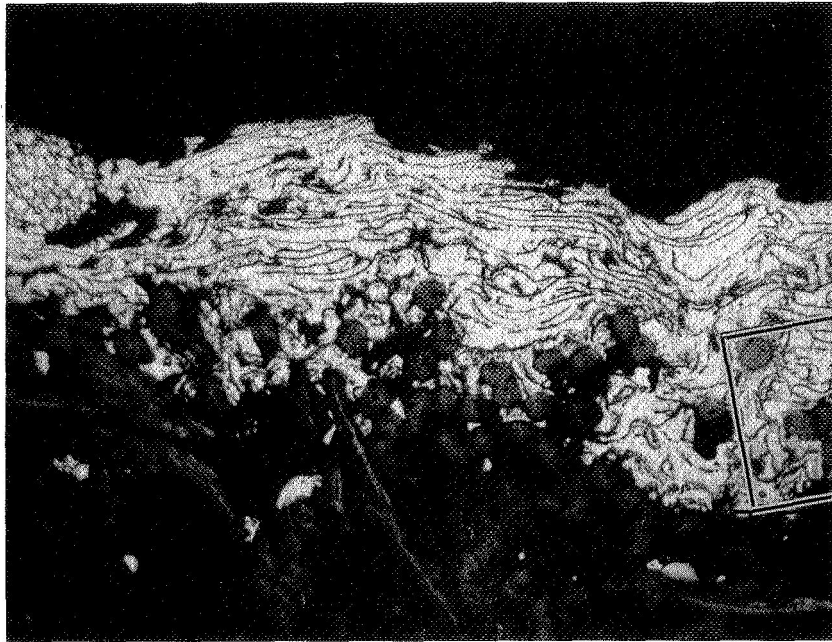
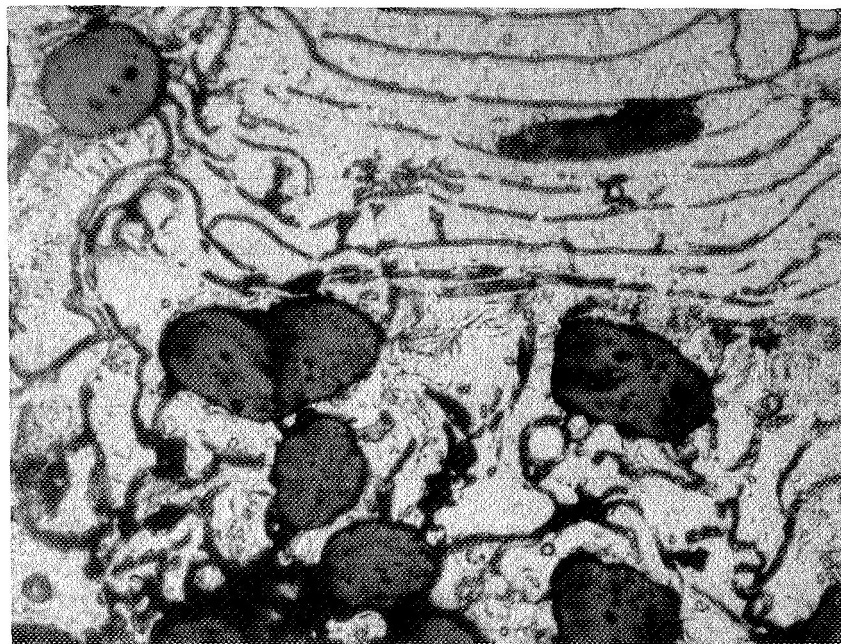
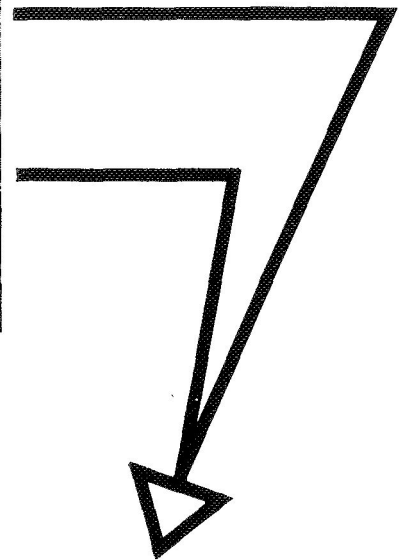


FIGURE 46. Typical Cycles of Thermal Cycling Test of Electrodeposited Nickel on RFG



(200 X)



Boxed Area (750 X)

FIGURE 47. Photomicrographs of Plasma Sprayed Nickel - RPG Interface

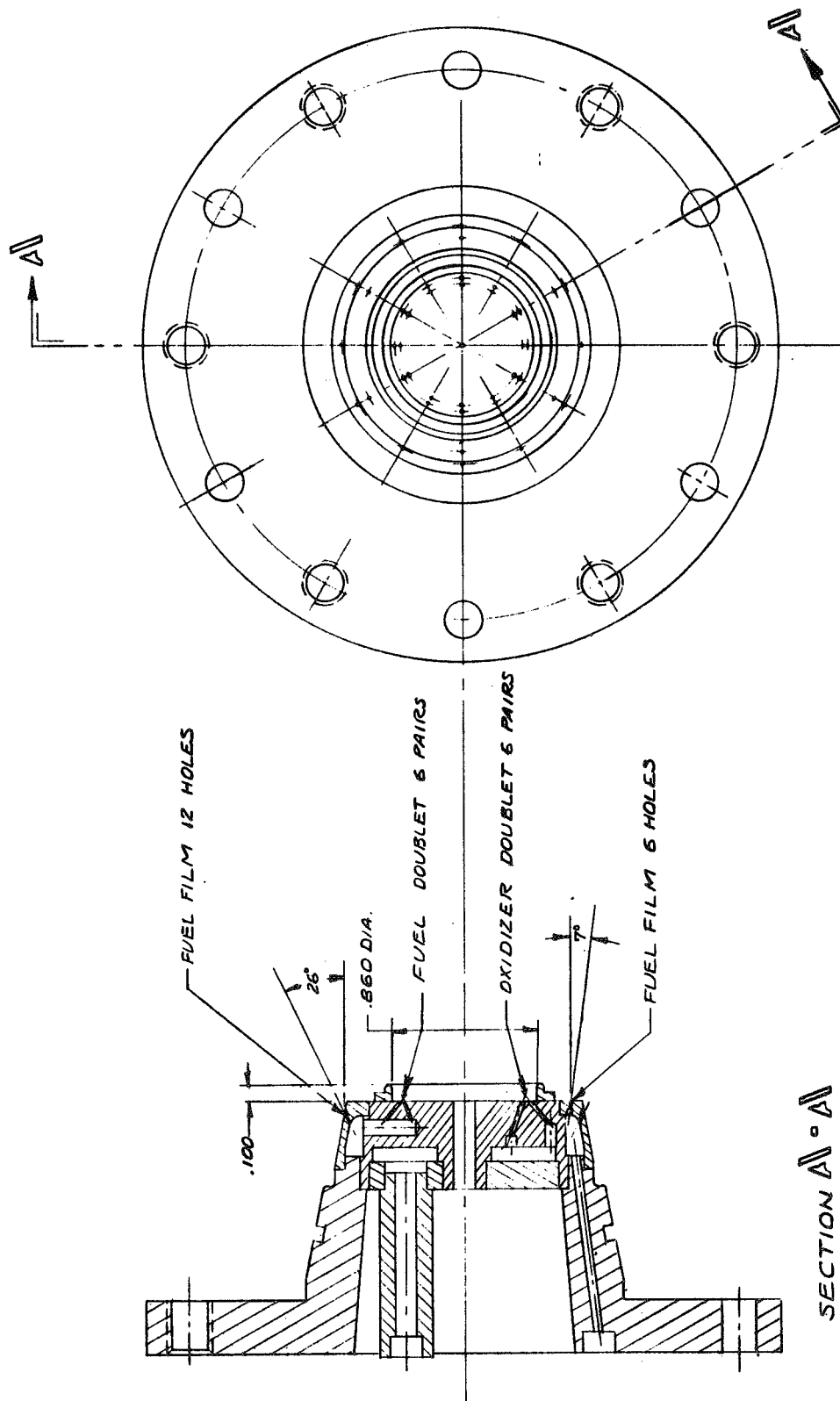


FIGURE 48. Final Configuration of the 100-pound Thrust FLOX Methane Injector, S/N002

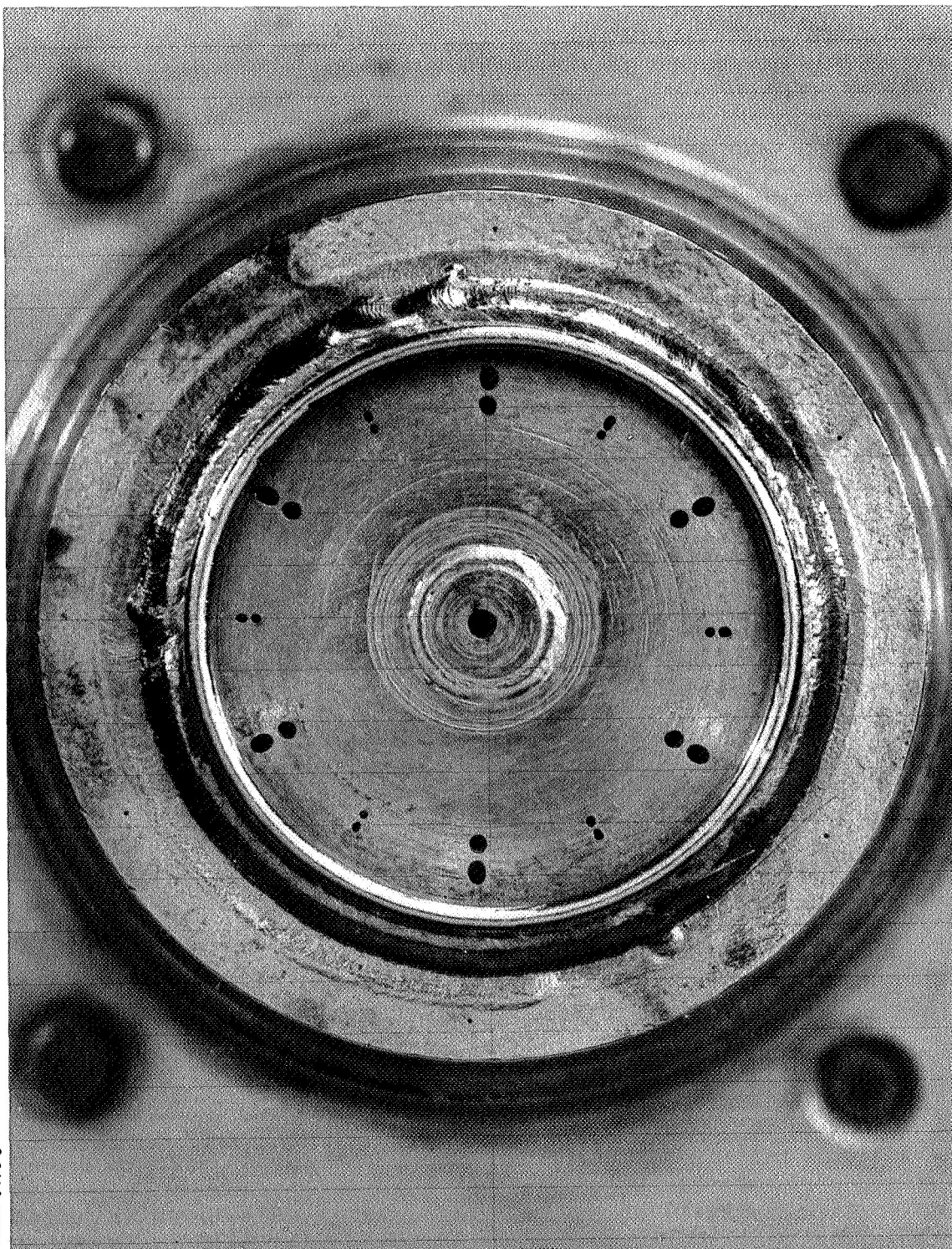


FIGURE 49. Final Configuration, S/N 002 Injector

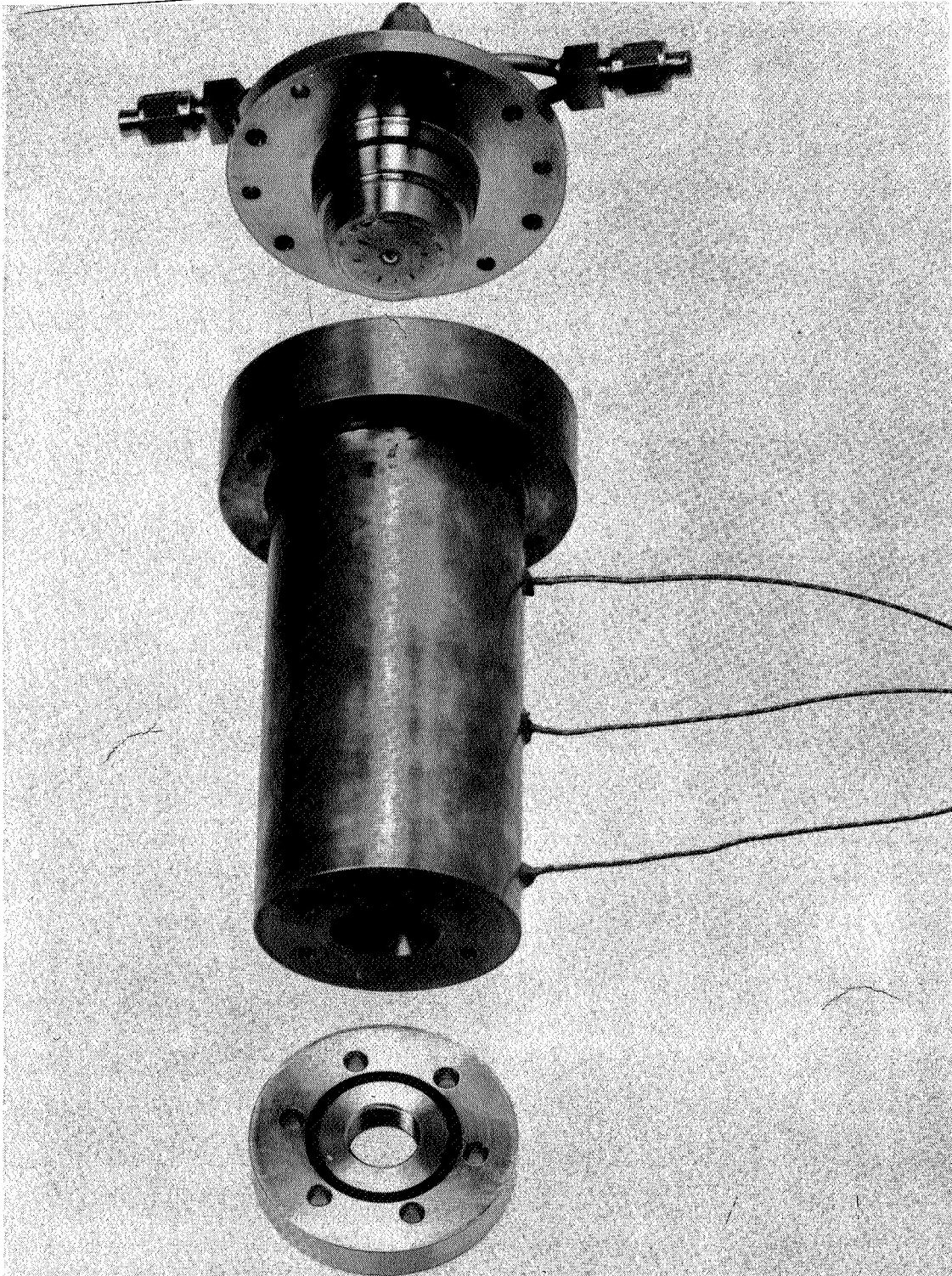


FIGURE 50. 100-pound Thrust FLOX/Methane Engine

NEG. 9157-1

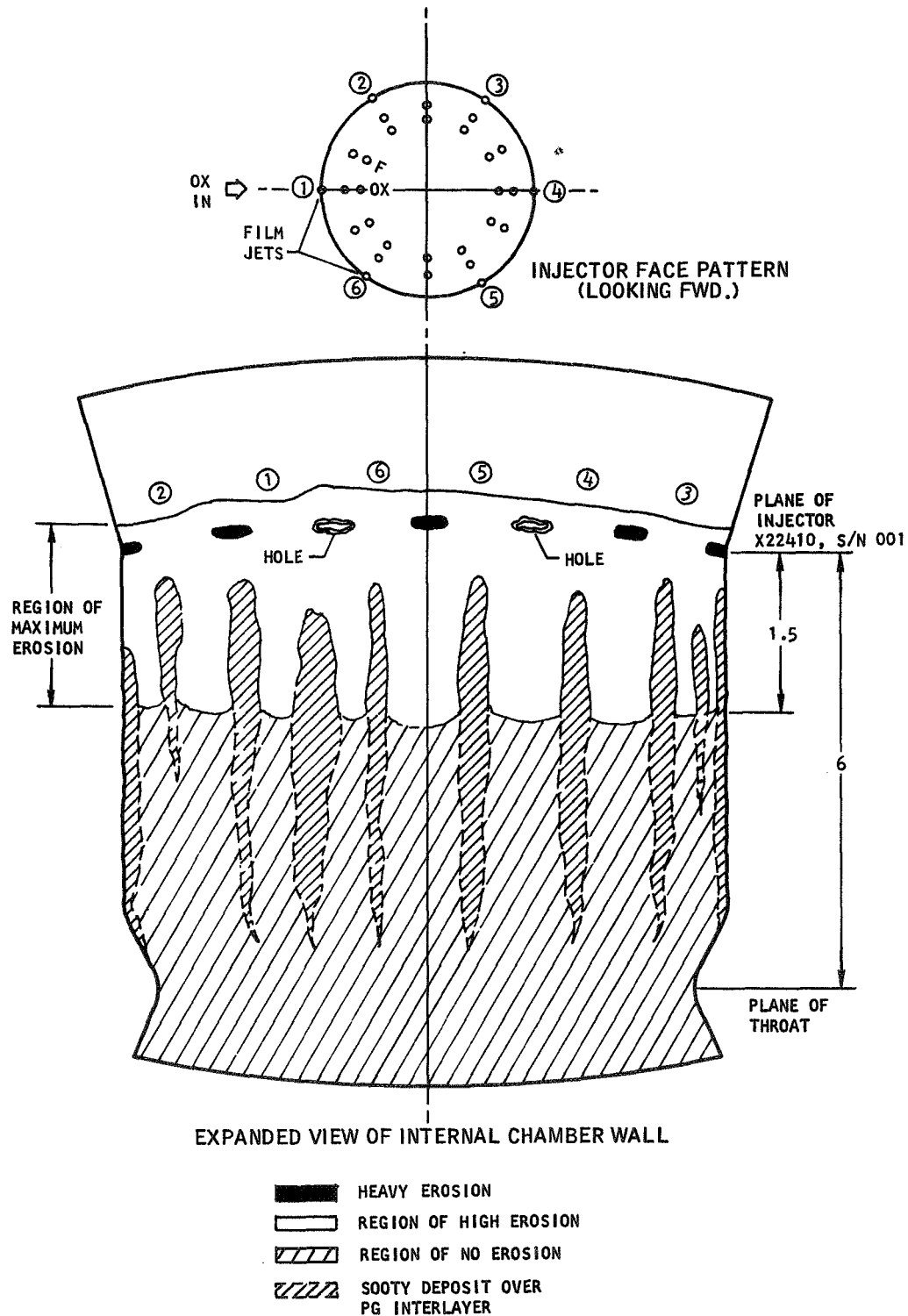


FIGURE 51. Erosion Pattern of PG Chamber S/N 006 after Test Run 45



NEG. 9421-1

FIGURE 52. Carbon Deposition in Sea Level PG Streak Chamber after 20 Seconds Firing

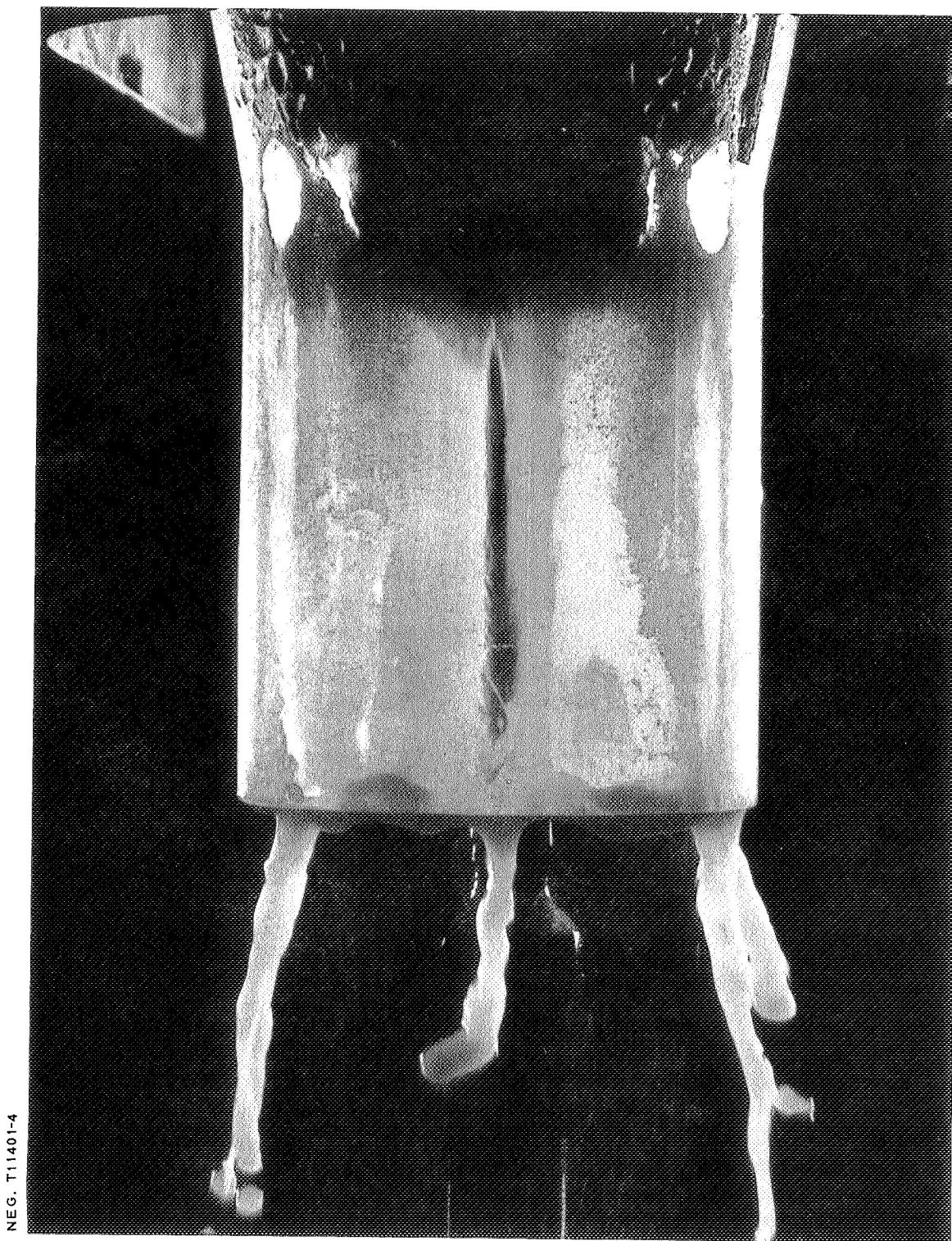
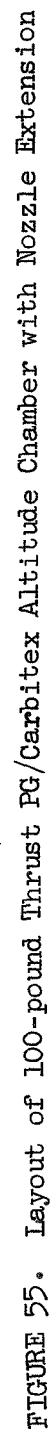


FIGURE 53. Water Flow Test of a Modified Injector Showing Film Spreading in a Lucite Chamber, $\Delta P = 80$ psi



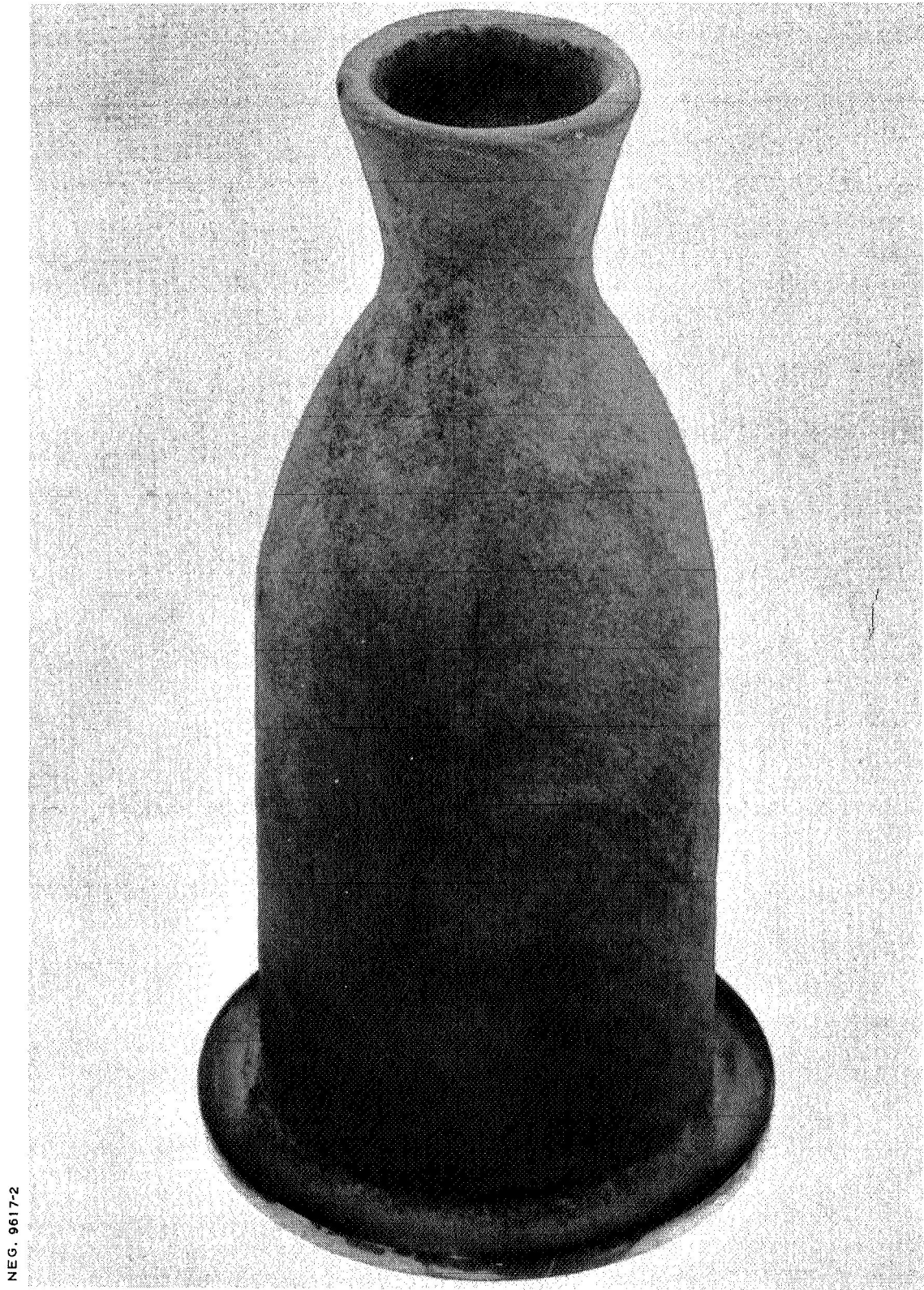
FIGURE 54. Spray Pattern from Cold Flow Tests of the 100-pound Thrust FLOX/Methane Injector with 18 Fuel Film Holes





NEG. 9472-2

FIGURE 56. PG/Carbitex Chamber with RPG Nozzle Extension after 322 Seconds Firing



NEG. 9617-2

FIGURE 57. HFC Coated Tantalum Tungsten Chamber

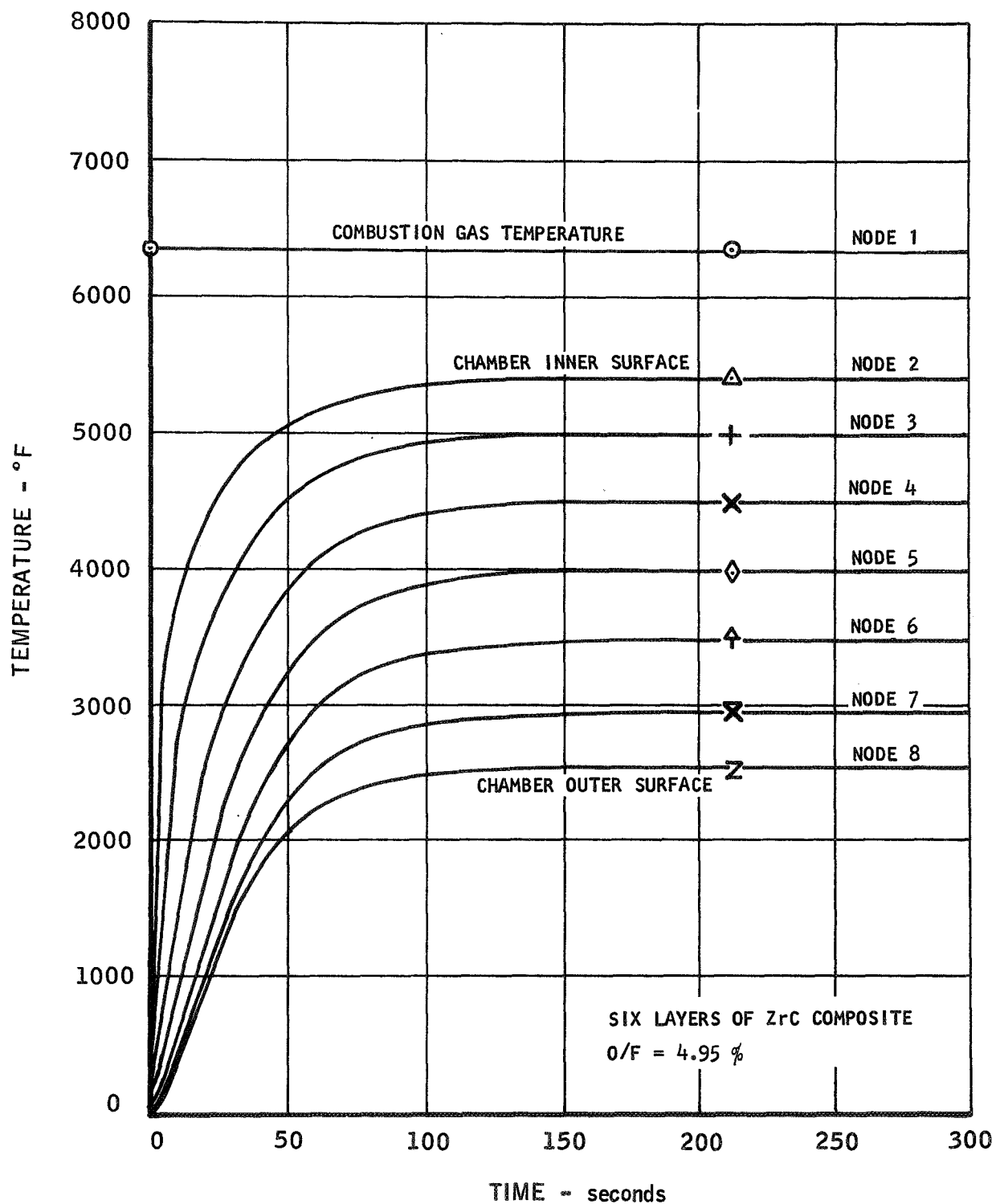


FIGURE 58. Predicted Transient Temperature Distribution in a ZrC Composite Chamber Fired with FLOX/Methane

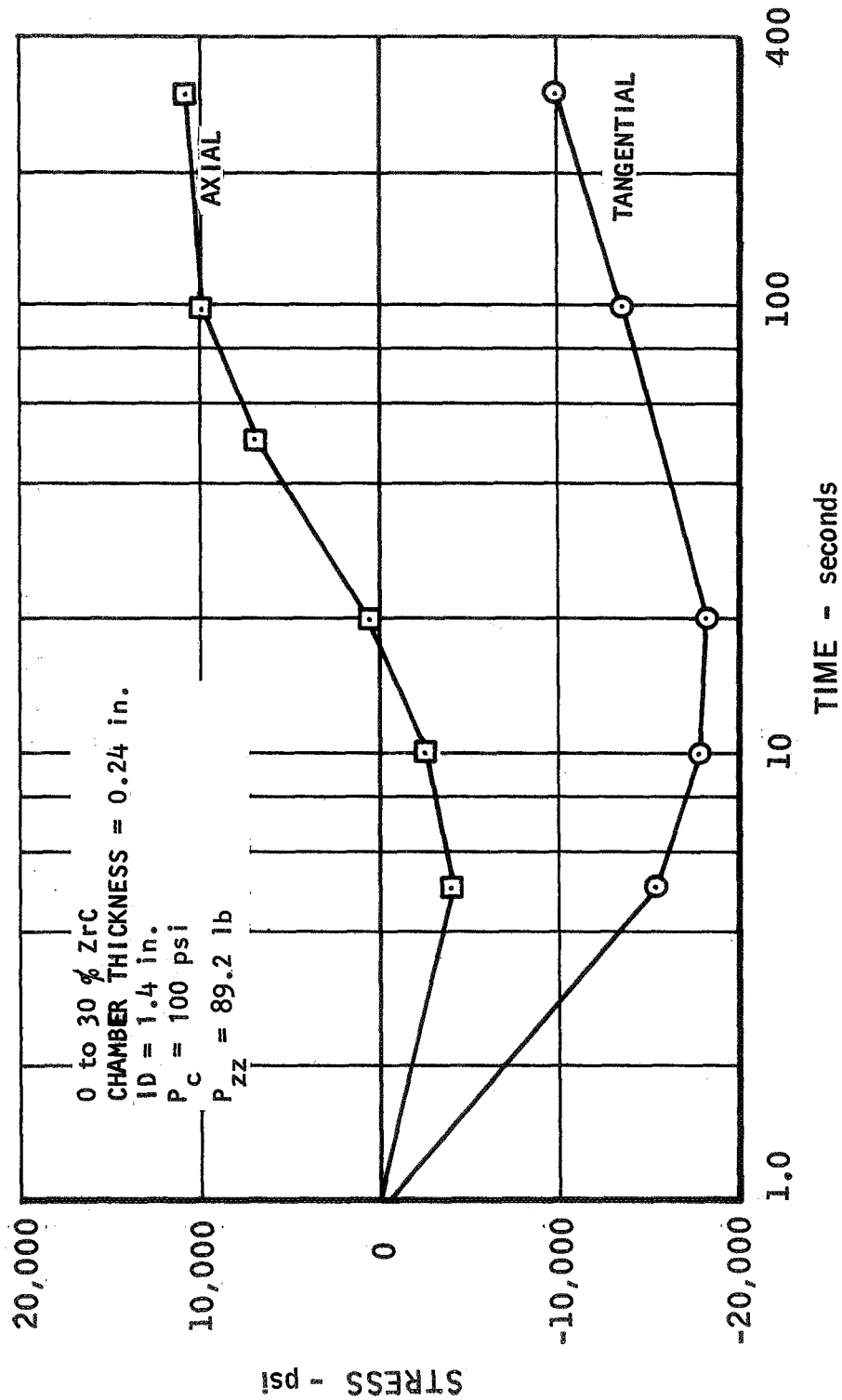


FIGURE 59. Inner Surface Stresses in a ZrC Composite Chamber Fired with FLOX/Methane

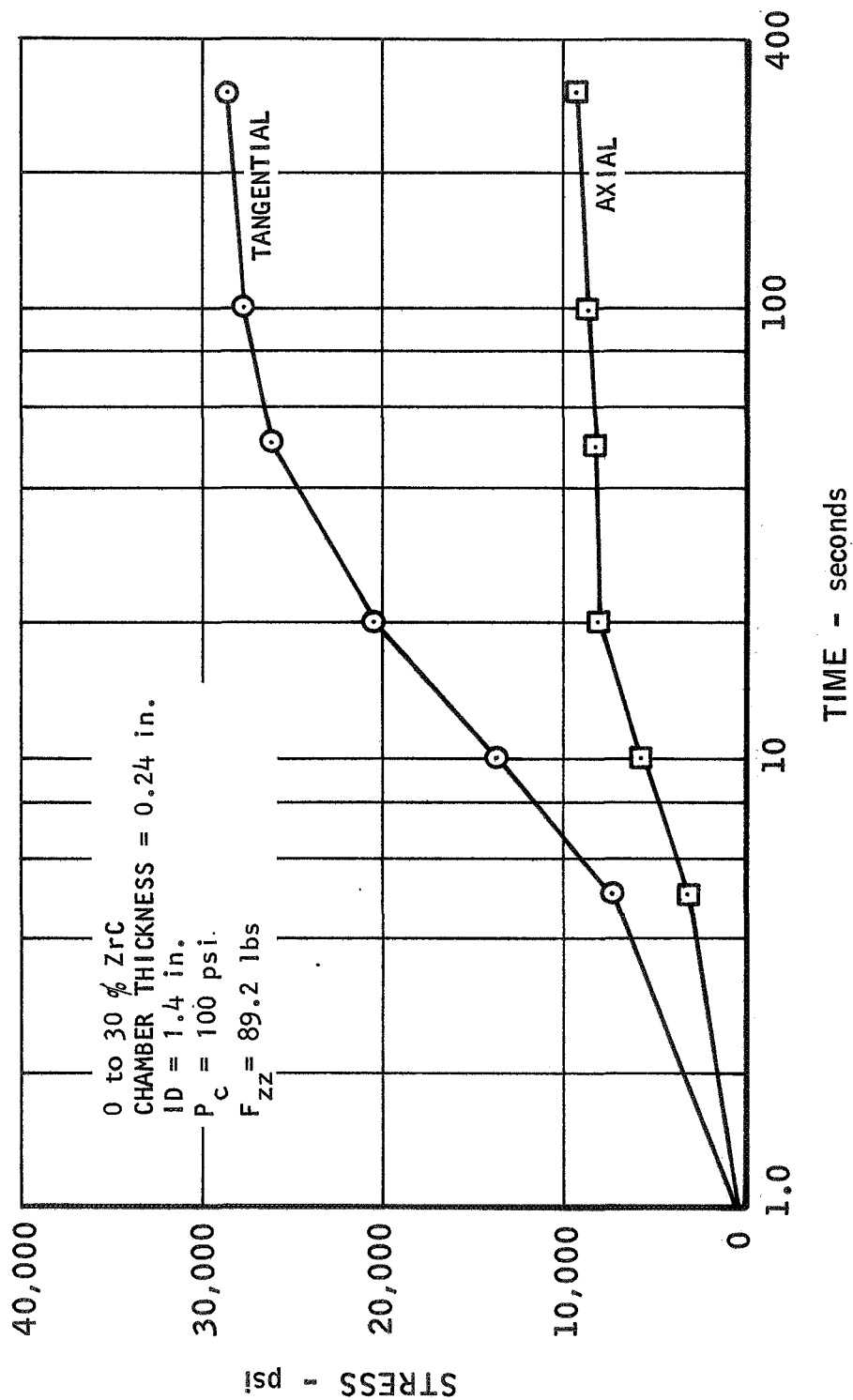


FIGURE 60. Outer Surface Stresses in a ZrC Composite Chamber Fired With FLOX/Methane

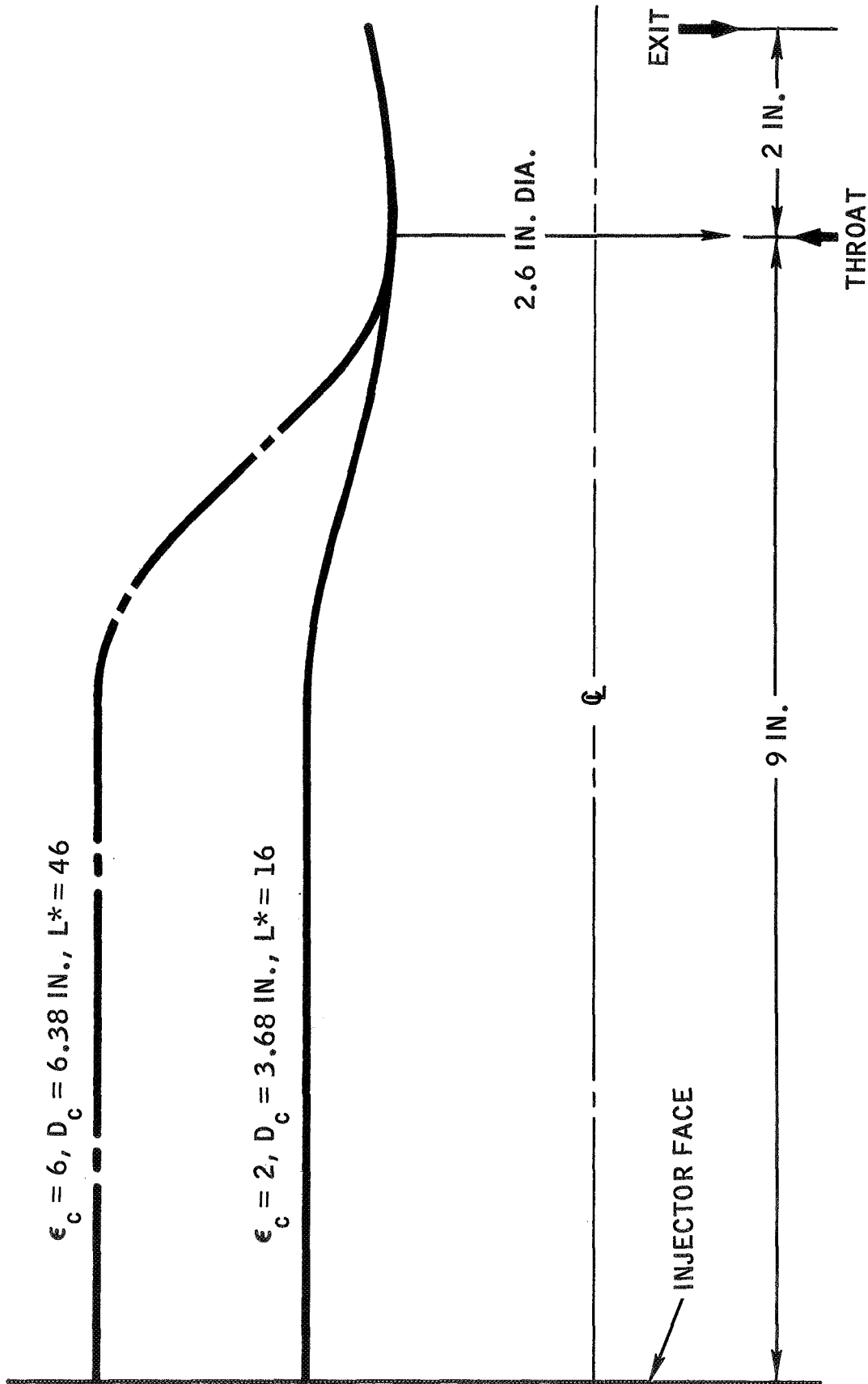


FIGURE 61. 1K Chamber Geometry for Thermal Analysis

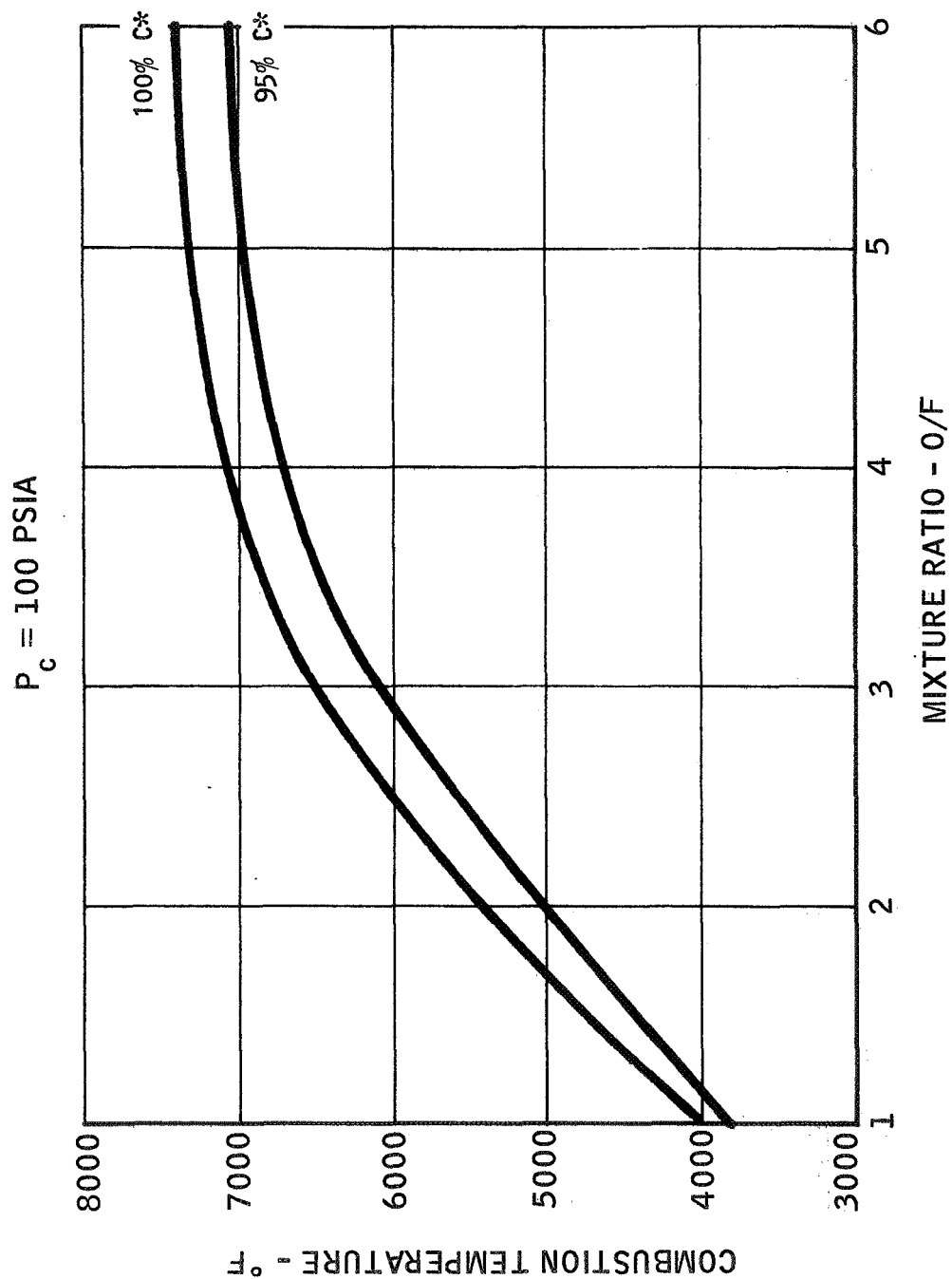


FIGURE 62. Combustion Temperature of $\text{OF}_2/\text{B}_2\text{H}_6$

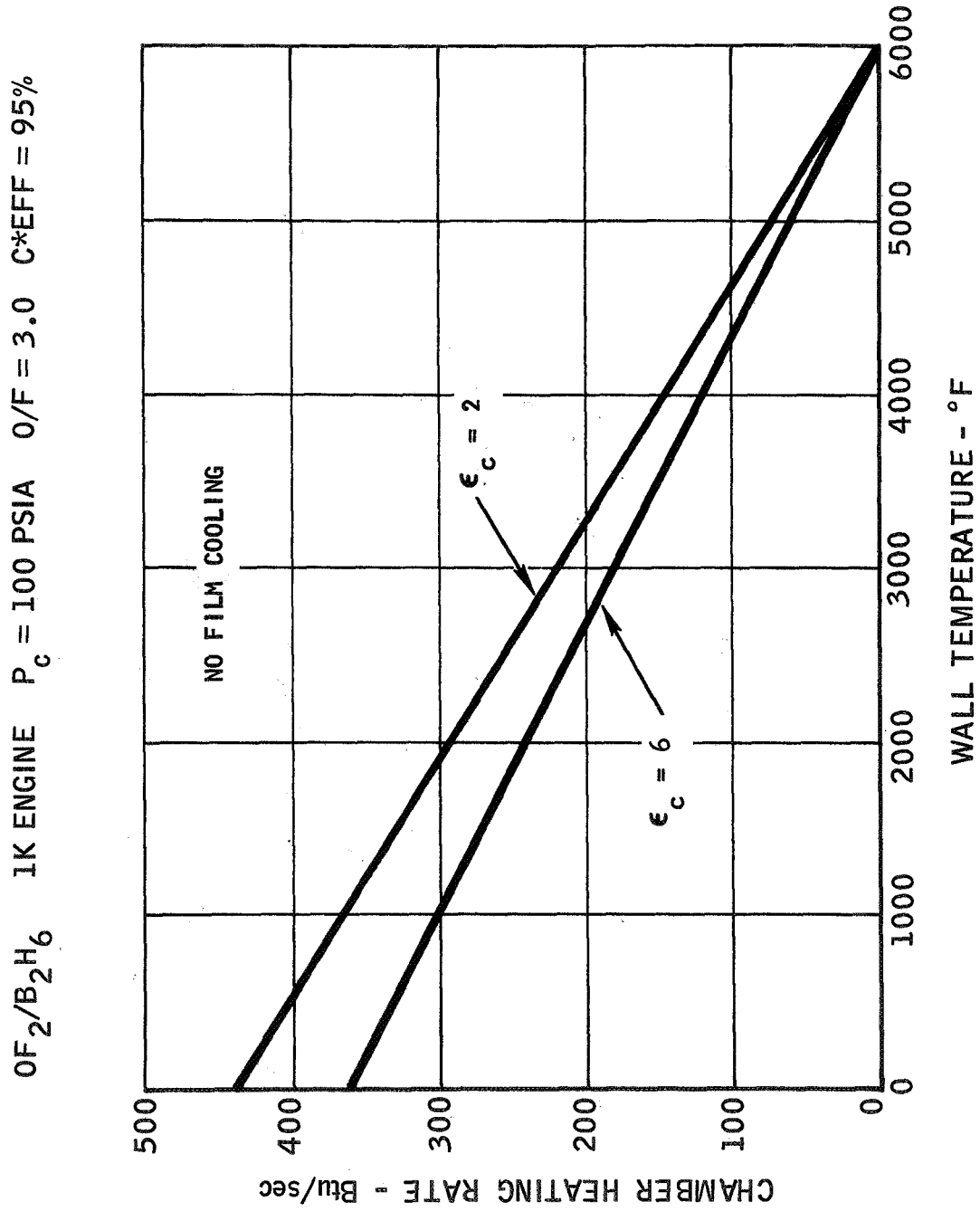


FIGURE 63. Chamber Heating Rate

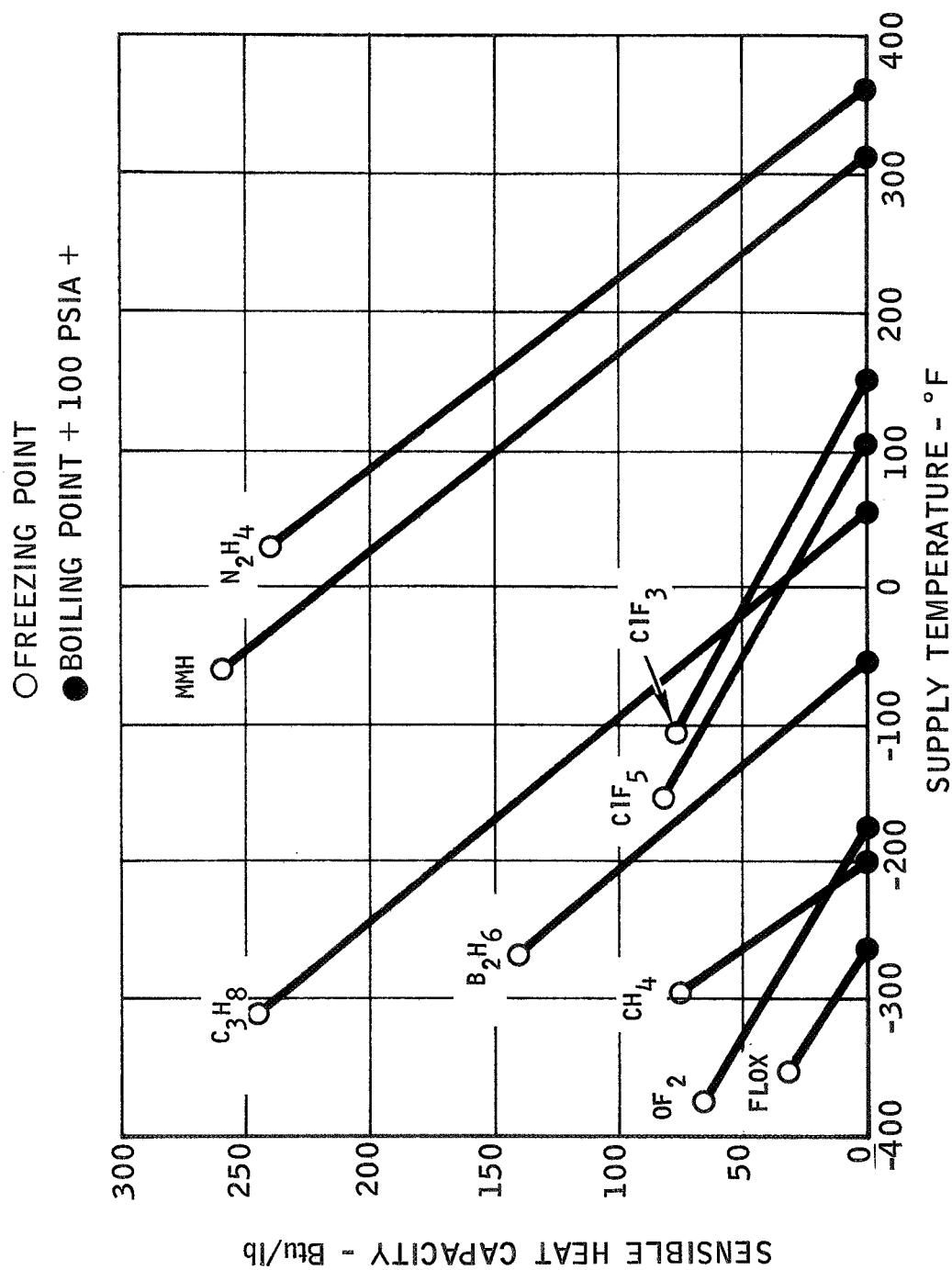


FIGURE 64. Sensible Heat Capacity versus Supply Temperature

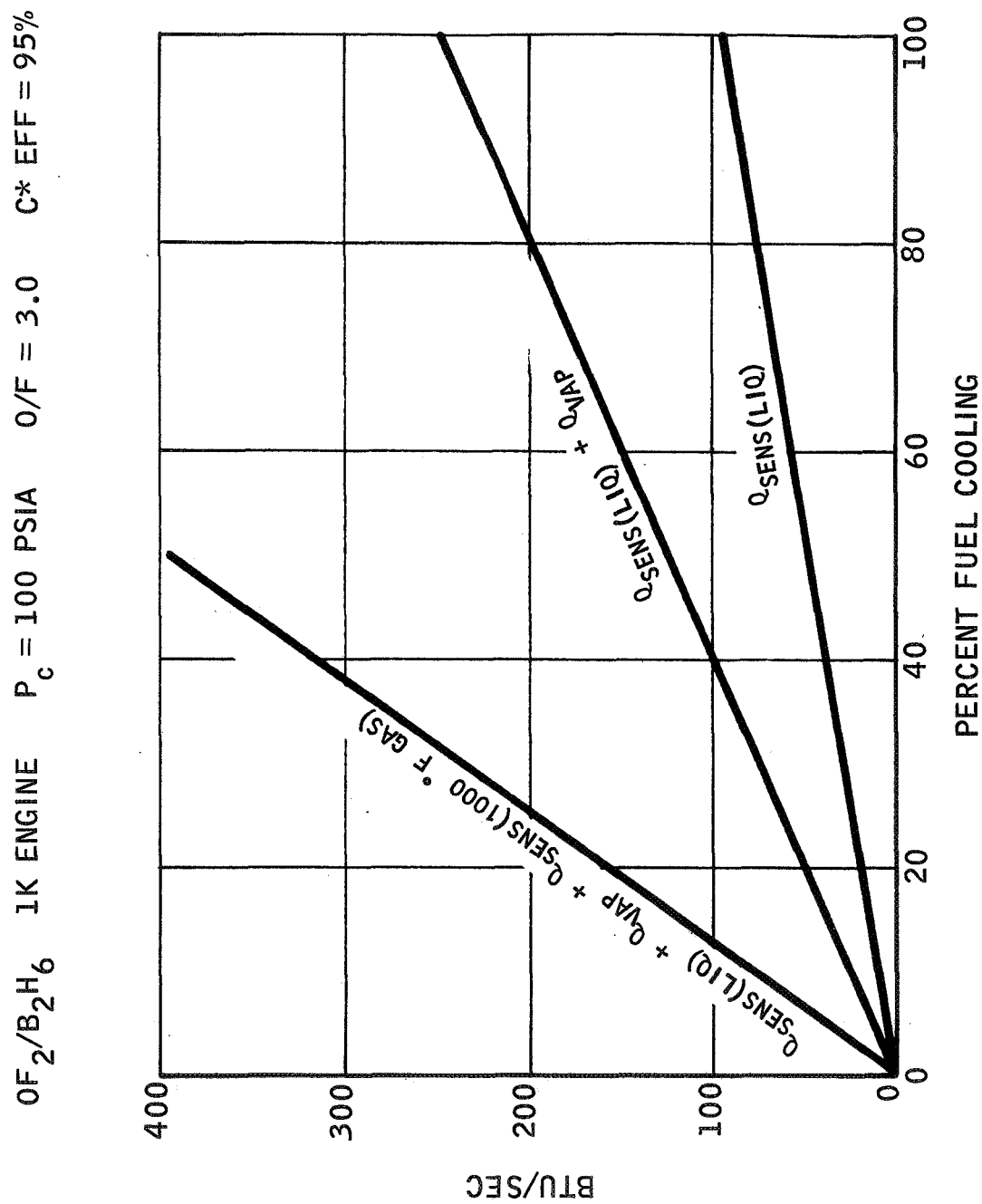


FIGURE 65. B₂H₆ Cooling Capacity

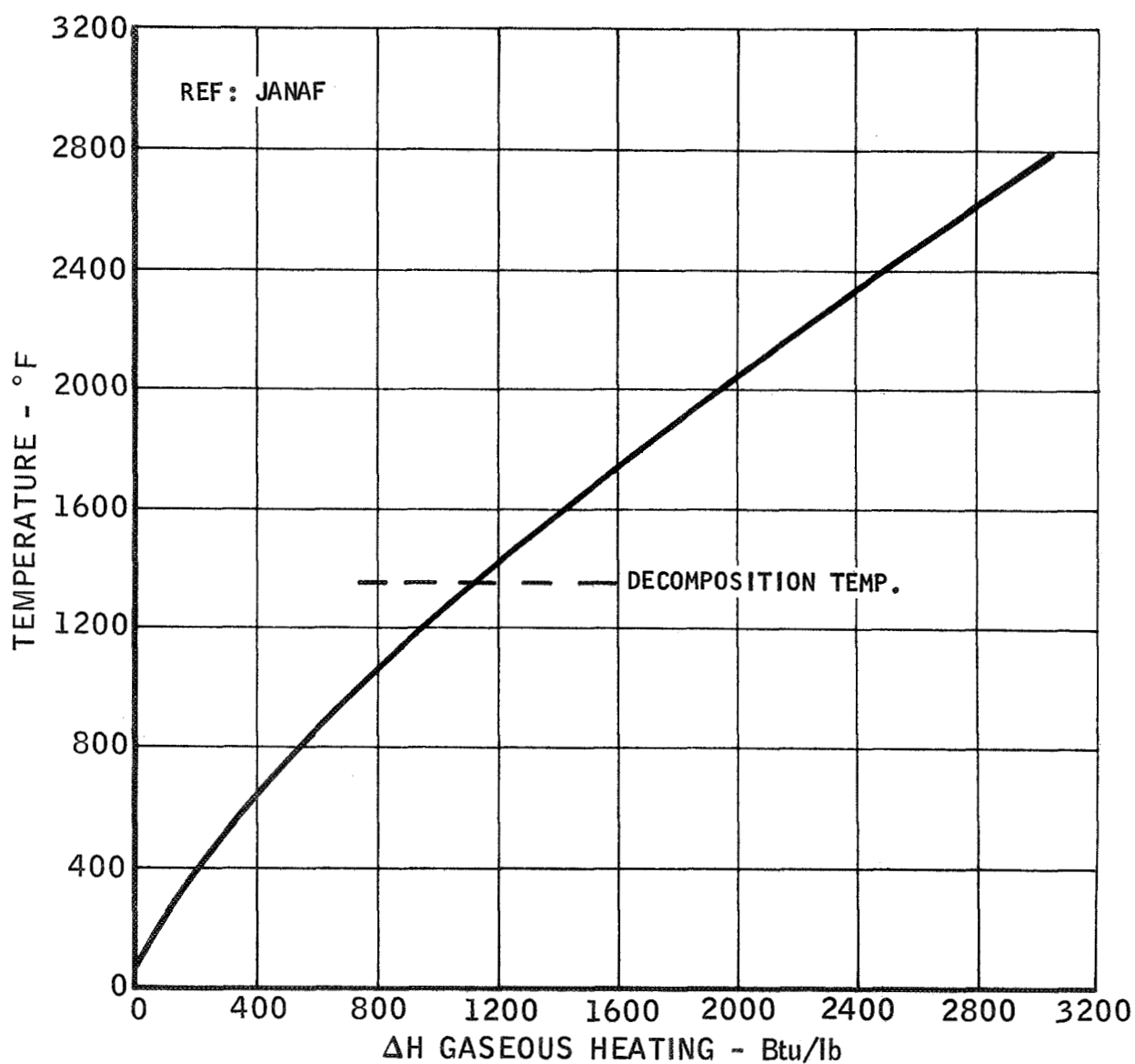


FIGURE 66. Enthalpy of Gaseous Diborane

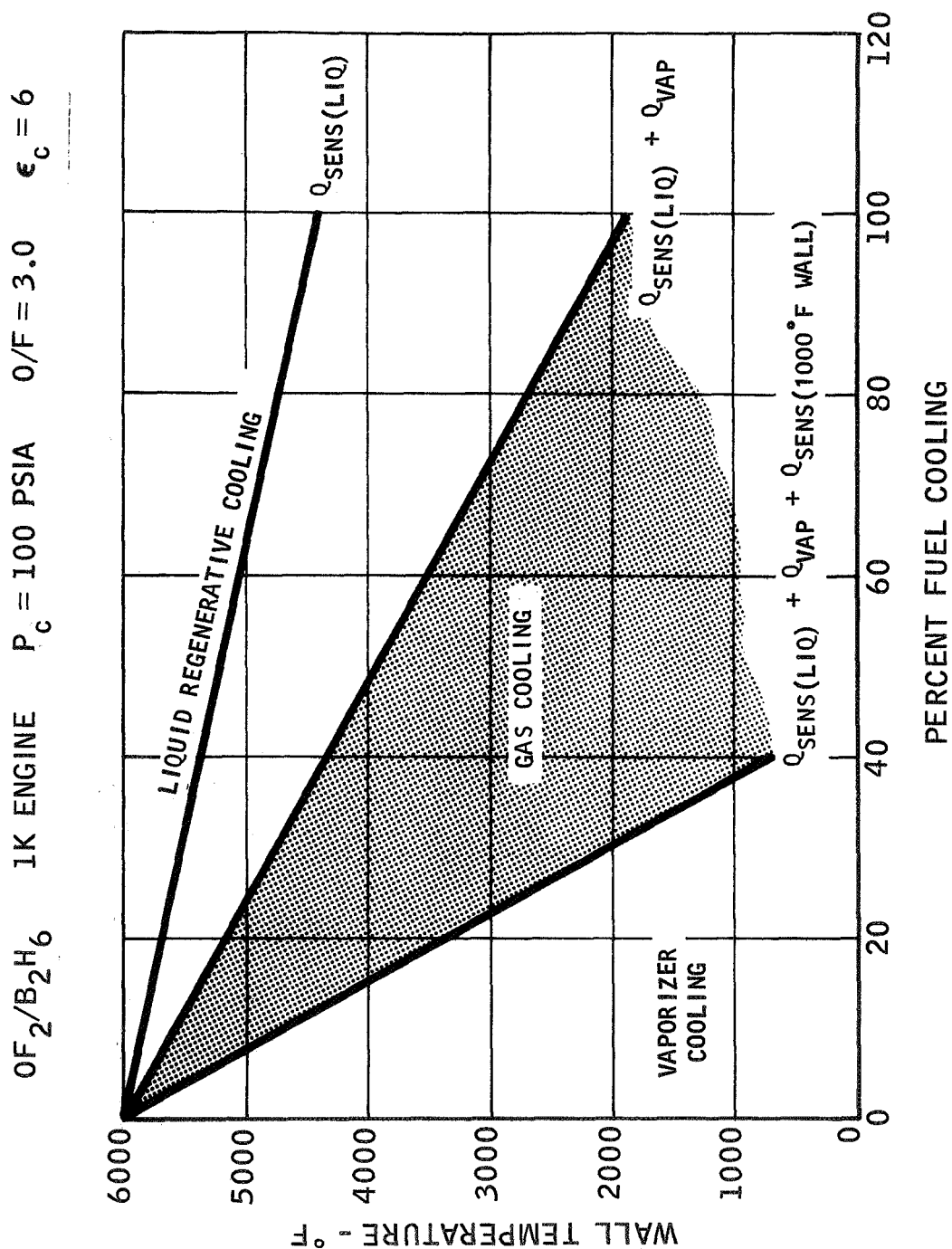


FIGURE 67. Equilibrium Chamber Wall Temperature

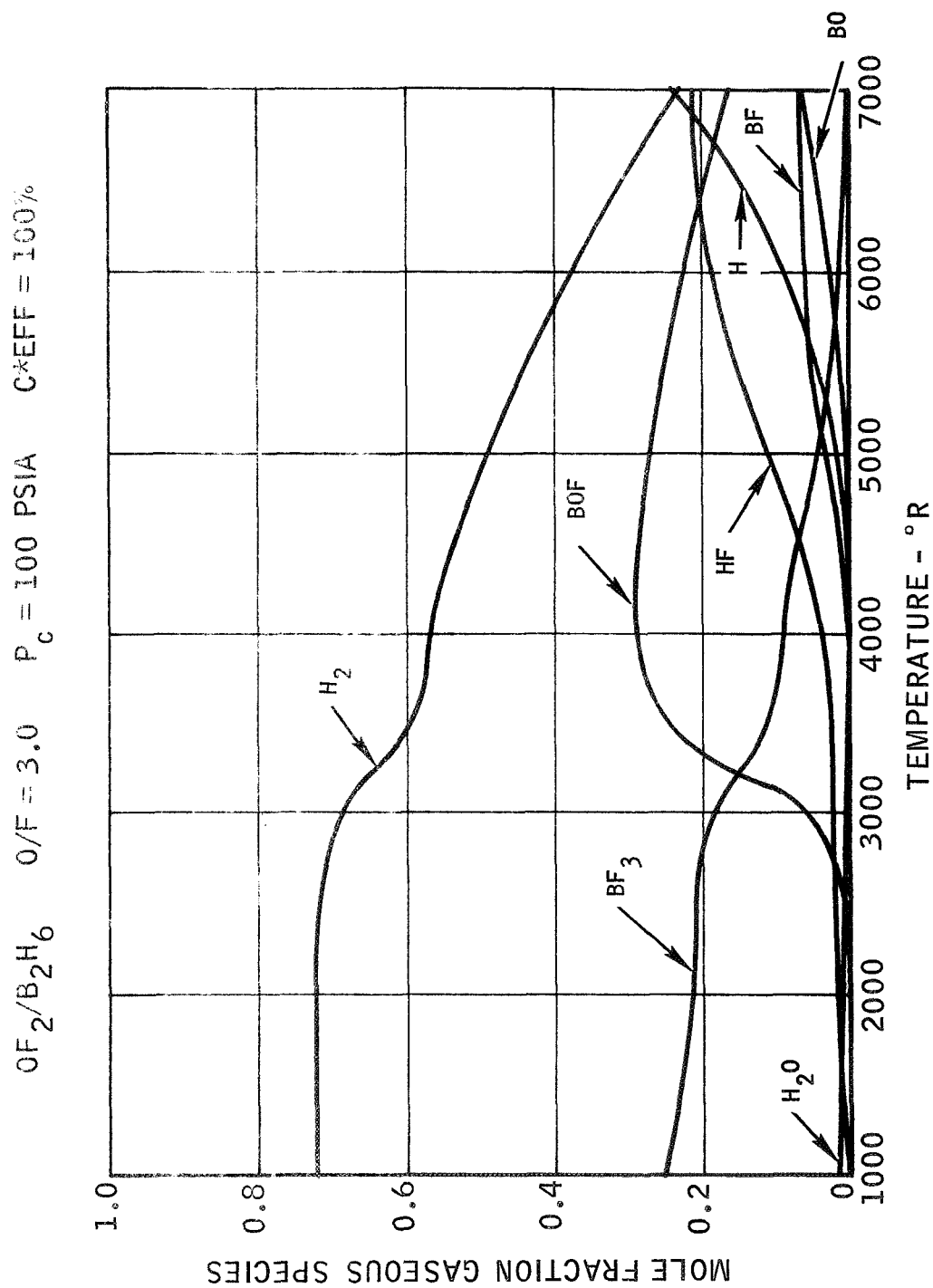


FIGURE 68. Combustion Products - OF OF_2/B_2H_6

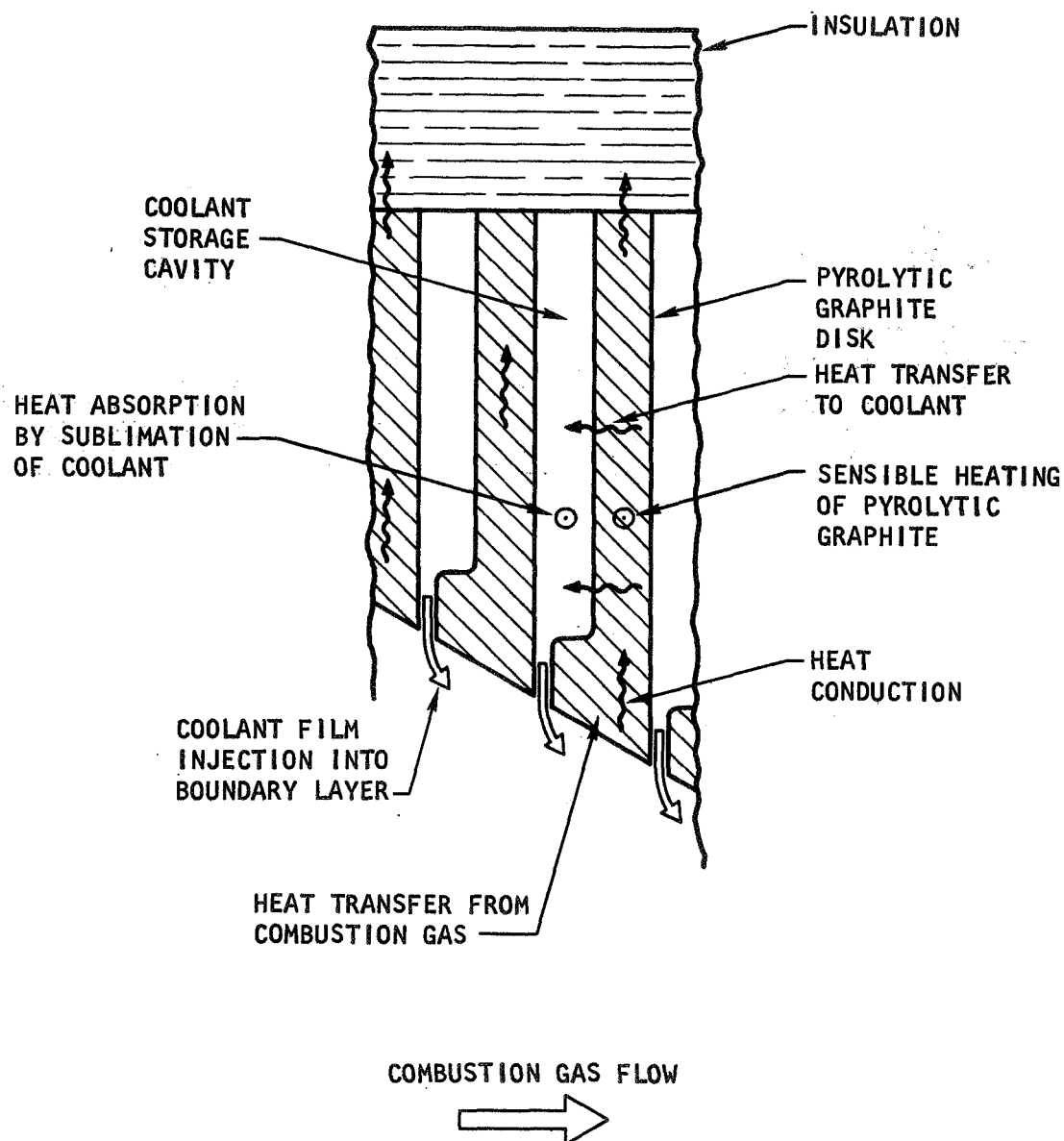
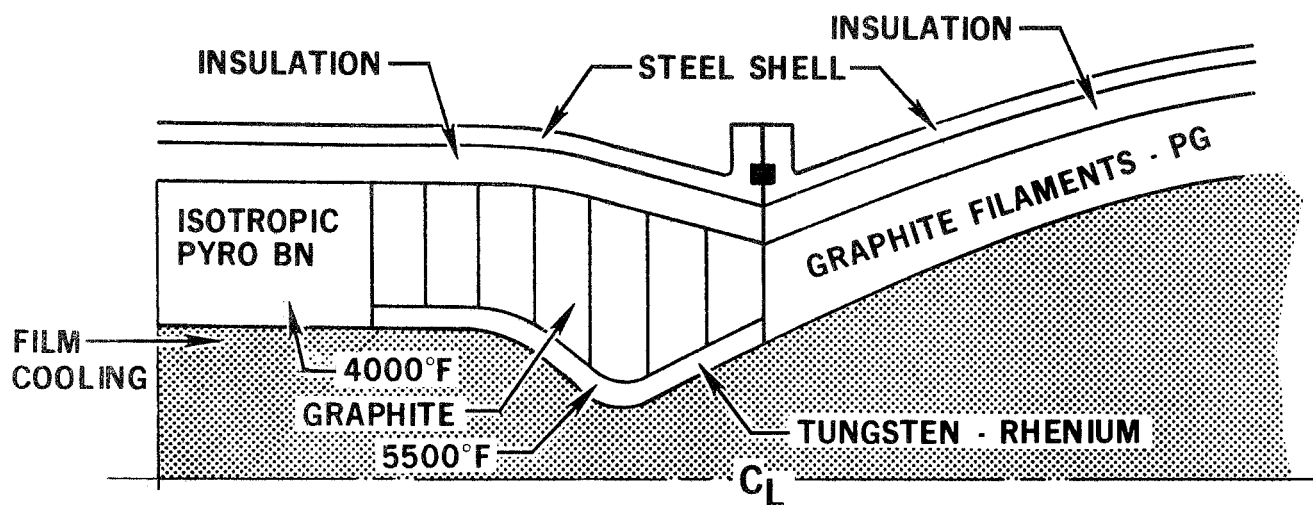


FIGURE 69. Heat Transfer Mechanisms in an Endothermically Cooled Pyrolytic Graphite Nozzle



- MODERATE AMOUNT OF B_2H_6 FILM COOLING
- INERT CHAMBER - BELOW 4000°F
- TUNGSTEN THROAT - BELOW 5500°F
- COMPOSITE GRAPHITIC EXPANSION NOZZLE - VERY LOW REACTION RATES IN LOW PRESSURE REGION

FIGURE 70. Composite Materials Chamber

DISTRIBUTION

<u>RECIPIENT</u>	<u>No. Cys.</u>
NASA Headquarters Washington D.C. 20546 Attn: Contracting Officer	1
Attn: Patent Office	1
NASA Lewis Research Center 21000 Brookpark Rd. Cleveland, Ohio 44135 Attn: Office of Technical Information	1
NASA Manned Spacecraft Center Houston, Texas 77001 Attn: Office of Technical Information	1
NASA Marshall Space Flight Center Huntsville, Alabama 35812 Attn: Technical Library	1
NASA Pasadena Office 4800 Oak Grove Drive Pasadena, California 91103 Attn: Patents and Contract Management	1
Jet Propulsion Laboratory 4800 Oak Grove Drive Pasadena, California 91103 Attn: Technical Manager	2
NASA Headquarters Office of Advanced Research and Technology Washington D.C. 20546 Attn: Chief, Liquid Propulsion Technology RPL	3

Distribution (Continued)

<u>Recipient</u>	<u>No. Cys.</u>
Director, Technology Utilization Division Office of Technology Utilization NASA Headquarters Washington, D.C. 20546	1
NASA Scientific and Technical Information Facility P.O. Box 33 College Park, Maryland 20740	25
Goddard Space Flight Center Greenbelt, Maryland 20771 Attn: Merland L. Moseson Code 620	1
Jet Propulsion Laboratory California Institute of Technology 4800 Oak Grove Drive Pasadena, California 91103 Attn: Henry Burlage, Jr. Propulsion Division 38	2
Langley Research Center Langley Station Hampton, Virginia 23365 Attn: Ed Cortwright Director	2
Lewis Research Center 21000 Brookpark Road Cleveland, Ohio 44135 Attn: Bruce Lundin Director	2
Marshall Space Flight Center Huntsville, Alabama 35812 Attn: Hans G. Paul Code R-P&VED	2

Distribution (Continued)

<u>Recipient</u>	<u>No. Cys.</u>
Manned Spacecraft Center Houston, Texas 77001 Attn: J. G. Thibodeux, Jr. Chief, Prop. & Power Division	2
John F. Kennedy Space Center, NASA Cocoa Beach, Florida 32931 Attn: Dr. Kurt H. Debus	2
Aeronautical Systems Division Air Force Systems Command Wright-Patterson AFB, Ohio 45433 Attn: D.L. Schmidt Code ASRONC-2	1
Space and Missile Systems Organization Air Force Unit Post Office Los Angeles 45, California 90045 Attn: Col. Clark Technical Data Center	1
Bureau of Naval Weapons Department of the Navy Washington, D.C. 20546 Attn: J. Kay RTMS-41	1
Defense Documentation Center Headquarters Cameron Station, Building 5 5010 Duke Street Alexandria, Virginia 22314 Attn: TISIA	1
Air Force Rocket Propulsion Laboratory Research and Technology Division Air Force Systems Command Edwards, California 93523 Attn: RPRPD/Mr. H. Main	2

Distribution (Continued)

<u>Recipient</u>	<u>No. Cys.</u>
U.S. Army Missile Command Redstone Arsenal Alabama 35809 Attn: Mr. Walter Wharton	1
U.S. Naval Ordnance Test Station China Lake, California 93557 Attn: Code 4562 Chief, Missile Propulsion Div.	1
Chemical Propulsion Information Agency Applied Physics Laboratory 8621 Georgia Ave. Silver Springs, Maryland 20910 Attn: Tom Reedy	1
Aerojet-General Corporation P.O. Box 1947 Technical Library, Bldg. 2015, Dept. 2410 Sacramento, California 95809 Attn: R. Stiff	1
Aerospace Corporation 2400 East El Segundo Blvd. P.O. Box 95085 Los Angeles, California 90045 Attn: John G. Wilder MS-2283	1
Atlantic Research Corporation Edsall Road and Shirley Highway Alexandria, Virginia 22314 Attn: Dr. Ray Friedman	1
Avco Systems Division Wilmington, Massachusetts Attn: Howard B. Winkler	1

Distribution (Continued)

<u>Recipient</u>	<u>No. Cys.</u>
Bell Aerosystems Company P.O. Box 1 Buffalo, New York 14240 Attn: W.M. Smith	1
Bellcomm 955 L'Enfant Plaza, S.W. Washington, D.C. Attn: H.S. London	1
General Dynamics, Convair Division Library and Information Services (128-00) P.O. Box 1128 San Diego, California Attn: Frank Dore	1
Missile and Space Systems Center General Electric Company Valley Forge Space Technology Center P.O. Box 8555 Philadelphia, Pa. Attn: Library	1
Arthur D. Little, Inc. 20 Acorn Park Cambridge, Massachusetts 02140 Attn: Library	1
Lockheed Missiles and Space Co. Attn: Technical Information Center P.O. Box 504 Sunnyvale, California 94088	1
Lockheed Propulsion Company P.O. Box 111 Redlands, California 92374	1

Distribution (Continued)

<u>Recipient</u>	<u>No. Cys.</u>
Astropower Laboratory McDonnell-Douglas Aircraft Company 2121 Paularino Newport Beach, California 92663 Attn: Dr. George Moc Director, Research	1
Missile and Space Systems Division McDonnell-Douglas Aircraft Company 3000 Ocean Park Blvd. Santa Monica, California 90406 Attn: Library	1
Space & Information Systems Division North American Rockwell 12214 Lakewood Blvd. Downey, California 90241 Attn: Library	1
Rocketdyne (Library 586-306) 6633 Canoga Ave. Canoga Park, California 91340 Attn: S.F. Jacobellis	1
Northrop Space Laboratories 3401 West Broadway Hawthorne, California 90250 Attn: Dr. William Howard	1
Aeronutronic Division Philco Corporation Ford Road Newport Beach, California 92663 Attn: D.A. Garrison	1
TRW Systems Group TRW Incorporated One Space Park Redondo Beach, California 90278 Attn: G.W. Elverum	1

Distribution (Continued)

<u>Recipient</u>	<u>No. Cys.</u>
United Technology Center 587 Methilda Ave. P.O. Box 358 Sunnyvale, California 94088 Attn: Dr. David Altman	1